HYDRODYNAMIC MODELING OF ANTHROPOGENIC STRESS IN A SHALLOW MICROTIDAL ESTUARY: ITAJURU CHANNEL, BRAZIL

by

Stephen Bryan Lippa

A research paper submitted in conformity with the requirements

for the degree of Master of Science

Graduate Department of Geography

University of Toronto

HYDRODYNAMIC MODELING OF ANTHROPOGENIC STRESS IN A SHALLOW MICROTIDAL ESTUARY: ITAJURU CHANNEL, BRAZIL

Stephen Bryan Lippa

Master of Science

Graduate Department of Geography

University of Toronto

ABSTRACT

The effect of an artificial morphological change on the hydrodynamics of the Itajuru Channel, Brazil is investigated using the RMA2 two-dimensional finite element hydrodynamic model. Two configurations were constructed to simulate the tidal wave and flow characteristics under existing conditions and conditions where the channel bathymetry is altered by dredging a -3 meter channel. Flood-dominant tidal current asymmetry and landward net sediment flux are predicted by the model simulation of the existing conditions, supporting the historical evidence describing internal sediment accretion. The channel dredging is shown to reduce the tidal amplitude along the channel, which in turn increases hydraulic gradients driving tidal currents. Greater increases in the ebb-directed current magnitudes relative to flood current magnitudes effectively eliminate the flood-dominant asymmetry to the extent that a small ebb-directed net sediment flux is predicted. Thus, the hydrodynamic results confirm that tidal propagation in the Itajuru Channel depend strongly on the bathymetric configuration.

ACKNOWLEDGEMENTS

In the course of writing this paper I have incurred three particular debts of gratitude. First, to Dr. Brian Greenwood, for his spirited criticism of hydrodynamic modeling and his informed arguments on coastal processes. His guidance has pushed me to think more deeply and communicate more accurately. To Dr. Guilherme Lessa, for his inspiration, energy, and expertise. Without his support and encouragement, I would never have believed it possible.

Most of all, I owe an unpayable debt to my wife, Janel. She has served as an exceptionally able critic and motivator; more, she is my unshakable friend and companion.

DEDICATION

This work is dedicated to Marcio Werneck da Cunha, a Brazilian historian who spent his life studying Cabo Frio. I met him at the start of this academic journey but, sadly, he is not with us now at its conclusion.

TABLE OF CONTENTS

LIST OF SYMBOLS

a	Basin area above the elevation contour at height h
a_t	Tidal amplitude
A	Maximum basin area
A_c	Channel cross sectional area
A_{bmax}	Maximum bay area
c	Celerity
ΔD	Duration difference
g	Gravitational acceleration
h	Height above the minimum basin elevation
h_{cd}	Average channel depth
H	Maximum height above minimum basin elevation
HW	High water
LW	Low water
n	Manning's roughness coefficient
R_{bay}	Tidal range inside the estuary
R_{sea}	Tidal range in the ocean
V_s	Volume of intertidal storage
V_c	Volume of the channel at mean sea level
wse	Water surface elevation
γ	Dimensionless parameter used to quantify the volume of sediment in a basin
ζ	Tidal amplitude
$\pm\sigma$	Plus or minus one standard deviation

LIST OF TABLES

LIST OF FIGURES

1. INTRODUCTION

Estuaries can be described as the geomorphological units that form the connection between terrestrial freshwater systems and the marine saltwater systems. They are ephemeral geological features that are created and consumed as a consequence of the interaction between sedimentation processes and sea-level fluctuations. Estuaries exhibit highly complex and inter-related processes governing their hydrodynamics, sediment dynamics, and biological productivity. Around the world, estuaries are recognized as economically important conduits for accessing harbours and inland waterways, and ecologically valuable breeding grounds and nurseries for a host of species. They also serve important roles in the dispersion of pollution, particularly from coastal cities. Global population growth is putting significantly greater pressure on estuarine ecosystems to accommodate the demands for larger and more frequent shipping traffic and to efficiently diffuse increasing pollution levels. Although estuarine research has grown steadily during the past 40 years, our understanding of the processes that govern estuarine dynamics still require refinement in order to build models which can be used to form adequate sustainable management strategies for these environments (Perillo and Kjerfve, 2005).

Estuaries exhibit large spatial and temporal variability due to the numerous factors influencing their formation, the water and sediment circulation within them, and their evolution (i.e. the magnitude and rate of sea level fluctuation, the volume of river inflow, the tidal and wave regime, climate, the type and stability of sediment, etc.). This infinite variability in the factors governing estuaries often prevents them from reaching a morphologic steady state; instead they frequently appear to be transient (Lanzoni and

Seminara, 2002; Medeiros and Kjerfve, 2005). Roy (1980) considered coastal lagoon estuaries to be shallow inland waters yet to be infilled by natural processes. They are usually oriented parallel to the coast, separated from the ocean by a barrier. One or more restricted inlets allow for varying degrees of tidal mixing resulting in salinity ranges from a coastal freshwater lake to a hypersaline lagoon (Kjerfve and Magill, 1989). Coastal lagoon estuaries occupy approximately 13% of the coastal zone worldwide, and are influenced by both natural and anthropogenic factors (Kjerfve et al., 1996).

Although wave activity and river discharge may become progressively more important towards the outer and inner portions of the estuary respectively, tidal currents play the dominant role with respect to sediment transport in the central zone (Lanzonni and Seminara, 2002). When considering the tidal oscillation in estuaries, it is important to note that the forcing mechanism does not originate directly from the gravitational effects of the moon and sun, as it does for ocean tides, but rather from the hydraulic gradient created by ocean tides at the estuary mouth. The form of the tidal wave within an estuary depends largely on its interaction with the bathymetry, and its frictional effect upon the barotropic wave.

In shallow estuaries, this effect can result in what is widely referred to as tidal asymmetry (Dronkers, 1986). The propagation of the ocean tide in shallow coastal systems, where the tidal wave amplitude is comparable to the total water depth, may be treated as the movement of a frictionless long wave, with celerity *c* given by

$$c = \sqrt{g\left(d + 1.5\zeta\right)} \qquad \text{(Equation 1)}$$

where g is gravitational acceleration, d is the water depth and ζ is the tidal amplitude (Pugh, 1987). This suggests that the wave speed decreases as a direct function of the water depth, which subsequently causes the crest of the wave to move faster and to become closer to the trough ahead. The result is a distorted wave shape with a steep face and a gentle backslope, ie. a shorter rising and a longer falling tide.

Observations of estuaries world-wide clearly indicate that estuarine hydraulics are also sensitive to external factors, such as the dredging of navigational channels (Thomas et al., 2002; Wang et al., 2002), land reclamation and channel training (Cheng et al., 1993; French and Clifford, 2000), major engineering works (Elias et al., 2003), and aquaculture (Bertin et al., 2005), all of which affect the estuary's geometry. Estuaries are also subject to natural changes through sea level rise (Fitzgerald et al., 2000; van der Spek, 1997) and sediment infilling or sediment removal (Lessa and Masselink, 1995).

Tidal circulation is especially important in well-mixed estuaries, i.e. where salinity is well distributed in the water column, and where fluvial discharge is negligible. In this case, gravitational circulation is dominated by the tidal "pumping" at the seaward margin. In such systems, the dynamic coupling between topography and the tide-induced water circulation is important, defining both the direction and magnitude of sediment transport. It has been shown that estuarine hypsometry (Boon and Byrne, 1981), amount of tidal distortion, the volume of intertidal storage, and tidal range (Freidrichs and Aubrey, 1988; Lessa, 2000) are important parameters influencing the net-transport direction in well-mixed estuaries. Boon and Byrne (1981) also suggest that radical changes in the net-sediment transport direction (from flood- to ebb-directed) may occur as a consequence of basin evolution due to sediment infilling (see also, Dronkers, 1998;

Fitzgerald et al., 1976; Freidrichs and Aubrey, 1994; Lessa and Masselink, 1995). Additionally, the morphology of an estuary is influenced by interaction between the terrestrial, estuarine, and marine environment, which determines the sediment supply to the system (Castainge and Allen, 1981). In a situation where sediment supply is limited, an estuary may indeed have the potential to import or export sediment, but is morphologically stable due to little or no available sediment for transport.

Morphological changes in estuaries can increase, decrease, cease altogether, or even reverse as a result of both natural and human-induced changes in sedimentation. Elias et al. (2003) examined both bathymetric and hydrodynamic change in the Texel Inlet (Dutch Wadden Sea) spanning a period of 60 years to explain changes that followed construction of the 32 km long *Afsluitdijk* dam. After completion of the dam in 1932, rapid sedimentation occurred for a period of 45 years due to an apparent shift in the magnitude of the ebb tidal currents from one inlet channel to a second channel. Unconsolidated sediment from the ebb tidal delta maintained by the antecedent hydrodynamics was forced into the basin by the subsequently more dominant wave-driven transport. Thomas et al. (2002) combined an analysis of bathymetric data, analytical methods, and hydrodynamic simulations to develop a conceptual understanding of the morphological changes that occurred in the Mersey Estuary between 1871 and 1997. They concluded that the construction of channel training walls initially increased accretion rates within the estuary; however, the landward sediment flux eventually consumed the transportable material at the estuary mouth, thereby, reducing sedimentation rates internally achieving channel stability. Lessa and Masselink (1995) postulated a reversal of the dominant tidal currents in Louisa Creek, Australia.

Hydrodynamic measurements of Louisa Creek showed generally ebb-dominant tidal asymmetry and sediment transport. However, sediment cores from the intertidal flats showed large volumes of marine-derived sand, characteristic of flood-dominant transport. They concluded that during the evolution of the estuary, intertidal storage increased to such an extent that it induced a change from flood- to ebb-dominance. Finally, Oliveira et al., (2006) constructed a numerical model to investigate the effects of dredging on the hydrodynamics and flushing properties of the Obidos Lagoon in Portugal. They concluded that the deepening and repositioning of the inlet channel increased tidal prisms effectively reducing the flood-dominant asymmetry improving the stability of the inlet.

Estuarine research is typically based on a combination of fieldwork, laboratory experiments, and/or numerical modeling. None of these three investigative methods alone are suitable to provide valid representation of the complexity of an actual estuary. Owing to the inherent variability in estuarine environments, a large number of field observations must be made in order to appropriately characterize the hydrodynamics. The costs associated with data collection are usually quite high and therefore field-based studies are generally limited. A possible solution to a small quantity of field data is the application of a numerical model to interpolate and extrapolate measurements in both the temporal and spatial domains. Over the last decade, great progress has been made in the development and application of numerical modeling techniques to estuarine and coastal waters (Uncles, 2002). The use of hydrodynamic models to hindcast changes in estuaries that have occurred as a result of human intervention or to forecast future changes from sea level rise predicted by modern climate change models is now commonplace, particularly in the field of engineering (French and Clifford, 2000). Despite the obvious advantages

of a three-dimensional model (see Fernandes et al., 2005), a wide range of hydrological and geomorphological problems can be adequately studied and evaluated through the creative application of well-validated, two-dimensional modeling schemes, especially those involving the interaction of well-mixed, shallow water flows with complex terrain (French and Clifford, 2000).

2. Aims and Objectives

In this study, the human-induced hydrodynamic and morphodynamic changes in the Itajuru Channel, Brazil are examined. The channel is part of a previously much larger estuary that connected the hypersaline Lagoa de Araruama to the ocean (Lessa, 1990). Rapid infilling of the estuary with marine sediment in the form of a flood tidal delta has rendered a historically bustling harbour inoperable (Cunha, 2004; Lessa; 1990, Primo, 2002). Analysis of satellite images, historical maps, bathymetric charts, and anecdotal evidence indicate that reclamation of the intertidal area for salt ponds has produced profound morphodynamic changes in the estuary. These data provide a basis for examining the changes induced by human impact and the subsequent hydrodynamic and morphodynamic responses. Localized dredging in the Itajuru Channel has occurred in the past to maintain a safe channel depth for shipping and recreational traffic. More comprehensive dredging of the channel has been proposed to stabilize the channel sedimentation and improve pollution dispersion (Freitas, 2004; Ribeiro et al., 2002).

Using recent field measurements and bathymetric charts, a two-dimensional numerical model is used to characterize the present conditions in the Itajuru Channel and assess the impact of a major human-induced morphological change upon the estuarine hydraulics and suggest implications for the general pattern of sedimentation. The

fundamental objective of this paper is to describe the present hydrodynamics of the Itajuru Channel and compare them with a modelled scenario where the channel has been significantly altered. In addition, the implications of human induced change on the sedimentation patterns within the estuary in the past 500 years will be discussed. To achieve this, four specific aims will be pursued:

1. construct and calibrate a two-dimensional numerical model of the estuarine hydrodynamics to simulate the water surface elevation and current velocities using field measurements from two locations within the Itajuru Channel;
2. characterize the tidal duration asymmetry, current asymmetry, water flux and sediment transport direction within the Itajuru Channel through numerical simulation and include: i) the conditions present when the field data was collected, and ii) conditions that are typically present;
3. compare the present tidal asymmetries and sediment transport trends with those that are predicted by the model following a hypothetical scenario where dredging of the Itajuru Channel is conducted;
4. discuss the morphological change that has been well-documented in the historic record in the context of the modelling results and suggest directions for further study.

3. STUDY AREA

Variations in global sea level during the Quaternary, wave-dominated longshore progradation, and the trapping of local freshwater runoff have produced and shaped the series of isolated lagoons observed along the southern coast of the state of Rio de Janeiro, Brazil (Figure 1, Muehe and Correa, 1989). High wave energy, small tidal prisms, and low fluvial discharges produce the narrow inlets that impede the exchange of lagoon water with the ocean.

Lagoa de Araruama is the largest among a series of lagoons located along the Atlantic coast between Rio de Janeiro and Cabo Frio. Tidal currents dominate the sedimentation of the inlet and lagoon. The Itajuru Channel is an excellent example of a human-impacted estuary and provides the only connection between Lagoa de Araruama and the ocean. It is located approximately at latitude 22º10'S and longitude 42º00'W, adjacent to the city of Cabo Frio (Figure 2). Geologically, the lagoon lies between two distinct terranes: Pre-Cambrian rocks to the north and Holocene marine sand barriers to the south.

Lagoa de Araraúma is considered the largest hypersaline coastal lagoon in Brazil (220 km^2). Hydrologic and climatic characteristics prompted the development of a salt extraction industry that flourished in the late 19^{th} century. Today, this region is an important tourist destination and the waterway is used for recreation and local fisheries. Owing to the early economic and historical significance of the city of Cabo Frio, the anthropogenic and morphologic development of the estuary has been documented for five hundred years in the form of bathymetric charts and other historical documents.

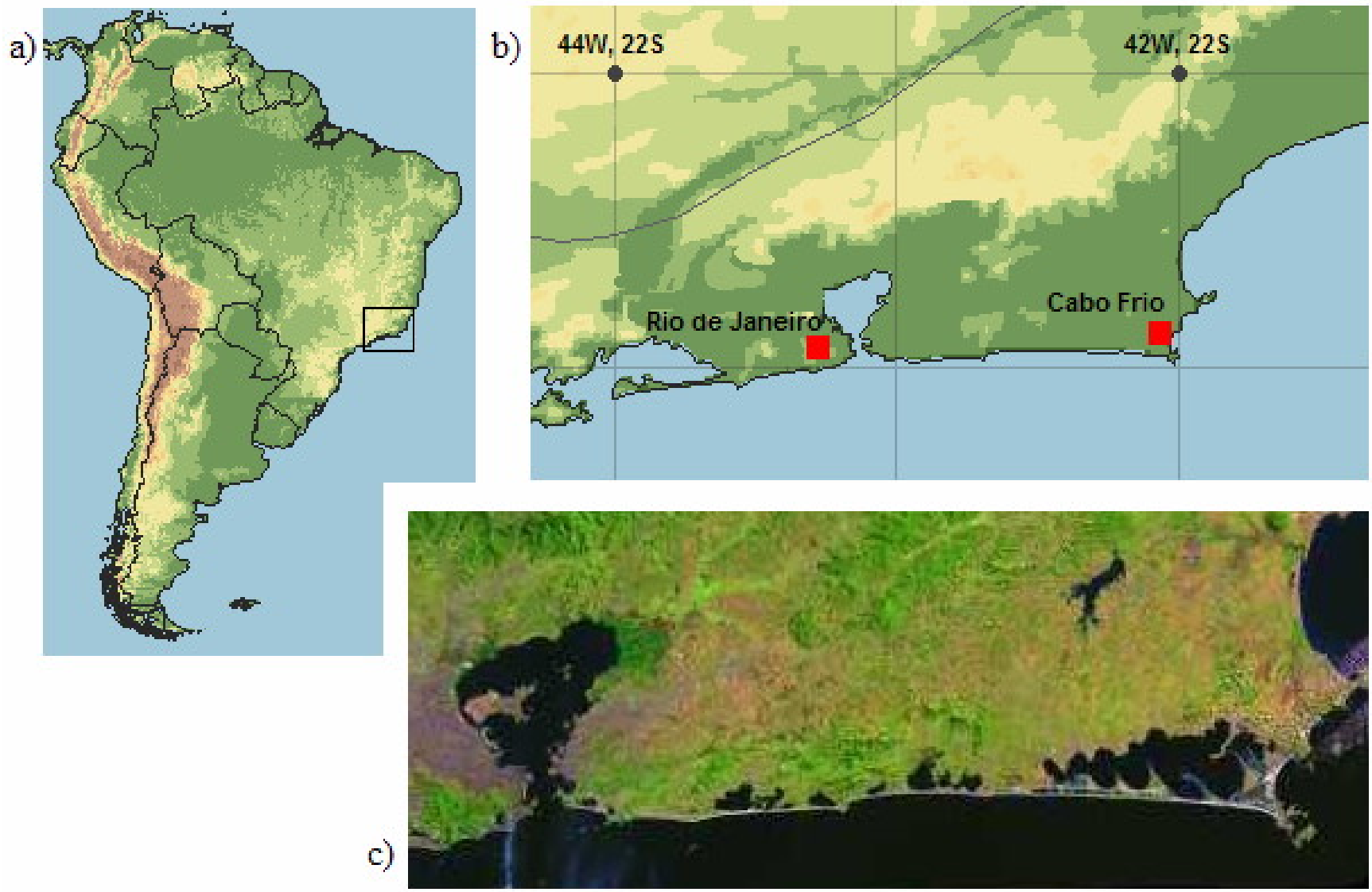

Figure 1 a) Map of South America with political boundaries. The State of Rio de Janeiro is highlighted with the rectangle. b) Location of Cabo Frio relative to Rio de Janeiro with longitude and latitude coordinates. c) Satellite image of series of isolated lagoons between Cabo Frio and Rio de Janeiro. Lagoa de Araruama is the largest, located in the lower right corner.

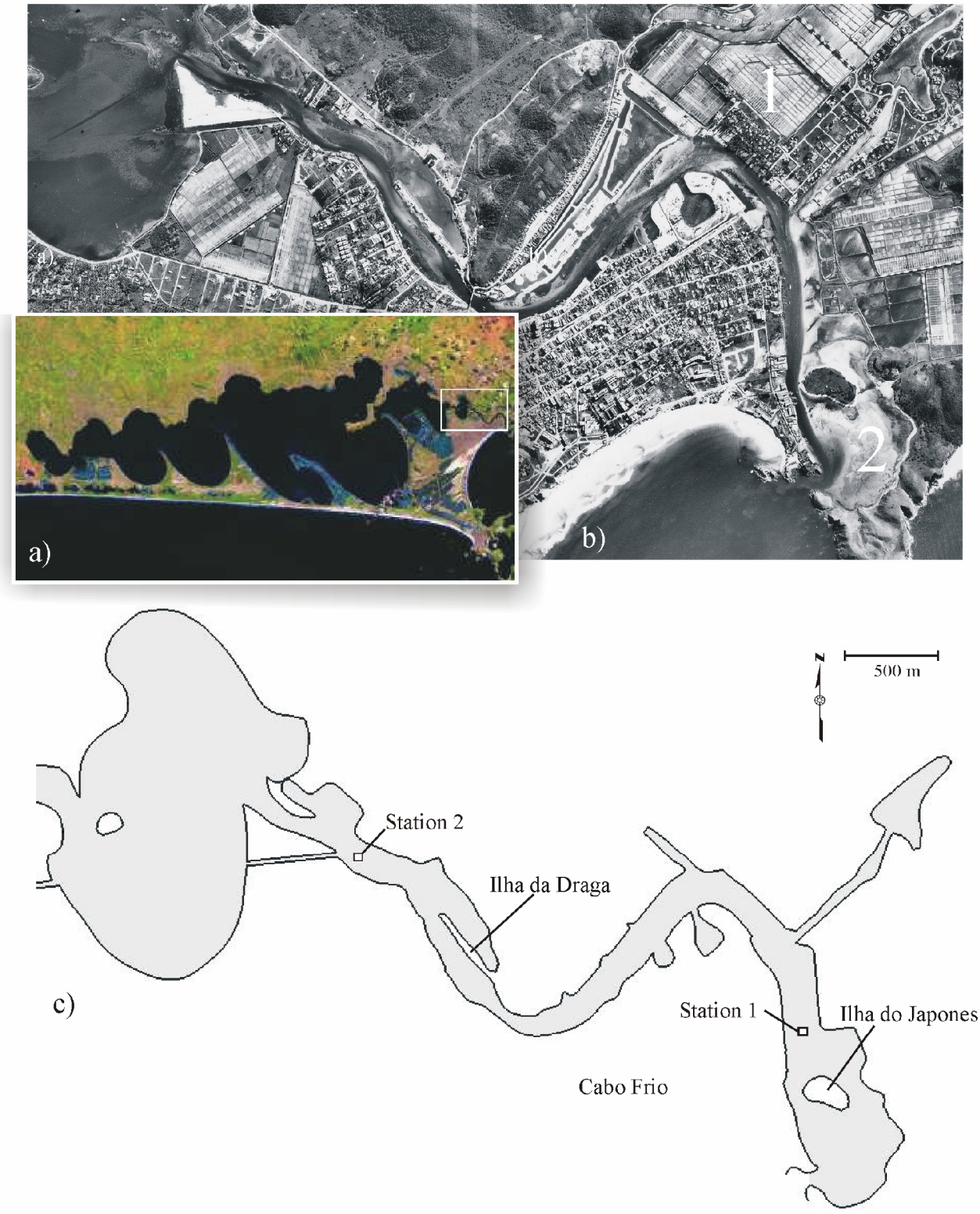

Figure 2 a) Satellite image of Lagoa de Araruama with the white box indicating the location of the Itajuru Channel. b) An air photograph of the Itajuru Channel where salt evaporation ponds (1) and sand shoals (2) are clearly visible. c) Map of the Itajuru Channel showing the two data stations where field data for model calibration were collected.

i) Environmental characteristics

Semi-arid conditions in this region have caused hypersalinity in Lagoa de Araruama; values up to 52 ppt have been recorded (Primo, 2002). Additionally, very high evaporation rates (1130 mm/year) offset precipitation (825 mm/year) to produce an average annual water balance which is negative (Kjerfve et al., 1996). Salinity measurements taken at stations along the Itajuru Channel show an increasing salinity toward the lagoon and a uniform salinity gradient in the vertical direction (Lessa, 1990).

Lagoa de Araruama has a very small watershed of ~350 km^2, and only two notable fresh water rivers; Rio das Mocas and Rio da Mataruna drain into it with a combined discharge of 2.3 m^3/s (Primo, 2002). River discharge varies seasonally in response to increased rainfall during the summer (November to January), and higher evaporation rates during the winter (July to September; Kjerfve, et al., 1996). The fresh water input is largely insignificant to the system hydrodynamics not only because of the negative water balance but also because it represents less than 1% of the 3.71×10^7 m^3 tidal prism (Lessa, 1990).

Lagoa de Araruama and the Itajuru Channel are bathymetrically complex, characterized by broad intertidal shoals and artificially walled, narrow channels. The Itajuru channel itself is ~8.3 km in length, with an average width of ~180 m, and an average depth of ~1.6 m. Depth distribution along the channel is highly variable, ranging from –7 m to +1 m (emergent during low tides). The geometry of the Itajuru channel is further complicated by the presence of Ilha do Japones, Ilha da Draga, and various salt evaporation ponds along its margins (Figure 2).

The channel mouth is at present ~82 m wide and ~4 m deep, bounded by two Pre-Cambrian rock formations oriented such that the inlet is protected from frontal wave attack from the Atlantic Ocean. Peak tidal currents limit sedimentation within the mouth; therefore, the cross sectional geometry in the absence of the human-induced changes can be assumed to remain constant over the short term (several centuries).

Sediment properties vary along the axis of the Itajuru Channel and Lagoa de Araruama. According to Lessa (1990), just inside the inlet, a large flood tidal delta is present, consisting of medium- to fine-grained sand (0.125-0.500 mm) of marine origin. Grain size becomes progressively finer inland with some sediments reaching very fine grained sand size (0.062 – 0.125 mm) at the confluence with the lagoon. Abundant carbonate shell deposits pave the lagoon bed and are periodically dredged for the production of calcium carbonate (Kjerfve et al., 1996).

The tidal pressure gradient is the principle factor causing the circulation of water in the Itajuru Channel (Lessa, 1990). The volume of water received through precipitation and runoff entering the lagoon is insufficient under normal climatic conditions to promote a constant water discharge toward the sea. The oceanic tides are mixed, with significant diurnal inequalities (Lessa, 1990, also see Figure 11). The M_2 and S_2 tidal constituents offshore of the channel mouth result in tidal ranges in the Itajuru Channel that vary from a maximum of ~1.20 m during spring tides to a minimum of ~0.30 m during neaps. Frictional effects progressively distort the propagating tidal wave along the channel, producing marked asymmetry in the tidal wave and tidal currents. Likewise, tidal amplitudes are progressively damped reducing to reach an average of only 0.02 m, 14 km from the ocean (Kjerfve et al. 1996). Of the many factors that affect tidal flow in the

channel, water depth is the most important factor controlling both magnitude, and arguably, the direction of the dominant tidal currents (Boon and Byrne, 1981).

ii) Historical Summary of Bathymetric Change

The first schematic map of the region was drawn in 1574 by the French explorer Jacques Vaulx de Clay. Of notable importance is the description of the tidal inlet, highlighted in Figure 3, which states (in French),

> "the basin is large enough to shelter five, 150 tonne ships".

Vaulx de Clay's description suggests that the dimensions of the basin must have been sufficient to accommodate the ships of that era. Ship building diagrams from the 16th century indicate that such a ship would typically have a draft of approximately 4 meters (Figure 4). Additionally, the official document of the birth of the City of Cabo Frio in 1615 contains descriptions of the harbour as (in Portuguese);

> "having an ample capacity that could accommodate ships of up to 200 tonnes and navigation into the lagoon is possible" (Cunha, 2004).

In 1615, a fortress built by the early Portuguese explorers was dismantled; according to Cunha (2004), the rubble from the fortress was deposited in the mouth of the inlet to impede unauthorized access to the harbour by pirates. Auguste de Saint Hilare described the inlet mouth in 1797 as clogged, no deeper than 2.5 m (Cunha, 2004) and it was subsequently illustrated in 1862 by M. A. Vital de Oliveira (Figure 5).

The semi-arid climate and hypersalinity of Lagoa de Araruama prompted a salt extraction industry in Cabo Frio that flourished in the 19th century. Construction of large commercial salt ponds began in 1824 and continued into the early 20th century. Today,

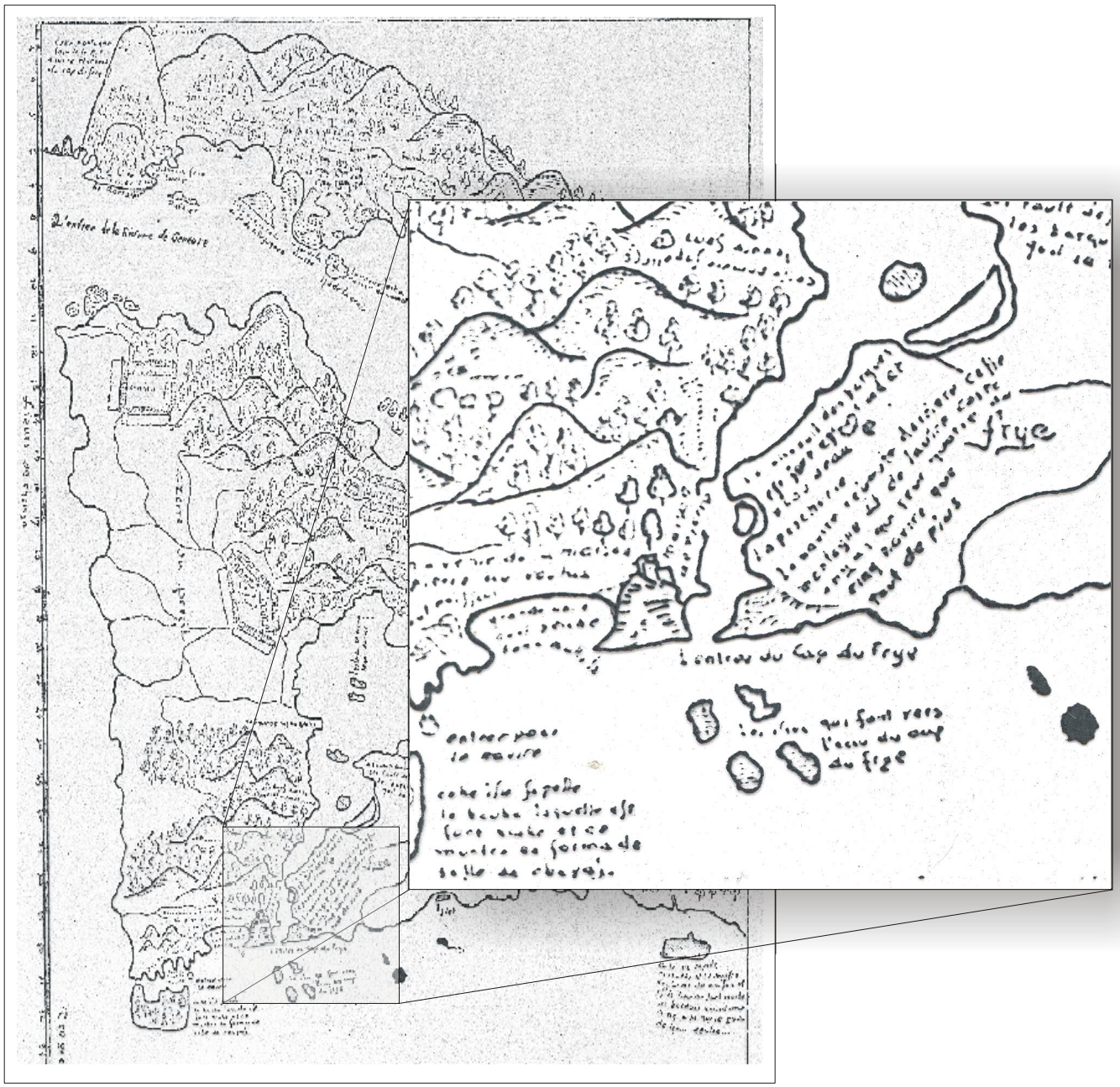

Figure 3 The first map of the region was drawn in 1574 by the French explorer Jacques Vaulx de Clay. A description of the tidal inlet is magnified.

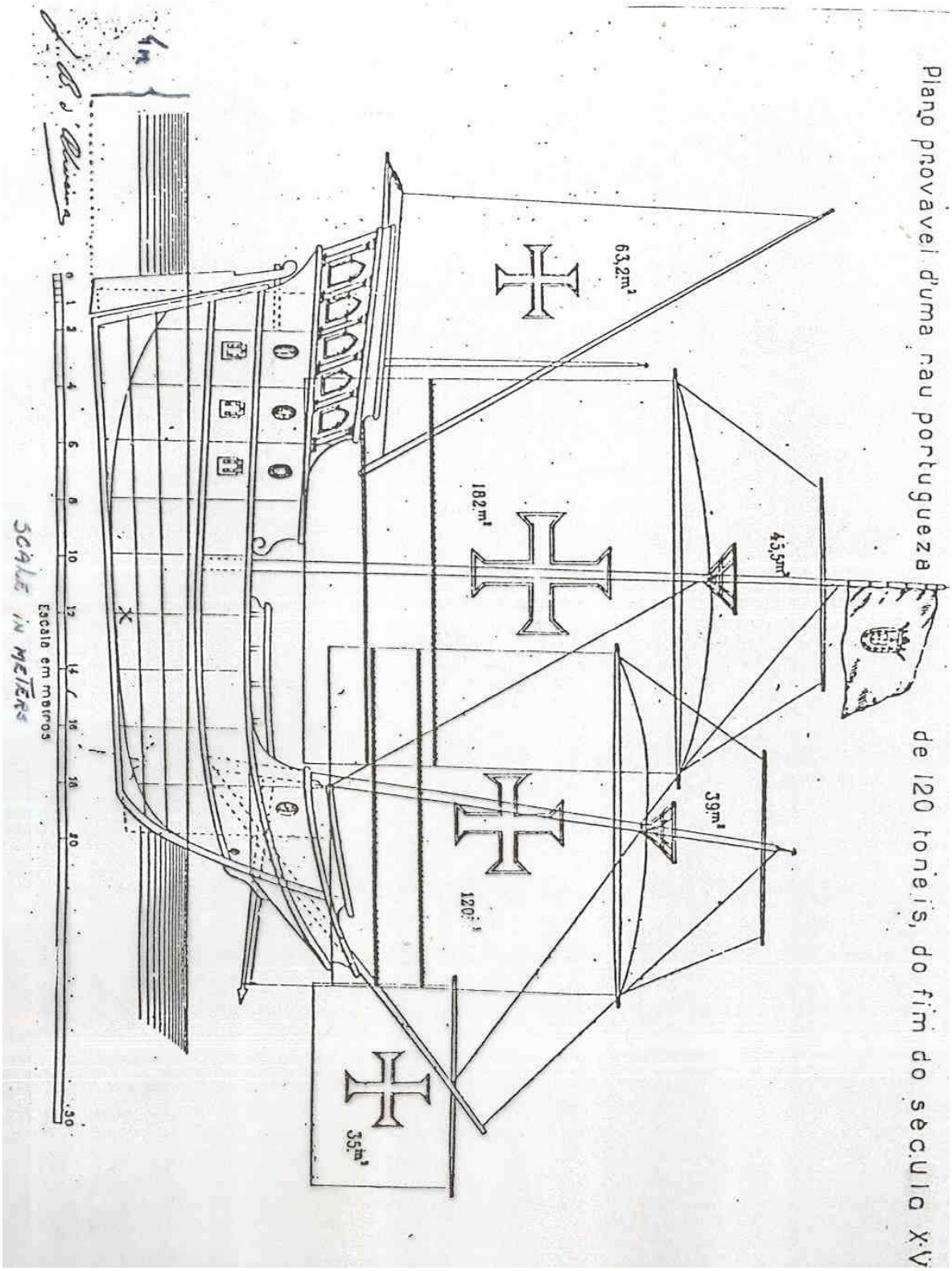

Figure 4 Diagram of typical fifteenth century Portuguese ship of 120 tonnes. The scale on the bottom is shown in meters and the draft is indicated as 4 m (Lessa, 1990).

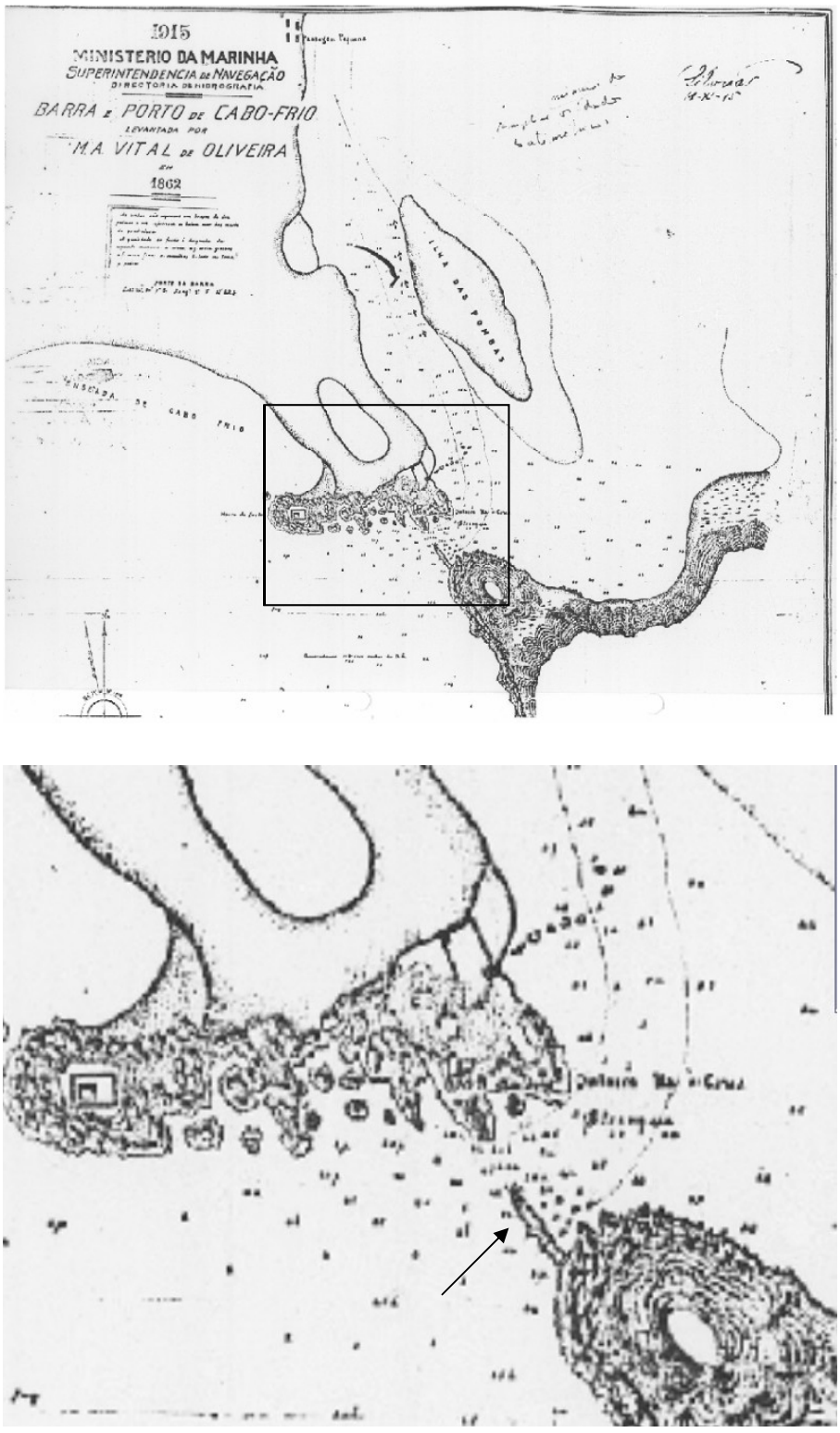

Figure 5 Chart drawn in 1862 indicating the constructed wall at the mouth of the Itajuru Channel. This effectively reduced the cross sectional area and depth of the mouth.

salt ponds occupy ~65 km^2 or 49% of the intertidal area of the Itajuru Channel and Lagoa de Araruama (Kjerfve et al., 1996).

The first chart to depict shoals in the harbour was published in 1788 by Luiz de Vasconcellos (Figure 6). Anecdotal concern over the shallowing harbour, however, did not follow until almost fifty years later. Orders sent from the governors of the Rio de Janeiro captaincy in 1836 instructed local officials to excavate the sand bars to improve the maneuvering capability of the 10-15 cargo ships arriving and departing from the harbour daily (Cunha, 2004). Unfortunately, for reasons that are unclear, the orders were never fully carried out. In 1862, an anonymous reference claimed that the average depth of the harbour was 0.9 m and that export goods needed to be transferred from smaller to larger boats along the channel (Cunha, 2004). Finally, in 1875 and 1880, two harbour improvement projects were started in order to build a shipping canal, remove debris obstructing the mouth (recognized by some to be causing the shoals), and excavate sand from the harbour.

The Itajuru Channel clearly has experienced numerous human-induced changes since its discovery by the Portuguese in 1587. In addition to the colonial documents presented here, land reclamation and salt production infrastructure has progressively reduced the area of the channel by 51%. The main conclusion to be drawn from historical documents is that sedimentation of the channel has been occurring since the 16^{th} century, possibly as a consequence of the anthropogenic stresses. Additionally, since no terrestrial sediment sources are evident, tidal processes have been primarily responsible for the sedimentation that has been documented.

Figure 6 The first indication of shoal formation the Itajuru Channel was documented in the chart published by Luiz de Vasconcellos (1788) is shown.

4. THEORETICAL MODELS OF ESTUARINE CIRCULATION – LITERATURE REVIEW

As astronomic tides propagate into estuaries, nonlinear processes generate higher frequency harmonics (Walters and Werner, 1991) that, as they grow, cause the tidal wave to become increasingly asymmetrical (Aldridge, 1997; Freidrichs and Aubrey, 1988). Although tides often have rising and falling limbs with similar durations, the deformation in shallow water usually leads to differences in these durations. When the tide rises faster than it falls, current velocities tend to be higher on the flood than on the ebb because of continuity (Fortunato and Oliveira, 2005).

i) Tidal asymmetry

Tidal asymmetry has important effects upon morphological change and hence human use, such as the navigability of estuaries. Understanding the processes that cause tidal asymmetry in specific cases is an important step towards deciphering the sedimentation history and evolution of estuaries and tidal inlets. Numerical modelling of fluid motion in tidal inlets and estuarine channels (Boon and Byrne, 1981; Mota-Oliviera, 1970; Speer and Aubrey, 1985) along with inlet field studies (Freidrichs and Aubrey, 1988; Lessa, 2000; Lessa and Masselink, 1996; Lincoln and Fitzgerald, 1988) have shown that the interaction of channel friction and basin geometry are primary sources of tidal distortion within inlet-lagoon systems.

The difference in duration between the rising and the falling limbs of the tide may be indicative of the tidal dominance, i.e. whether an estuary is flood dominant (maximum current velocities during the flood stage of the tide) or ebb dominant (maximum current velocities during the ebb stage of the tide). In shallow estuaries, the depth distribution within the basin strongly influences the frictional resistance to the tidal wave propagation

and the shape of the tidal curve. This produces differences in ebb or flood duration. Several mechanisms interact to varying degrees to determine both the magnitude and the direction of the tidal asymmetry. Friction at the bed can slow down the propagation of the tidal troughs relative to the propagation of the crests, resulting in a longer ebb duration relative to flood (Speer & Aubrey, 1985). Boon and Byrne (1981) demonstrated that tidal asymmetry can develop as a consequence of the basin hypsometry (the distribution of basin surface area with height). Estuary cross-sections with large intertidal areas relative to the whole tend to be ebb dominant because of the greater roughness and thus frictional resistance of the large expanses of salt marshes and mangrove forests. During high water stages, the flow is conveyed through the hydraulically inefficient intertidal area; however, during low water the flow is conveyed through hydraulically efficient channels resulting in a shorter duration for the ebb and greater magnitude flow velocities (Dronkers, 1986; Friedrichs and Aubrey, 1988). Several studies have provided a theoretical foundation for velocity patterns through the analysis of water level records and basin hypsometry, and these studies highlight the importance of tidal asymmetries to the transport and accumulation of sediments in tidal systems (Aubrey and Speer, 1985; Boon and Byrne, 1981; Dronkers, 1986; Friedrichs and Aubrey, 1988; Lessa 1996; Lessa, 2000; Oliveira et al., 2006; Ranasinghe and Pattiaratchi, 2000; Wang et al., 1995).

ii) Flood dominance

Shallow channels are inefficient at exchanging water at low tide, resulting in a time lag between low tide in the ocean and in the estuary. This inefficiency also means that the tide in the ocean can be rising at the final stages of the falling tide in the estuary. By the time the water starts to flow into the estuary, the tide on the open coast is rising,

and a steep pressure gradient is created, inducing fast flows which peak at approximately mid-tide. As the estuarine area varies almost linearly with the rising tide in the estuary, all of the water which rushes into the estuary forces rapid change in elevation of the water level. Since changes in water level occur faster at high water, when frictional resistance is minimized, tidal lag at points along the estuary is small. During the initial stages of the falling tide, the deeper channel provides efficient water exchange, and the falling tide in the estuary follows the pace of the ocean tide. Relatively gentle water surface gradients are then developed. The hydraulic gradient increases as the water depth decreases and the tide level in the estuary starts to lag behind the ocean tide. Friction is enhanced, however, resulting in flow retardation, and peak velocities are smaller than those during the flood tide.

iii) Ebb dominance

Estuaries with deeper channels and broad intertidal areas are more efficient in exchanging water at low tide, and usually low water in the estuary coincides with low water in the ocean. Because there is a broad intertidal area to be flooded, the water flowing gradually into the estuary cannot induce a quick rise in the water level, and the rising tide in the estuary lags behind the rising tide in the ocean. Although this causes a steepening of the surface gradient, cross sectional areas are wide enough to absorb the increased discharge, and stronger currents do not result. High water in the basin lags behind high water in the ocean, meaning that the ocean level is already falling before the falling tide in the estuary is initiated. The falling tide in the estuary tends to occur at the same time at various locations, but because the channels are deeper than the intertidal areas, the flow velocities are faster and the water level drops more quickly. This causes a

flow into the channel, slowing the rate of the falling tide in the channel adjacent to intertidal areas. A more abrupt surface gradient then develops, and coincides with the time when the cross-sectional area is confined only to the channel. Stronger ebb currents are then observed.

iv) *Asymmetry induced sediment transport*

There are two well-known lags between the sediment response and flow which are used to explain the transport of suspended matter: the scour lag is due to the difference between the current velocity which is required to erode the sediment and the velocity which is sufficient to maintain it in the suspension; the settling lag is measured by the time when the dynamics can no longer maintain the sediment in suspension and the time when the sediment reaches the bed (Stanev et al., 2004). The settling lag will bring a particle further up an intertidal area due to its inertia in the fluid on the flooding tide. When currents reverse, a large part of the ebb tide will have passed over the particle before the water reaches the required velocity for entrainment. In general, a sediment particle will come to rest at a site further landward than from which it was entrained. However, in an environment where there are asymmetrical current magnitudes over a flood/ebb cycle, large quantities of sediment can be transported in one direction if the flow in a single direction exceeds the threshold of entrainment and in the other direction it does not. Additionally, weakly ebb dominated estuaries may not have sediment transported in the ebb direction due to the effects of scour and settling lag.

The magnitude of the tidal asymmetry does not have to be large in order to translate directly into a net landward or seaward sediment transport (Masselink and Hughes, 2003) assuming that sediment is coarse enough that settling and scour lag effects

are small. The sequential evolution of estuaries is often characterized by a positive feedback between the sedimentation and the flow hydraulics (Freidrichs et al., 1992). For example, increasing the proportion of intertidal area changes the way the tidal wave propagates, which can cause a change in the net sediment transport direction (Boon and Byrne, 1981). This feeds back to the evolution of the estuary, changing the pattern of erosion or deposition within the basin (Lessa and Masselink, 1996).

v) *Estuarine basin evolution*

a) Numerical Modelling

Using a numerical model of an idealized estuary, Mota-Oliveira (1970) observed that ebb-dominant transport was the result of a situation where the basin area varied significantly with different stages of the tide. These conditions would be expected as an estuary fills with sediment and thus Byrne and Boon (1976) hypothesized that a reversal in the direction of sediment transport can occur as shoaling becomes advanced. Boon and Byrne (1981) provided further insight into tidal hydraulics using a numerical model and showed that the formation of shoals and tidal flats, in a previously open channel, could be responsible for a modification of the tidal wave asymmetry and a shift from flood to ebb dominance. Speer & Aubrey (1985) supported this hypothesis, evaluating the sensitivity of an inlet/bay system to the size of the flats and channel cross-sectional geometry.

Direct insight into the effects of sedimentation upon tidal hydrodynamics was provided by Boon and Byrne (1981), who modified the hypsometric formula of Strahler (1952) to represent evolutionary profiles of an estuarine basin. These profiles were used in numerical calculations of tide levels to determine duration asymmetry. Figure 7 shows

four different hypsometric curves for Swash Bay, Virginia for four different degrees of basin infilling, progressing from an open basin with nearly vertical banks ($\gamma = 5.0$, γ = dimensionless parameter used to quantify the volume of sediment in a basin) to a nearly infilled basin ($\gamma = 1.8$, Boon and Byrne, 1981). In a hypsometric curve one compares the dimensionless horizontal inundation, a / A, (A maximum basin area, a = the basin area above minimum elevation contour at height h) to the dimensionless vertical inundation, h / H, (h = height above minimum basin elevation, H = maximum height) over a tidal cycle. If a/A increases faster than h / H, a large basin area is flooded with only a small rise of the tide level. Conversely, faster rates of change in h / H means that the tide level is rising without a significant change of the inundated area. In Figure 7, four data points representing the present hypsometry of Swash Bay are included, as well as the relative elevation for high and low water. The shaded area indicates the relative tidal prism for each of the basin configuration; the tidal prism diminishes, and shaded area becomes smaller, as the basin infills.

The range of horizontal inundation in Figure 7 increases as the bay is infilled, due to formation of intertidal areas. For instance, the wet area in an open embayment ($\gamma = 5.0$) changes only 10% while in an infilled estuary ($\gamma = 1.8$) it varies four-fold. In an open bay environment ($\gamma = 5.0$)), since there is little variation in wet bay area during the rising or falling tide, the water level varies swiftly. However, with the addition of a large intertidal area ($\gamma = 1.8$), a swifter change in the water level occurs at the beginning of the flooding tide ($a/A \approx 0.9$ and $h/H \approx 0.78$), when the water flows along a defined channel. As the tide rises, the water gradually floods wide intertidal areas and a relatively fast change in the horizontal inundation rates slow down the vertical inundation rate.

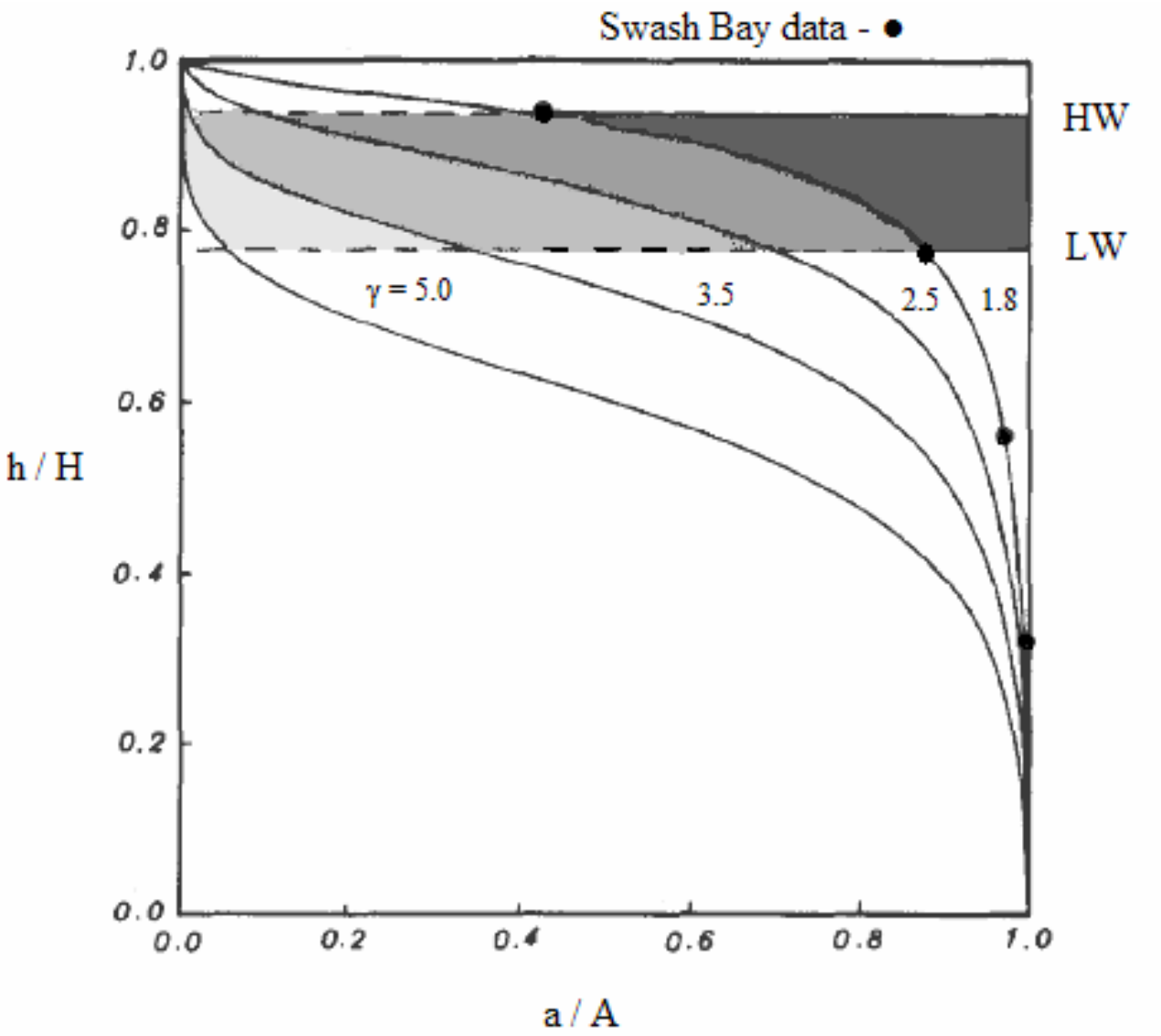

Figure 7 Four different hypsometric curves for Swash Bay, Virginia, representing different basin evolutionary stages, progressing from an open basin with nearly vertical banks ($\gamma = 5.0$) to a nearly infilled basin with large tidal flats ($\gamma = 1.8$). Data points representing the present hypsometry of Swash Bay are included on the $\gamma = 1.8$ curve. The shaded areas, bounded by the high (HW) and low water (LW), indicate the relative tidal prism for each of the basin profiles; the tidal prism diminishes and the shaded area becomes smaller as the basin infills. Note: h = height above minimum basin elevation, H = maximum height, γ = dimensionless parameter used to quantify the volume of sediment in a basin (area under the hypsometric curve) , A maximum basin area, a = the basin area above minimum elevation contour at height h.

Figure 8 shows the effect of varying the dimensionless inlet cross sectional area with respect to the tidal attenuation inside the estuary and the difference in time between the rising and falling tide, for different degrees of basin infilling. The duration difference is indicated by ΔD, with negative values indicating shorter rising tides (flood dominance) and positive values indicating shorter falling tides (ebb dominance). The dimensionless cross sectional area is given by the ratio of the channel cross sectional area A_C to the maximum bay area A_{bmax}.

It is noticed that as the basin fills in (γ from 5 to 1.8), the duration difference changes from $\Delta D < 0$ (shorter flood flow) to $\Delta D > 0$ (shorter ebb flow) (Figure 8). In addition, the attenuation of the tidal wave within the estuary decreases as demonstrated by the larger values for R_{bay} / R_{sea} (R_{bay} = tidal range inside estuary, R_{sea} = tidal range in ocean). The effect of varying the cross sectional area is visible along the x axis. Decreasing the cross sectional area increases the flow impedance and reduces the tidal range within the basin (i.e. water will not inundate as far). This results in a reduction of the effect of varying basin hypsometry and promotes shorter flows. Since the same amount of water passes in either direction during a tidal cycle, shorter flows will have to be faster and thus more competent. In summary, Boon and Byrne (1981) suggest that, given unrestricted flow conditions, a flood dominant open basin will change into an ebb dominant salt-marsh estuary as the sedimentation evolves and its hypsometry changes.

Friedrichs and Aubrey (1988) investigated the relationship between estuarine geometry and the asymmetry of tides in 26 tide-dominated estuaries along the US East Coast, and compared measured tidal elevations with the results of numerical modelling. A simple one-dimensional numerical model, developed by Speer and Aubrey (1985), was

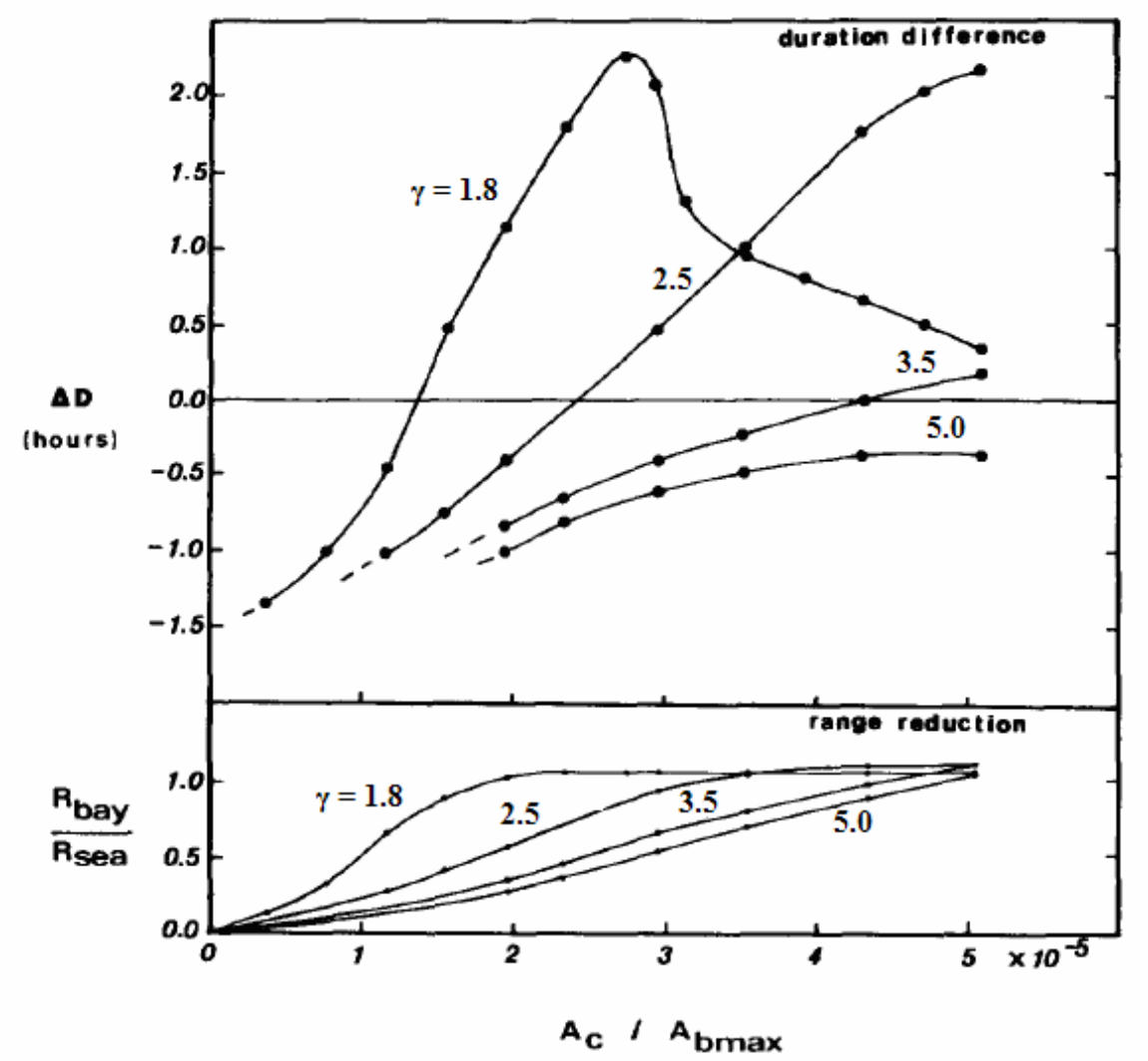

Figure 8 Results of the numerical simulations performed by Boon and Byrne (1981). Tidal duration differences (ΔD) representative of flood dominant tidal asymmetry (negative values) and ebb dominant tidal asymmetry (positive values) and range ratios between basin and sea tides are given as a function of the dimensionless cross-sectional area of the estuary's channel for four hypsometric basin profiles. Note: A_c = channel cross-sectional area, A_{bmax} = maximum bay area, R_{bay} = tidal range inside estuary, R_{sea} = tidal range in ocean.

used to establish preliminary quantitative relationships between tidal forcing, system geometry and tidal distortion (Friedrichs and Aubrey, 1988). Their results indicate that flood and ebb dominance in shallow estuaries is controlled by the relative tidal amplitude in the estuary, a_t / h_{cd} (a_t = tidal amplitude, h_{cd} = average channel depth), and the relative intertidal storage, V_s/V_c (V_s = volume of intertidal storage, V_c = volume of the channel at mean sea level). A plot of these two parameters was used to predict if an estuary is flood or ebb dominant.

Flood dominance occurs where the tidal amplitude is large relative to the channel depth, whereas ebb dominance takes place when the relative intertidal storage is large. They pointed out, however, that the relative tidal amplitude alone may be sufficient to dictate overall tidal asymmetry, with deep estuaries ($a_t / h_{cd} < 0.3$) being ebb-dominant and shallow estuaries ($a_t / h_{cd} > 0.3$) being flood dominant. Friedrichs and Aubrey (1988) further suggested that the effect of tidal distortion on bed-load sediment transport is to make shallow systems shallower and deep systems deeper, and that a hydrodynamic evolution from flood to ebb-dominant systems may be only possible for very weakly flood-dominant systems. For the latter, the transition from flood to ebb dominance would require that infilling does not decrease channel depth but only raises the intertidal area.

Friedrichs et al. (1992) examined the specific feedback mechanisms between morphology and the hydrodynamic processes. Estuaries with shallow basins and narrow intertidal flats tend to be flood dominant, whereas those with deep basins and wide intertidal flats tend to be ebb dominant. In both cases, the dominant current will reinforce the morphology. Flood dominance will enhance landward sediment deposition and basin

infilling, whereas ebb dominance enhances seaward sediment transport and sediment scouring.

b) Field Studies

Relatively few studies have attempted to examine the stratigraphic evidence for the morphodynamic interactions that occur in estuarine evolution. Lessa and Masselink (1995) studied Louisa Creek, Australia, which is a mature estuary with large intertidal areas. The direction of sediment transport in this estuary changes from flood dominant during neap and intermediate tides to ebb dominant during spring tides. On an annual basis the estuary was shown to be ebb dominant through both hydrologic analysis and the presence of an ebb delta outside of the inlet. However, the stratigraphic model of the basin derived from sediment core data indicates that a significant portion of the infilled sediment volume is marine sand, deposited under conditions of flood dominance. Lessa and Masselink (1995) proposed that a hydrodynamic change must have occurred during the evolution of Louisa Creek resulting from an increase in intertidal water storage capacity as a consequence of the intertidal accretion over several centuries and lateral growth of mangrove forests.

vi) Summary

The concept of positive feedback between morphology and hydrodynamics, as presented by Freidrichs and Aubrey (1988) and Freidrichs et al., (1992), refutes the hypothesis of Boon and Byrne (1981) that during the evolution of a basin the character of the tidal asymmetry and sediment transport direction will change from flood to ebb dominant. Freidrichs and Aubrey (1988) assumed that the hydrodynamic characteristics of a system are inherited from the antecedent topography and do not alter during basin

evolution. The results derived by Boon and Byrne (1981) reflect the assumptions made in their representation of the basin evolutionary profiles. Essentially, Boon and Byrne (1981) allowed for the aggradation of the intertidal area while maintaining a constant channel bed elevation (or the channel remains relatively deep and hydraulically efficient), whereas Friedrichs et al. (1992) assume channel and intertidal accretion will occur simultaneously. The applicability of either theoretical model to a particular estuary will depend on the morphological characteristics of the channel bed (i.e. type and size of sediment). However, the geologic evidence presented by Lessa and Masselink (1995) shows that a change from flood to ebb dominance occurred in Louisa Creek during its evolution, and therefore supports the results of Boon and Byrne (1981). The model of Friedrichs et al. (1992), however, appears more universally applicable since it describes the evolution of the entire estuary rather than just the intertidal area.

5. THE NUMERICAL MODEL – RMA2 (RESEARCH MANAGEMENT ASSOCIATES)

Numerical models are mathematical representations of complex systems, such as estuaries, which can simulate the hydrodynamics through 1, 2 or 3-dimensional approaches. Any model must be able to resolve conditions that would be found typically in the environment being simulated. For example, in the case of estuaries, an appropriate representation of intertidal emergence and submergence and the ability to handle a variety of boundary conditions must be accounted for in the model construction. Finite-element schemes, based upon a mesh that can be formed over irregular terrain features, are a logical choice for this kind of problem (French and Clifford, 2000). For well-mixed

estuaries, such as the Itajuru Channel (Lessa, 1990), a two-dimensional depth-averaged hydraulic/hydrodynamic model is adequate.

A number of commercially available, two-dimensional, finite-element models are available to represent the complex hydrodynamic behaviour found in estuaries. RMA2 (Research Management Associates, Version 4.35) developed by Norton, King, and Orlob (1973) and King (1990) with more recent refinements undertaken by the United States Army Corps of Engineers, Waterways Experiment Station (WES) Hydraulic Laboratory, uses the Reynolds form of the Navier-Stokes equations to compute water surface elevations and horizontal depth-averaged velocities for unsteady, subcritical, free-surface flow. It is designed to be applied to unstratified water bodies where vertical accelerations are negligible and velocity vectors generally point in the same direction over the entire depth of the water column. RMA2 can simulate wetting and drying and therefore is suited to computing the hydrodynamics in tidal flats and wetlands.

The selection of this model was based primarily on the availability of an interactive graphical user interface that augments the model with a pre- and post-processing environment. The Surface-water Modeling System (SMS - Version 8.1), developed at the Environmental Modeling Research Laboratory at Brigham-Young University includes a variety of interfaces and tools specifically designed to assist the user in integrating the required data into a stable finite element mesh (King et al., 2005). Additionally, the interface has several tools that can be applied to visualize the model output, edit the finite-element mesh, and calibrate the model with field data.

An interactive user interface is a necessary requirement for the application of RMA2 in complex estuarine environments. The manipulation of bathymetric data and the

design of a computational mesh that is stable and representative of reality accounts for a significant portion of the overall modeling effort (King et al., 2005, Burau and Cheng, 1989) and should not be taking lightly (Cheng et al., 1993). Without some level of automation for mesh generation and mesh quality assessment, the task of creating a computational mesh that produces a valid and meaningful output would be significantly more difficult, if not impossible, to achieve.

French and Clifford (2000) applied the RMA2 hydrodynamic model to the Blyth Estuary in Suffolk, England. Their results indicated that, once the computational and methodological challenges were overcome, it was relatively straightforward to achieve an acceptable degree of fit between modeled and observed tidal water surface elevation curves within the estuary. Current velocities were not as well represented in detail, although a good representation of the peak velocities was obtained within the areas of interest (French and Clifford, 2000). They concluded that the model performed satisfactorily at the estuary scale but computational issues arising from areas of wetting and drying reduce the accuracy of quantitative results at higher resolutions. For example, bathymetric accuracy is particularly important for modelling applications; however, this data must be edited to remove depressions that pool water at low tide to achieve model stability. Therefore, this change can impact the model predictions at that location, making them less accurate at high resolutions.

6. Model of the Itajuru Channel

The prerequisites for constructing a hydrodynamic model of the Itajuru Channel using the RMA2 modelling scheme include: (i) a detailed bathymetric representation of the estuary (ii) data characterizing the boundary conditions, such as the magnitudes of the

discharge of freshwater (either as a mean flow or temporally variable) and time series of tidal water surface elevation; (iii) estimates of the input and losses of water over the lagoon surface area due to rainfall and evaporation; (iv) the spatial distribution of the various bed sediments necessary to estimate values for the bed roughness, flow turbulence, and eddy viscosity; and (v) calibration data consisting of both water surface elevation and horizontal flow velocity. The quality of each of these items is critical to the ultimate performance of the model.

i) Bathymetric Data

Obtaining a reasonable bathymetric representation of the Itajuru Channel was achieved through both field surveys and the manual digitization of bathymetric charts (chart codes: 028/85, 029/85, 030/85) obtained from the Companhia Brasileira de Dragagem (1985). Scanned digital images of the bathymetric charts at a scale of 1:2000 were imported and mutually referenced using Environmental Systems Research Institute (ESRI) ArcView Version 3.2. The channel boundary and the 9200 bathymetric survey points were then digitized manually using the scanned images as a reference. Gaps in the bathymetric data were surveyed directly with an electronic level and staff. Where bathymetric data could not be obtained or surveyed, estimates were made based on regional contour maps at larger scales or interpolated from the measured values (Figure 9).

ii) Boundary conditions

The data necessary to characterize the boundary conditions and water budget were obtained primarily from the literature. Regional hydrologic data for Lagoa de Arauama are available in Lessa (1990), Kjerfve et al. (1996), and Primo (2002). A net loss of water occurs in the lagoon because the magnitude of evaporation exceeds the inputs from runoff, rainfall,

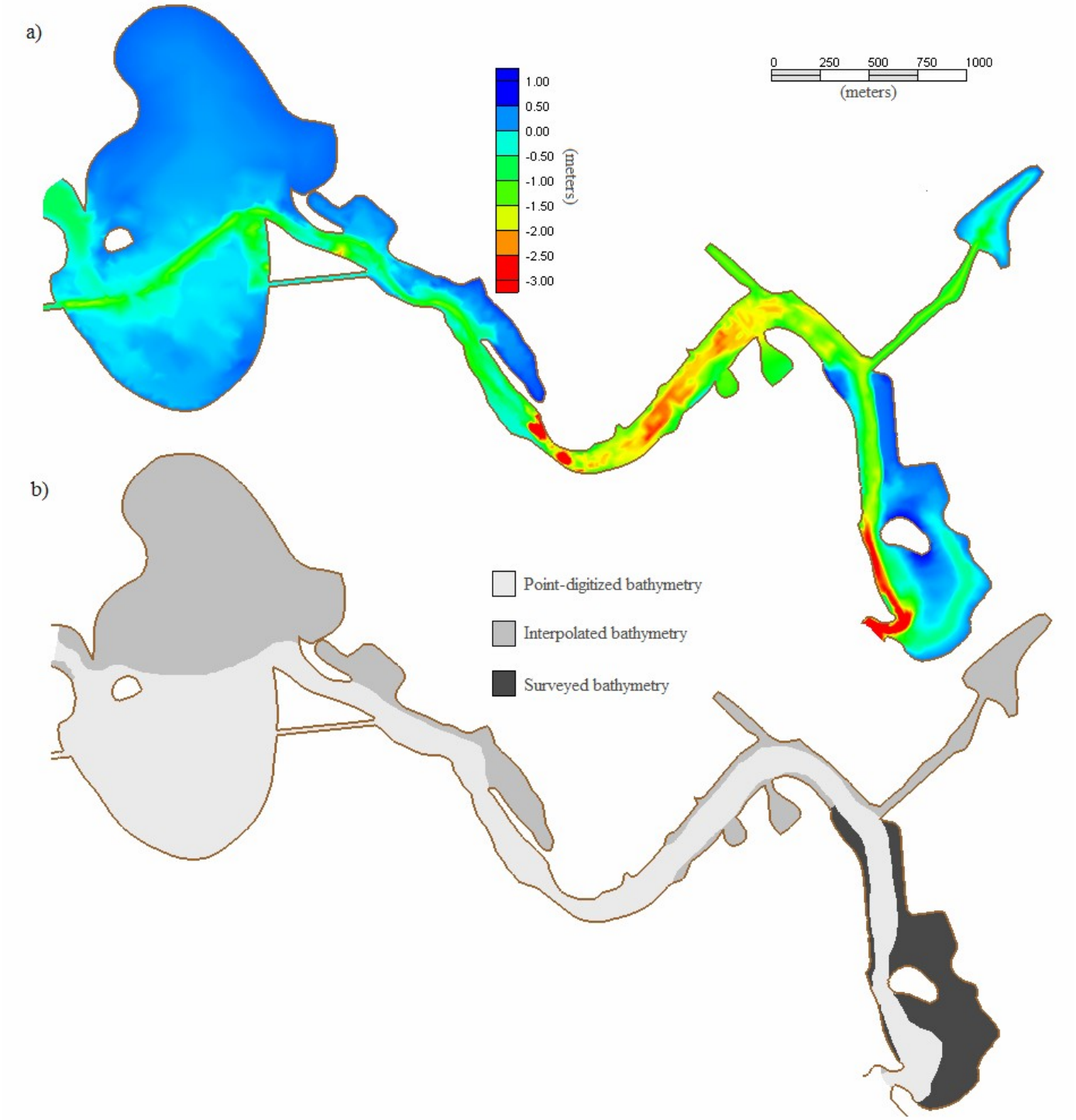

Figure 9 a) The bathymetric representation of the Itajuru Channel used in the RMA2 model was based on published bathymetric charts, field surveys, and interpolated values as indicated in b). The bathymetry shown is referenced to mean low low water.

and groundwater (Kjerfve et al., 1996). Only an annual mean value for the net loss of water through evaporation was applied to the final model configuration. A hindcast of the ocean tides for the period of time when the calibration data were collected was obtained through a computational algorithm for harmonic analyses and prediction (Franco, 1988) using the principal harmonic constituents at the ocean boundary. The principal tidal constituents are shown in Table 1 and the input tidal curve is shown in Figure 10.

iii) Roughness Distribution

The roughness of the actual bed is a function of grain size, bedforms, and vegetation. Unfortunately, no data is available on the characteristics of the bedforms or the type of vegetation that may be present in the Itajuru Channel. However, during the field campaign little vegetation was noted within the channel and along its margins. Any effects caused by vegetation or bedforms on bed roughness was neglected in the model construction. The surface sediment grain size distribution presented by Lessa (1990; Figure 11a) provided spatial guidance for the distribution of Manning's *n* roughness that was eventually applied to the model (Figure 11b). The RMA2 user manual (King, 2005) and the U.S. Geological Survey report (Arcement and Schneider, 1989) provide a range of roughness values (*n*) for various grain sizes, sediment types, and environmental circumstances. Large values (0.033-0.045) were applied for highly constricted channels or rough surfaces, such as the rocky inlet mouth; mid-range values (0.024-0.029) in the intertidal areas; and low values (0.020-0.022) for straight unrestricted channel sections with coarse or fine sandy beds. Values within these recommended ranges were used initially to represent the bed roughness. Small adjustments, within the recommended

Table 1 - Principal harmonic constituents of Porto de Arraial do Cabo (42.0W, 22.1S; Ribeiro et al., 2002).

Description	Tidal Constituent	Period x 10^4 (s)	Amplitude (m)	Phase (rad)
Principal lunar	M2	4.47	0.33	1.37
Principal solar	S2	4.32	0.17	1.54
Principal lunar diurnal	O1	9.29	0.10	1.52
Lunar/solar diurnal	K1	8.62	0.05	2.57
Lunar/solar semidiurnal	K2	4.31	0.05	1.55
Larger lunar elliptic	N2	4.56	0.04	1.61
Larger lunar eliptic	Q1	9.67	0.03	1.31
Smaller solar elliptic	L2	4.39	0.02	1.61
Principal solar diurnal	P1	8.66	0.02	2.49
Smaller lunar elliptic	M1	8.94	0.01	0.80
Larger solar elliptic	T2	4.33	0.01	1.53
Small lunar elliptic	J1	8.32	0.01	2.16

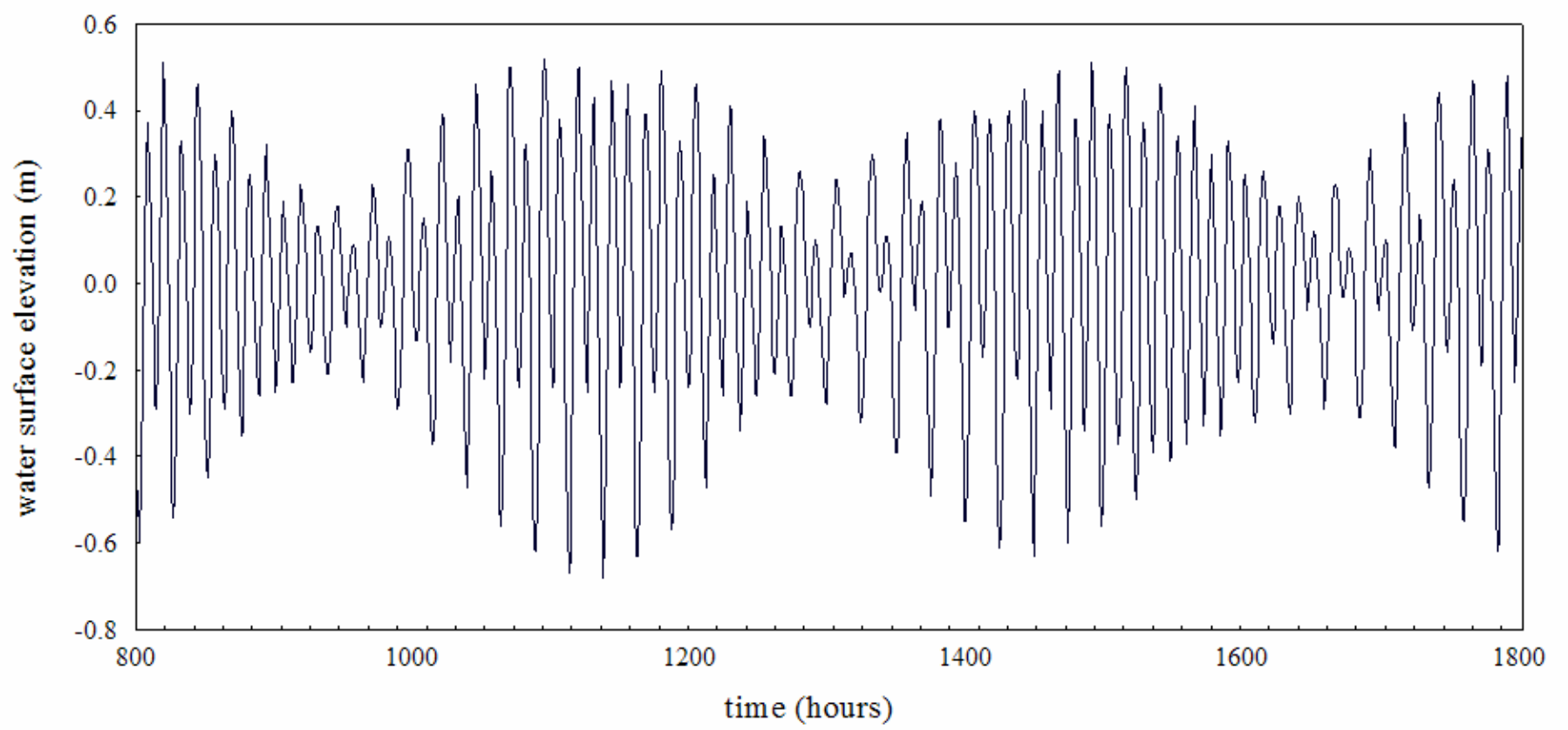

Figure 10 Tidal forcing curve generated using the principal harmonic constants shown in Table 1. This curve is used as the input for the RMA2 model and is the primary forcing mechanism.

ranges, to roughness and eddy viscosity were made both during the initial stabilization of the model and the calibration with field data. The Manning's *n* values applied for the different material types and eddy viscosities are listed in Table 2.

Table 2 Final values of dimensionless Manning's *n* and eddy viscosity applied to the model material types determined though calibration.

Material type	**Manning's n**	**Eddy Viscosity** (Pascal-sec)
concrete	0.033	2600
channel sand	0.020	2500
coarse sand	0.022	2500
rock	0.045	2500
fine sand (intertidal)	0.029	2500
beach sand	0.024	3000
island sand	0.026	2700
ocean floor	0.028	2500
silt/mud	0.025	2500

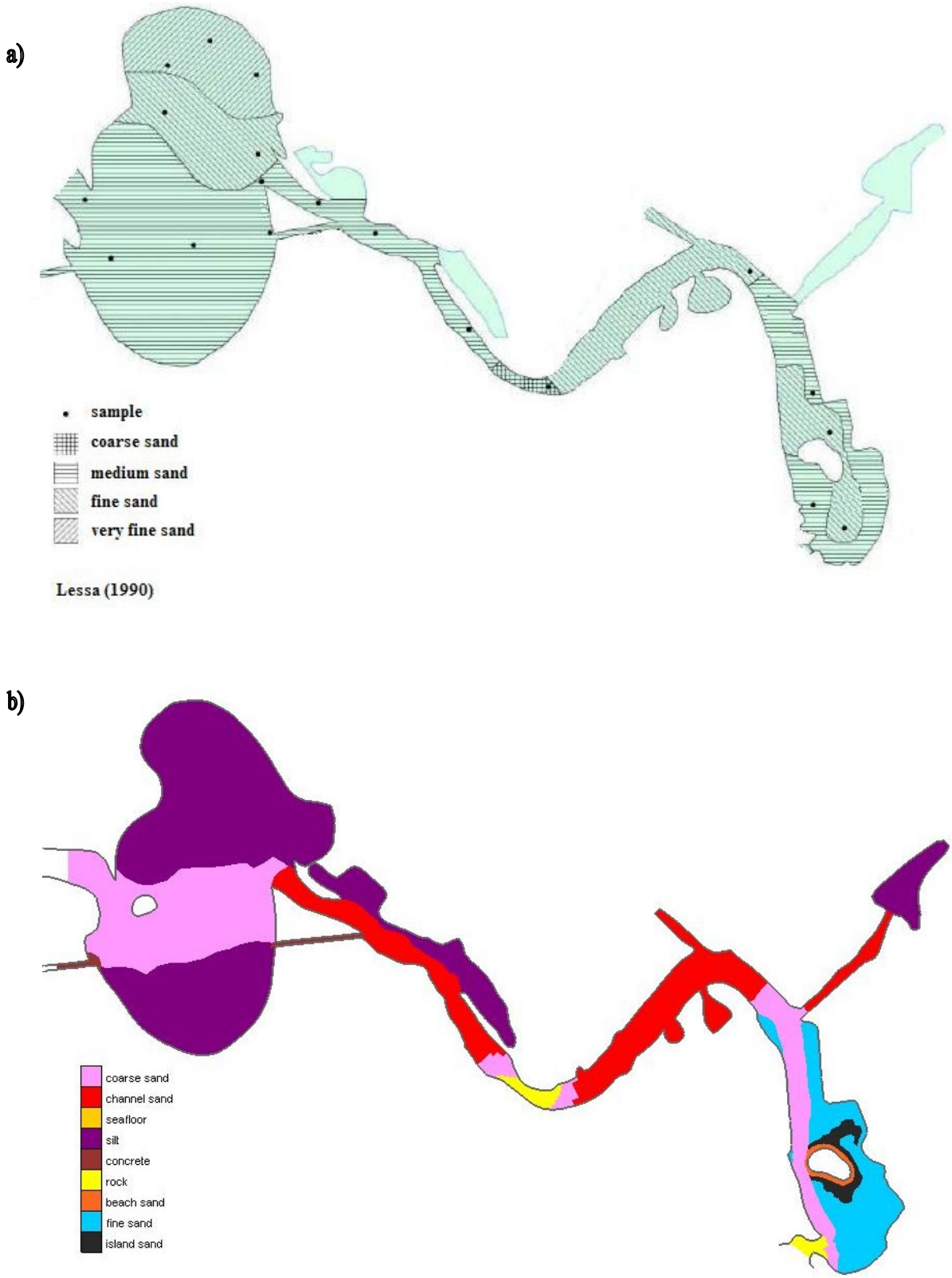

Figure 11 a) The sediment distribution in the Itajuru Channel (Lessa, 1990) and b) sediment roughness distribution applied in the RMA2 model. See table 1 for specific values of Manning's *n.*

7. THE FINITE ELEMENT MESH

The final mesh was produced from several polygons delimiting distinct terrains, including: the ocean, inlet mouth, sub-tidal channel, concrete walled canals, intertidal sand, intertidal mud, and lagoon. The mesh generating algorithms within SMS allowed the creation of both triangular and quadrilateral elements within each polygon. The final mesh contained a total of 6037 elements of which 65% were triangular and 35% quadrilateral (Figure 12). In general, channel sections were represented with quadrilateral elements, whereas intertidal areas were represented with triangular elements. In the intertidal regions the structure of the mesh was manually aligned along bathymetric contours to minimize instabilities arising from wetting and drying.

i) Calibration data

Lessa (1990) collected instantaneous water depth and flow velocity data from four stations: two along the Itajuru Channel and two inside Lagoa de Araruama . Data from the two stations located in the main channel (Station 1 and Station 2, Figure 2) were used for model calibration. Calibration data for the additional data stations within the Lagoa de Araruama were omitted due to extremely poor agreement during calibration. In general, predicted water surface elevations and current velocities were significantly less than the field measurements. Several attempts were made to modify the model parameters to perform better within the lagoon but will need further investigation beyond the scope of this paper.

Each station was equipped with a Savonius Rotor current meter oriented into the flow within the channel thalweg. Measurements were taken simultaneously at all stations at 30-minute intervals over two 25-hour periods, one during a spring tidal cycle and the

a)

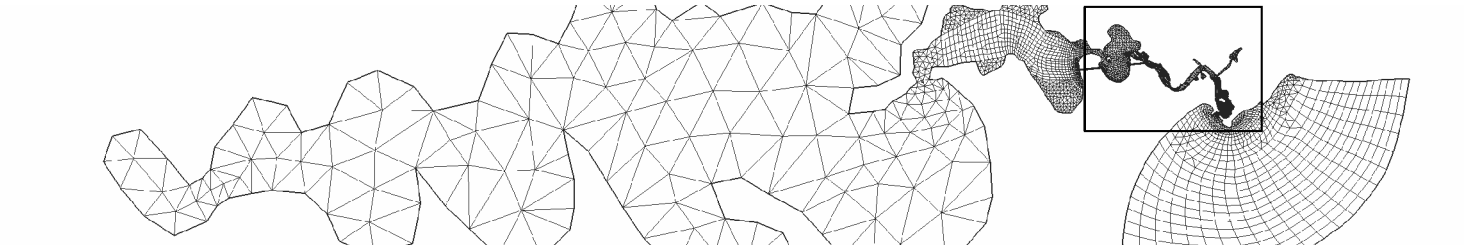

b)

Figure 12 a) Finite element mesh of Lagoa de Araruama and b) the Itajuru Channel.

other during a neap cycle. Flow velocity measurements were obtained by lowering the current meter through the water column at 1-m intervals and recording the mean flow at each elevation over 30-second intervals. The current velocity used to calibrate the numerical model was the mean current velocity integrated over the water column. At the same time, the water level variation was obtained with a graduated staff. Water surface elevation measurements from each of the stations were referenced to the computed mean sea level.

8. Model Implementation and Stability

The successful application of a numerical model depends heavily on the accuracy of the model bathymetry and proper specification of the boundary conditions (Cheng et al., 1993). Bathymetric change is expected to occur from the hydrologic interaction of the fluid and the channel bed but is not represented in the model. The bathymetry at the start of the simulation is assumed to be the same as the bathymetry at the end. It is unclear to what extent this assumption effects the validity of the model. Additionally, RMA2 does not support the formation of pools of trapped water. Shallow topographic depressions become disconnected from the active mesh as a consequence of the drying of adjacent elements. These “pools” cause instabilities in the solution that often will prevent solution convergence and editing of the bathymetric data is required. Thus, alteration of the bathymetry to accommodate this limitation is necessary to achieve model stability but effectively reduces the accuracy of the representative bathymetry and the model results.

Lagoa de Araruama experiences strong north-easterly winds year-round which have an average speed of 5·2 m/s and are the primary forcing mechanism of the lagoon hydrodynamics and produce setup, wind-driven currents, and low-frequency lagoon

water level fluctuations (Kjerfve et al., 1996). The effects of wind are clearly important in tidal circulation and residual circulation of the lagoon and channel. Unfortunately, these properties have been neglected in the present investigation due to a lack of sufficient data.

Two open boundary conditions for the model were implemented at opposite sides of the mesh consisting of the hindcast tidal level curve at the ocean boundary and a constant freshwater discharge into the lagoon. Given the relatively insignificant volume of freshwater discharge, this effectively has limited influence on the model results. Of potentially greater importance, is the representation of rainfall and evaporation from the lagoon and the Itajuru Channel. Using annual averages for evaporation and rainfall, an annual average water deficit of 0.012 mm/hour was adopted for the lagoon and channel system. This value was calculated using the water budget data available in Kjerfve et al. (1996). In the absence of more detailed climatic data from the period modeled, this rate of evaporation from the lagoon only serves to approximate the influences of rainfall and evaporation. The lateral shoreline boundary conditions are satisfied automatically within the model parameters as a closed or “no flow” condition.

Measurements of the variations in fluid density in the channel are documented in Lessa (1999), and Kjerfve et al. (1996). These measurements were used to estimate an average fluid density to be applied in the model. Fluid density progressively increases from the ocean to the lagoon primarily due to a gradual increase in salinity from the ocean to the lagoon. Lessa (1990) measured fluid density at four stations along the channel ranging from minimum values of 1024 kg/m^3 to maximum values of 1031 kg/m^3. The mean value of 1027 kg/m^3 was applied to the calibrated model and thus does not

account for variations that are present. Although differences in fluid densities are potentially significant, the shallowness of the inlet restrains flow stratification.

The RMA2 model has two distinct methods for handling intertidal wetting and drying: element elimination and marsh porosity. Both methods were tested but the element elimination technique was found to be simpler to employ. Elements were set to turn off when one node achieved a depth less than 0.01 m and reactivate when all nodes had a depth of 0.076 m.

Numerical methods used in RMA2 solve the equations for fluid flow employing a Newton-Raphson iteration procedure. Iterative solution methods require a computational convergence criterion that is used to determine when the iterations can be terminated and computations at the subsequent time step initiated. A poorly chosen convergence criteria can lead to either poor results (when too large) or long computational times (when too small). Several convergence criteria values were utilized at different stages of the model development and a value of 0.01 was found to achieve adequate balance between reasonable results and computational time.

The RMA2 model allows the user to select an appropriate time step for the problem being investigated. Here, a time step of 0.5 hours was used to correspond to the interval between subsequent field observations used in the calibration procedure.

The initial solution (cold start) of the model requires all elements in the mesh to be completely inundated. The initial water level was therefore set above the highest nodal point (1.1 m) in the computational mesh. The model was then left to stabilize over a period of 1450 simulated hours (approximately 120 tidal cycles). Subsequent runs of the

model would start from this initial solution. Experimental runs were 600-750 simulated hours to produce output at both spring and neap tides.

9. Model Calibration

The calibration of a numerical model is typically accomplished by a comparison of field data for flow velocity and water surface elevation with the spatially and temporally equivalent values predicted by the model. A numerical model is considered validated when the model output fits the field data. However, this fit is rarely perfect; this is the nature of modelling. Although a variety of statistical methods can be used to analyze the relationship between model results and field data to measure model performance, nevertheless, calibration often involves some degree of subjective judgment (Cheng et al., 1993).

Several historical documents describe that sedimentation near the mouth of the channel has been occurring over at least three centuries (Cunha, 2004; Lessa, 1990; Primo, 2000). The field data used to calibrate the model however, indicates that the maximum ebb current velocities are greater than the flood currents; and thus, the infilling of the channel should not be occurring under these conditions (Lessa, 1990). Higher than average rainfall, prior to the field campaign, increased the level of the lagoon by ~0.10 m for the period of calibration data collection. Therefore, a constant discharge of water through the channel from the lagoon was occurring. Calibration of the model using these data had to account for this higher than normal level of the lagoon. This was achieved by monitoring the water surface elevation of the lagoon during the initial 700 simulated hours until it had reached 0.10 m above the calculated mean sea level and then extracting sufficient data to analyze it with the field data.

Model calibration for the Itajuru Channel was achieved through an iterative process involving numerous simulation runs, comparison of model output with field data, applying appropriate mesh modifications where necessary, and adjusting the values for the Manning's roughness coefficient (*n*) and eddy viscosities. The results of the final calibrated configuration for spring and neap tidal cycles are shown in Figure 13 and Figure 14, respectively. Time series cross correlations were performed to validate the model output. In all cases, the curves were found to be in phase (zero lag) and have correlation coefficients above the 95% confidence band. Figure 15 shows the correlation output for the current velocity at Station 1. Correlation coefficients for all other data sets are listed in Table 3. Additionally, the field data were plotted with the model output to evaluate the variation between the predicted and actual values. The predicted values were then plotted against the field data and a least squares linear regression used to determine the R^2 values for the resulting fit. These values are shown in Table 4. Agreement between the model output and field data was excellent during the spring tides, but only satisfactory during neap tides.

Although the model reproduction of the field data was considered reasonable, several limitations in both the model and in the field data sets may explain why a better agreement could not be achieved: (i) the effect of wind forcing was not simulated in the model, and (ii) the tidal input water surface elevation curve was generated by a hindcast, incorporating the tidal constituents and ignoring any possible anomalies due to meteorological effects; thus, the actual tidal curve may have been slightly different when the field data was obtained than the one applied in the simulation.

Further refinement of the model parameters may achieve a closer agreement between the available field data and model output, particularly during neap tides; however, due to the paucity of field data for calibration, without additional data collection, any effort to achieve greater agreement would be of limited value. Based on the results of the calibration simulation, the numerical model for the Itajuru Channel is considered validated for tidal time scale processes.

a)

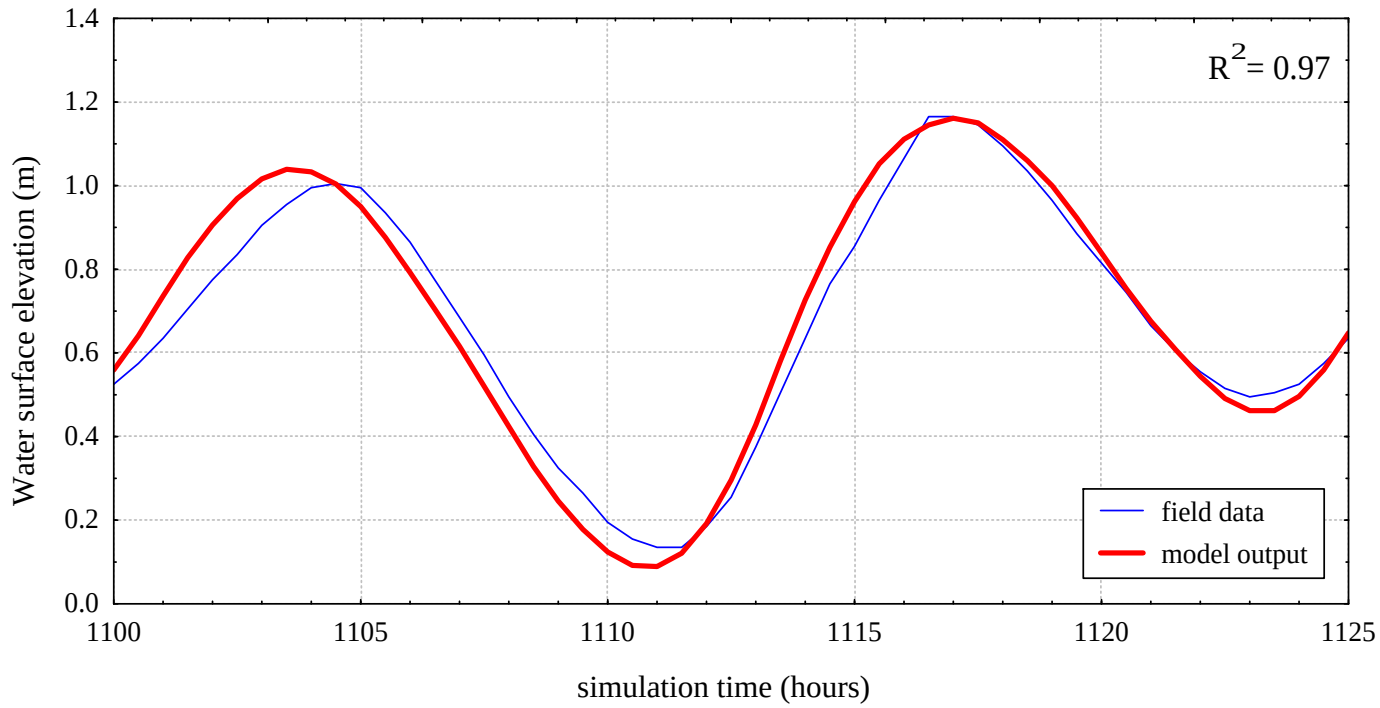
Station 1 - Water Surface Elevation (Spring Tide)
R2= 0.97
Water surface elevation (m)
1.4
1.2
1.0
0.8
0.6
0.4
0.2
0.0
1100
1105
1110
1115
1120
1125
simulation time (hours)
field data
model output

b)

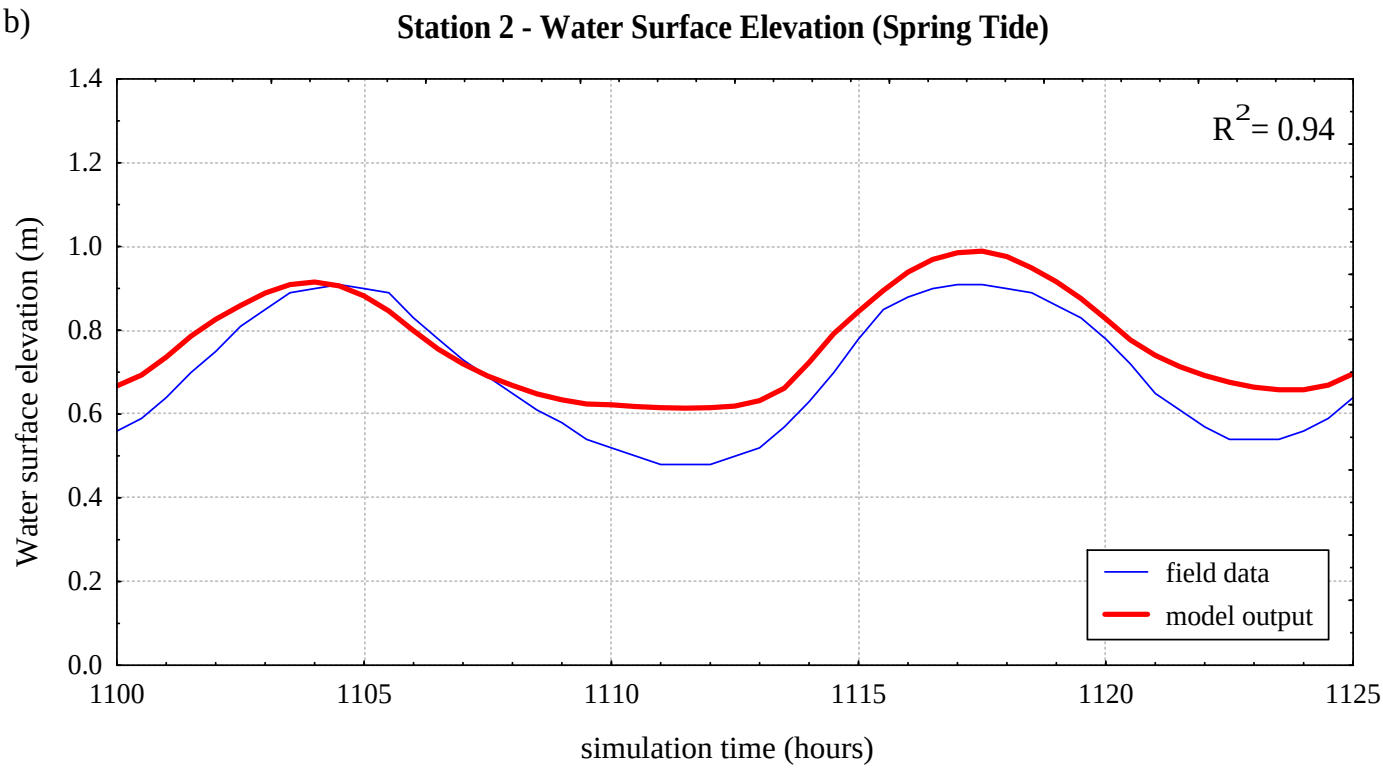
Station 2 - Water Surface Elevation (Spring Tide)
R2= 0.94
Water surface elevation (m)
1.4
1.2
1.0
0.8
0.6
0.4
0.2
0.0
1100
1105
1110
1115
1120
1125
simulation time (hours)
field data
model output

c)

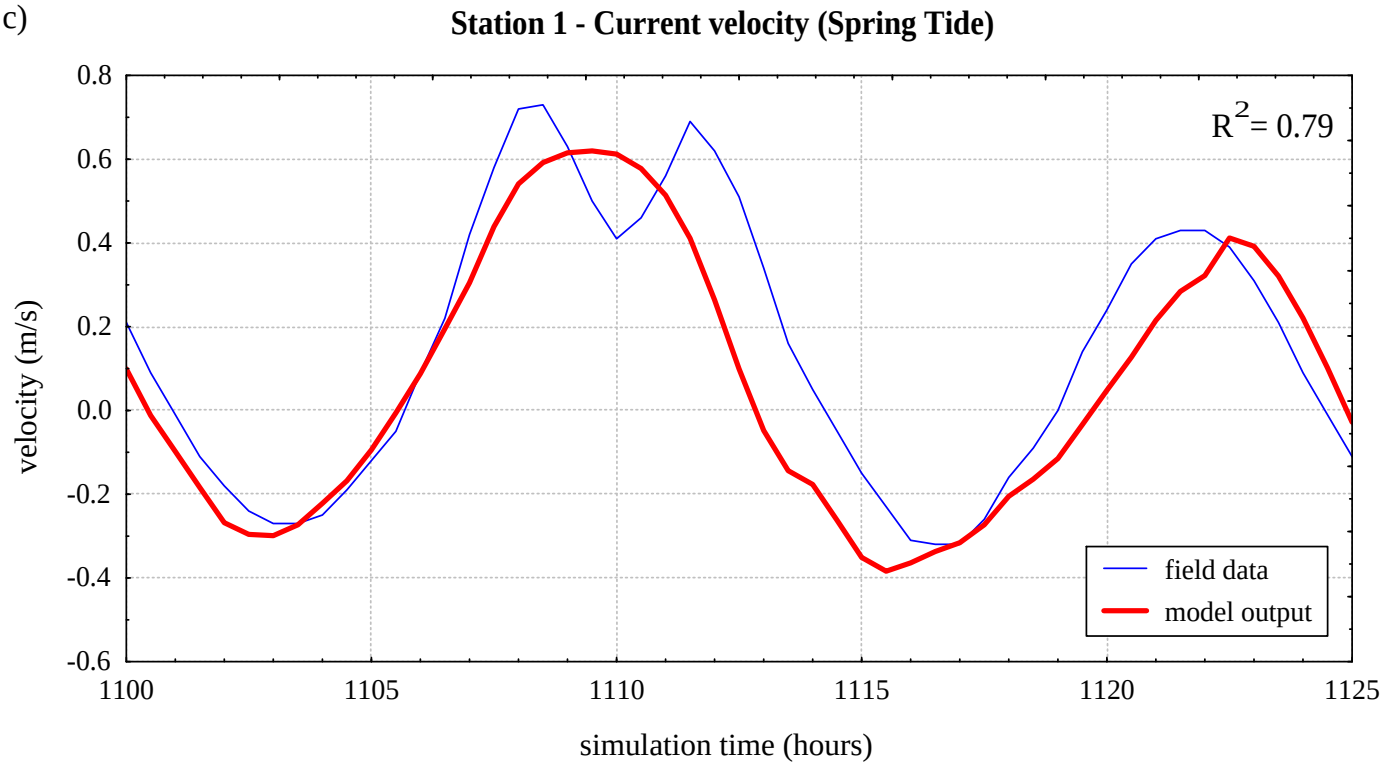

d)

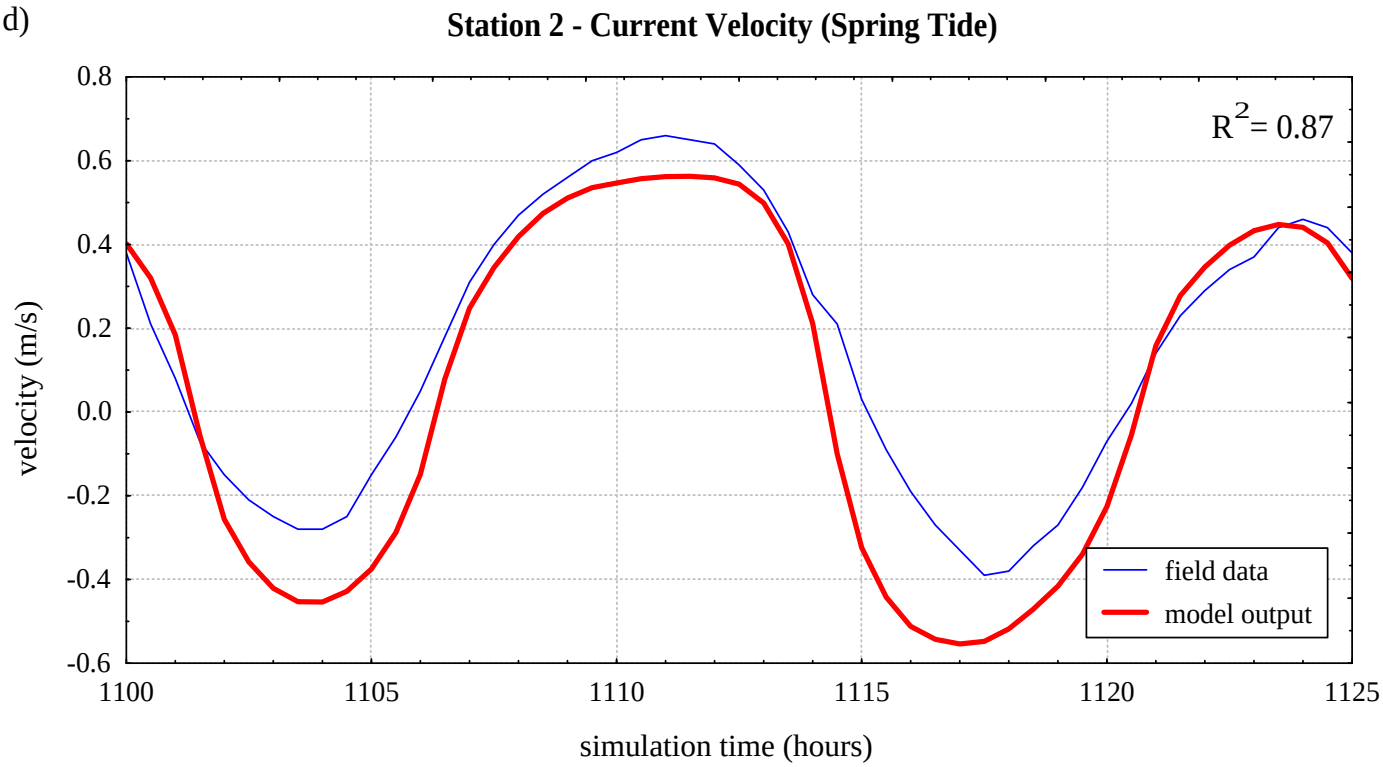

Figure 13 – Graphs showing the model output plotted with the calibration field data during spring tide for the water surface elevation and current velocity at field stations 1 (a, c) and 2 (b, d).

a)

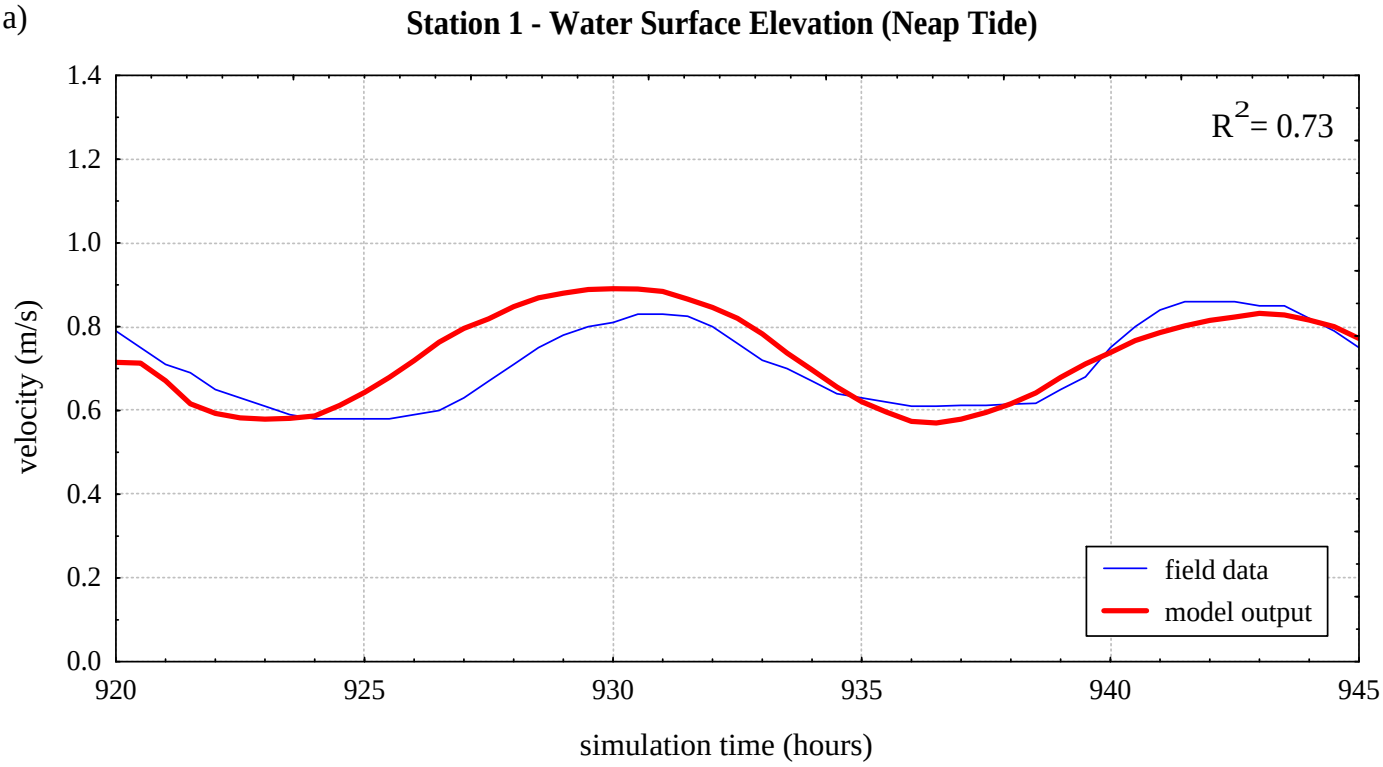
Station 1 - Water Surface Elevation (Neap Tide)
R2= 0.73
velocity (m/s)
simulation time (hours)
field data
model output
1.4
1.2
1.0
0.8
0.6
0.4
0.2
0.0
920
925
930
935
940
945

b)

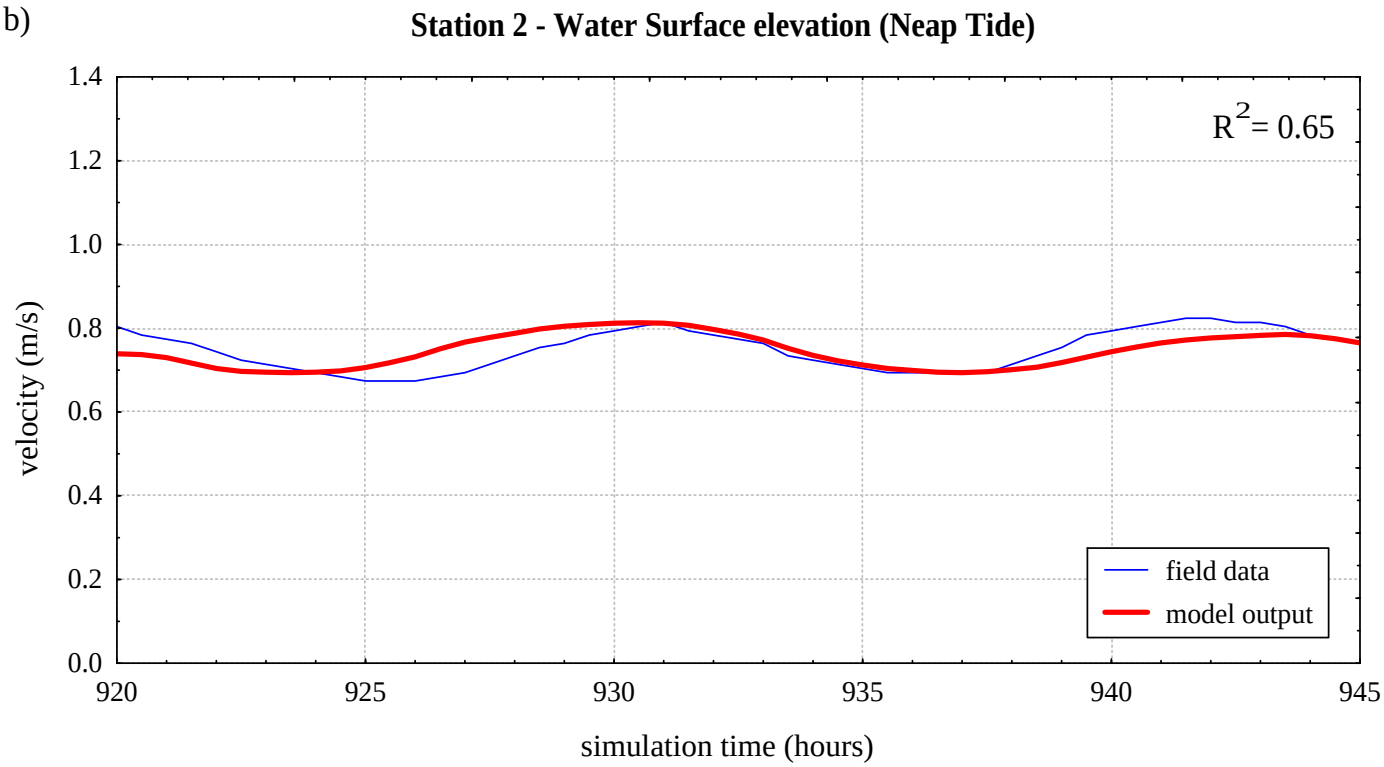
Station 2 - Water Surface elevation (Neap Tide)
R2= 0.65
velocity (m/s)
simulation time (hours)
field data
model output
1.4
1.2
1.0
0.8
0.6
0.4
0.2
0.0
920
925
930
935
940
945

c)

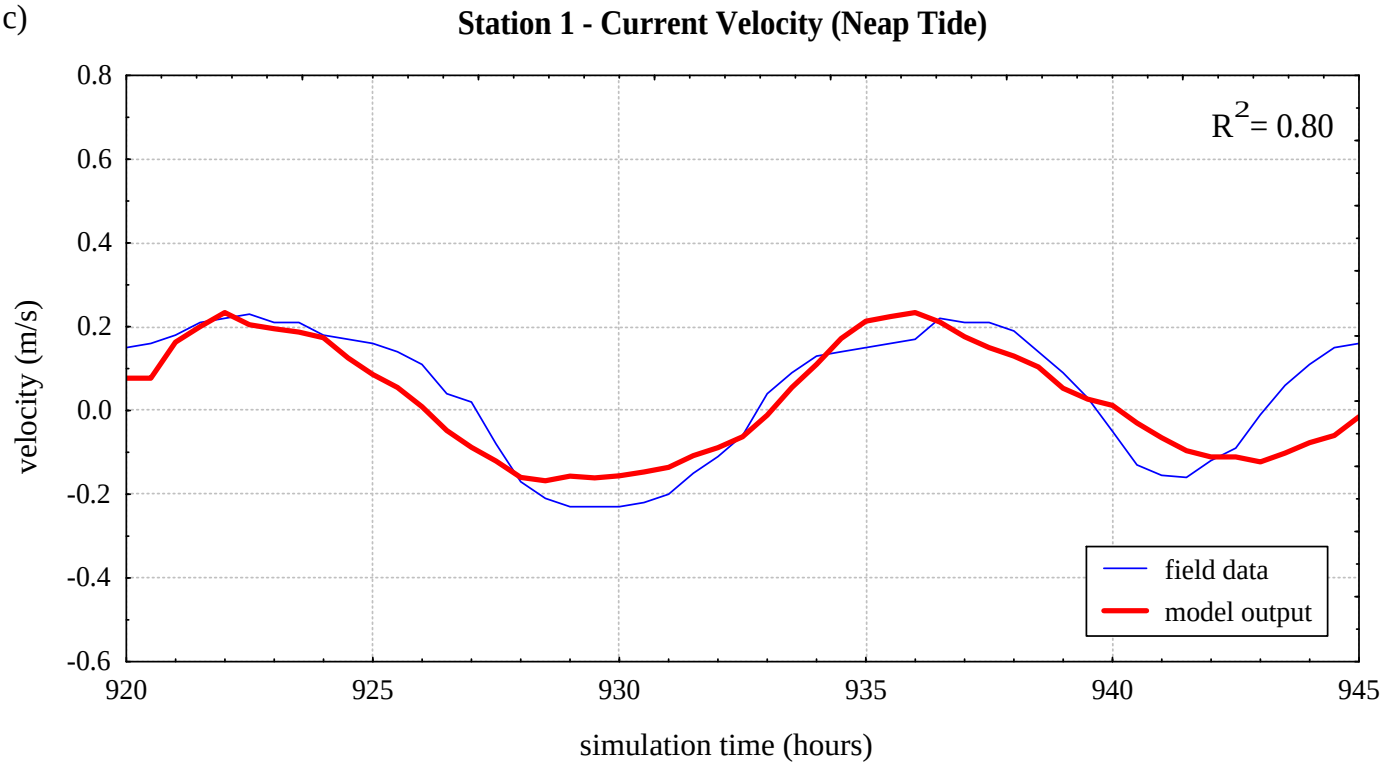

d)

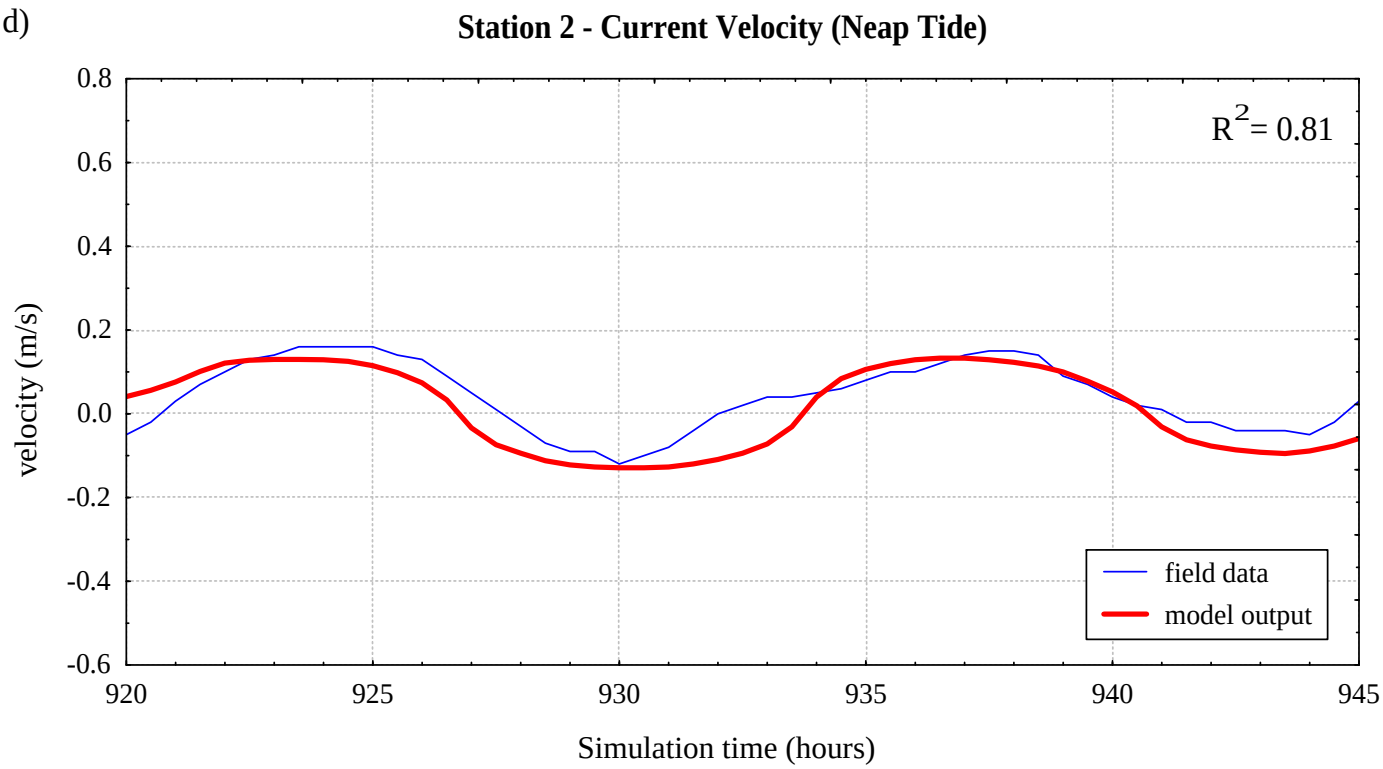

Figure 14 – Graphs showing the model output plotted with the calibration field data during neap tide for the water surface elevation and current velocity at field stations 1 (a, c) and 2 (b, d).

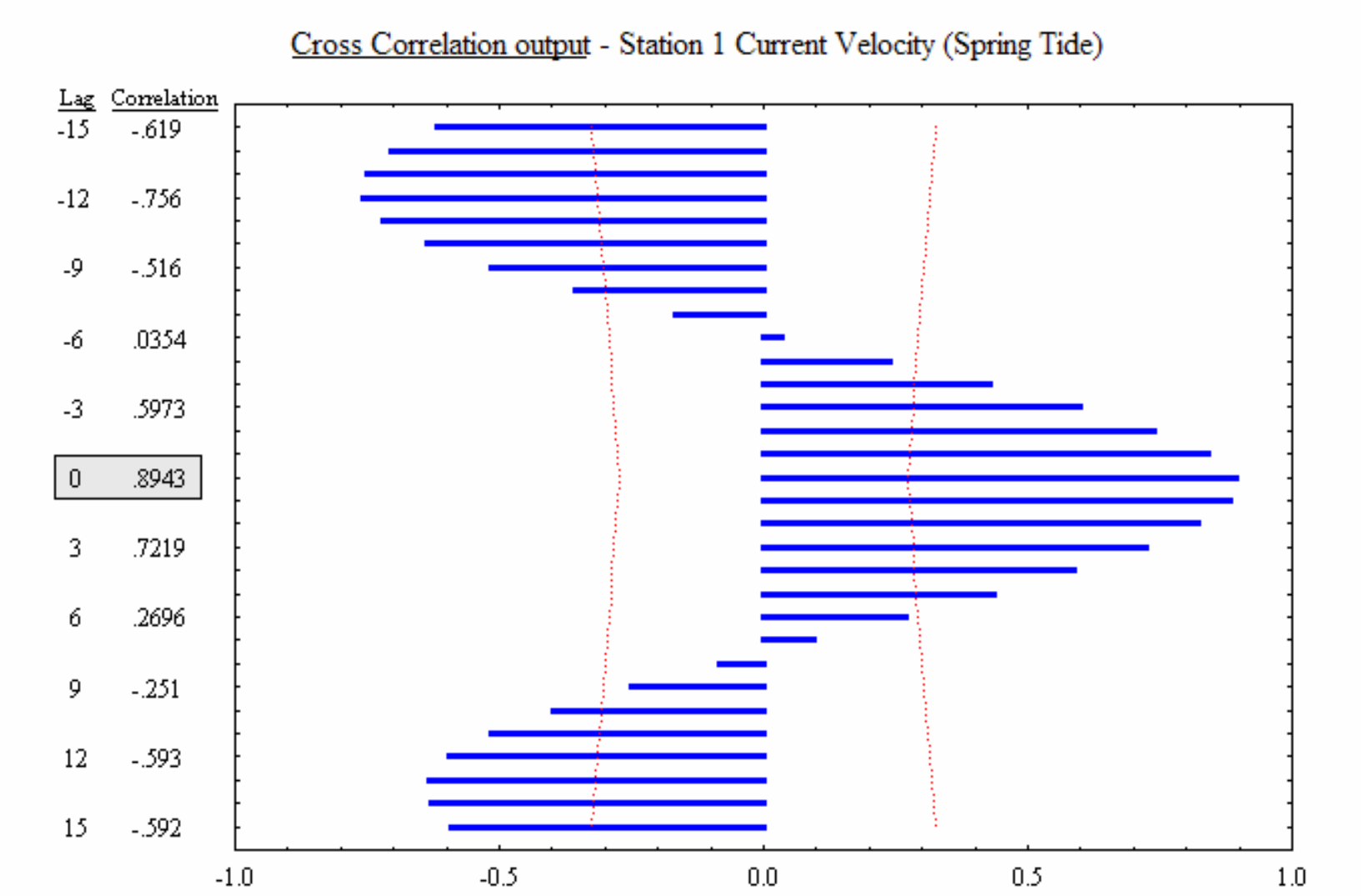

Figure 15 Sample cross-correlation output comparing spring tide current velocities of the model output and field data. Highest correlation is at zero lag. The red dotted line indicates the 95% confidence band.

Table 3: Cross-correlation coefficients for field data and model output time series. All values are at zero lag.

	Correlation Coefficients
Spring Tide	
Station 1	
Water surface elevation	0.981
Current velocity	0.894
Station 2	
Water surface elevation	0.961
Current velocity	0.979
Neap Tide	
Station 1	
Water surface elevation	0.640
Current velocity	0.436
Station 2	
Water surface elevation	0.721
Current velocity	0.366

Table 4: R^2 values of scatter plots of model output vs. field data.

	R^2 values
Spring Tide	
Station 1	
Water surface elevation	0.97
Current velocity	0.79
Station 2	
Water surface elevation	0.94
Current velocity	0.87
Neap Tide	
Station 1	
Water surface elevation	0.73
Current velocity	0.80
Station 2	
Water surface elevation	0.65
Current velocity	0.81

10. Results and Discussion

Water surface elevation and current velocity data are extracted from the model using a single point centred in the thalweg of the channel at the positions indicated in Figure 16. Water flux data is extracted using an arc that spans the channel at each position. For both the baseline conditions and the dredged channel scenario, short model runs of 600 simulated hours (including a single spring and neap cycle) were performed to evaluate the performance of the model, highlight the general characteristics of the estuary, and establish baseline conditions with which a comparison with a hypothetical dredged channel could be made.

Results are presented for the vertical cross-sections at the inlet Mouth, Station 1, 2, and 3 (Figure 16), illustrating the tidal wave and flow structure through time. The cross-sectional area at the Mouth varies by an average of 13% from high to low water over the period examined. Stations 1 and 3 are much shallower sections of the Itajuru Channel and therefore the channel geometry and cross-sectional area are significantly influenced by the change in water surface elevation (wse). The cross-sectional area varies by an average of 34% at Station 1 and 38% at Station 2.

The output data presented herein is shown in 3 segments of 75 simulated hours (6 tidal cycles) to highlight the hydraulic conditions at spring, intermediate, and neap tides. The behaviour of the flow structure is discussed in terms of the tidal range (amplitude), tidal asymmetry, tidal current flow dominance, water flux, and sediment transport implications.

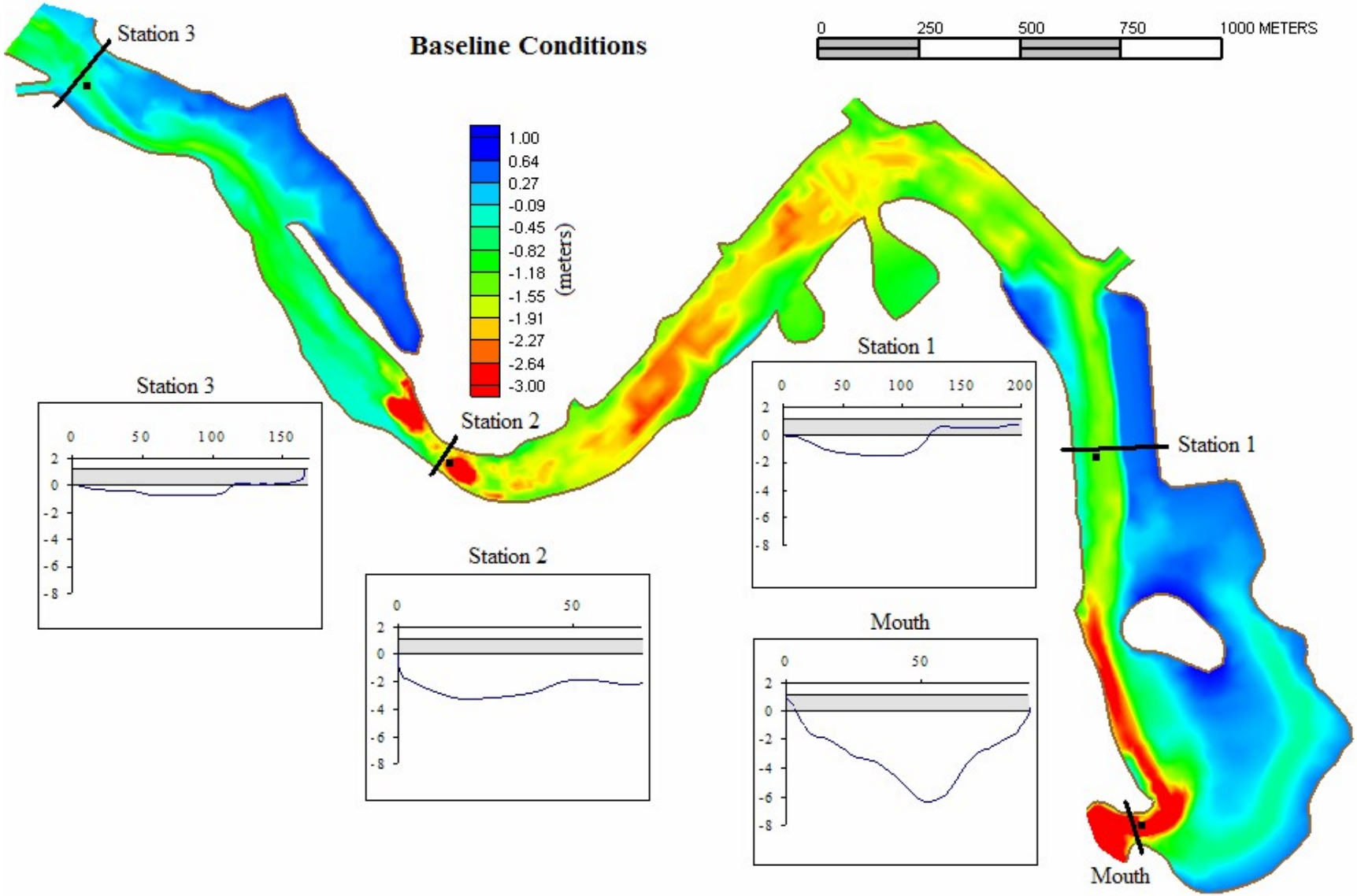

Figure 16 Bathymetry used in the baseline conditions simulation. The locations of the four data stations are represented by the dark squares. The cross sectional profiles of the four stations are shown with vertical exaggeration (scale in meters). Dark bands in the cross-sectional profile diagrams show the maximum tidal range occurring at the highest spring tides.

i) Baseline Conditions

a) Water surface elevation

Asymmetry of the wse curves is apparent at all 3 phases of the tidal cycle. The crest and trough of the tidal wave at Stations 1 through 3 arrive consistently later than the equivalent point at the mouth of the channel, demonstrating the wave propagation up the channel in the form of a progressive tide (Figure 17). Due to the small phase lag between stations, the hydraulic gradient is proportional to the change in the wse between the data stations at a particular time step. As the tidal wave begins to enter the Itajuru Channel the hydraulic gradient is eliminated between the Mouth, Station 1 and Station 2 producing a brief period of slack water. As the wave progresses a hydraulic gradient is gradually established which causes flow acceleration, which appear to be the greatest at Stations 2 and 3. The increasing water depth minimizes friction and the rise of the wse at all stations keeps pace with the rising ocean water well. The hydraulic gradient reaches its maximum just before the crest of the wave enters the Itajuru Channel producing peak current velocities (Figure 18). Current velocities do not change significantly as the wave enters the channel because the hydraulic gradient does not increase. During the initial stages of the falling tide, the deeper channel provides efficient water exchange and the hydraulic gradient is minimized, producing slack water when the wse at each station passes the mean sea level. However, flow reversal does not occur simultaneously because of inertia. As water levels continue to drop, areas of the channel margins dry and the cross-sectional area diminishes at Station 1 and Station 3. The hydraulic gradient increases as the water depth decreases and the tide level in the estuary starts to lag behind the ocean tide. Friction is enhanced, resulting in flow retardation at low water.

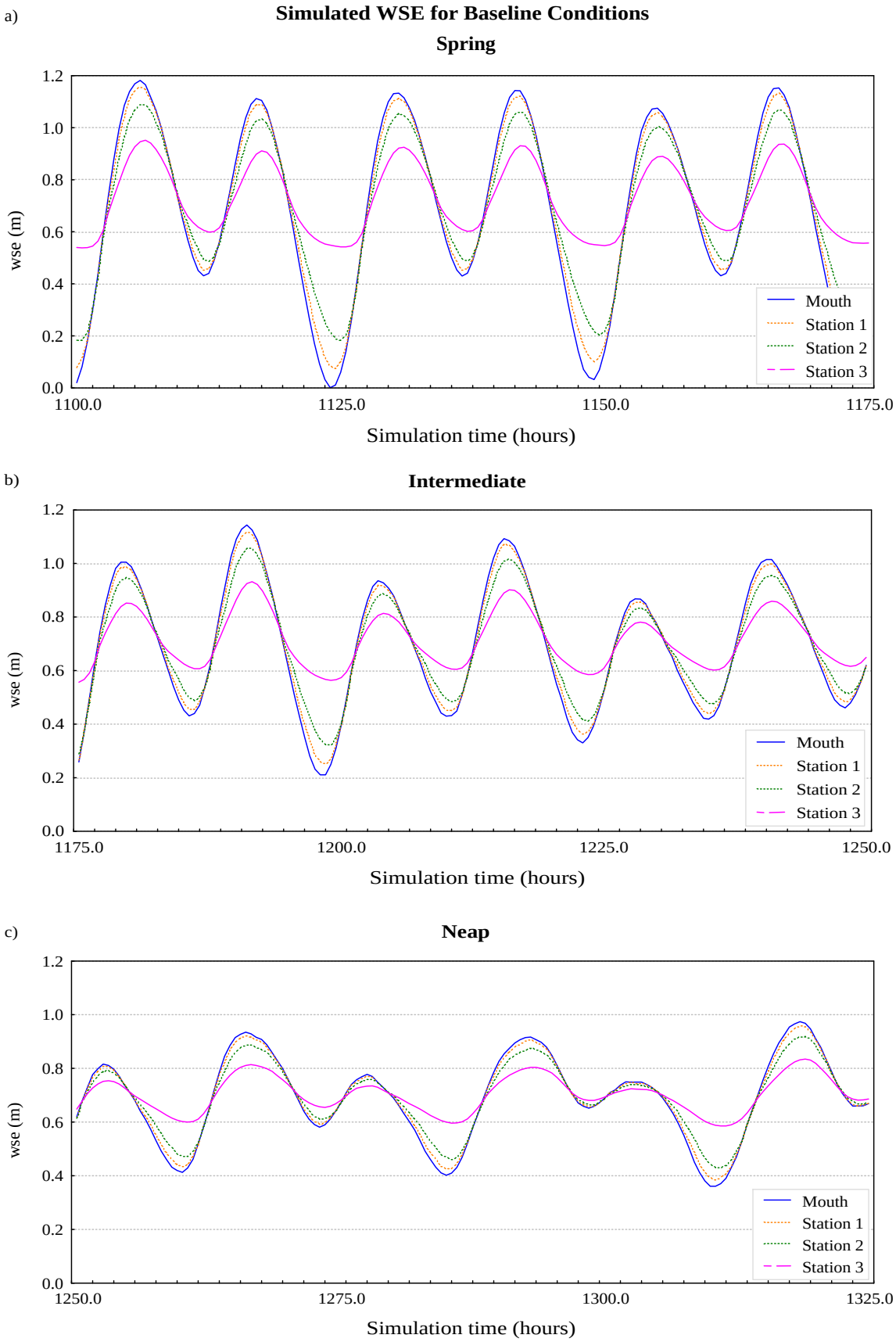

Figure 17 Three consecutive segments of the water surface elevation output for a) spring, b) intermediate, and c) neap tides.

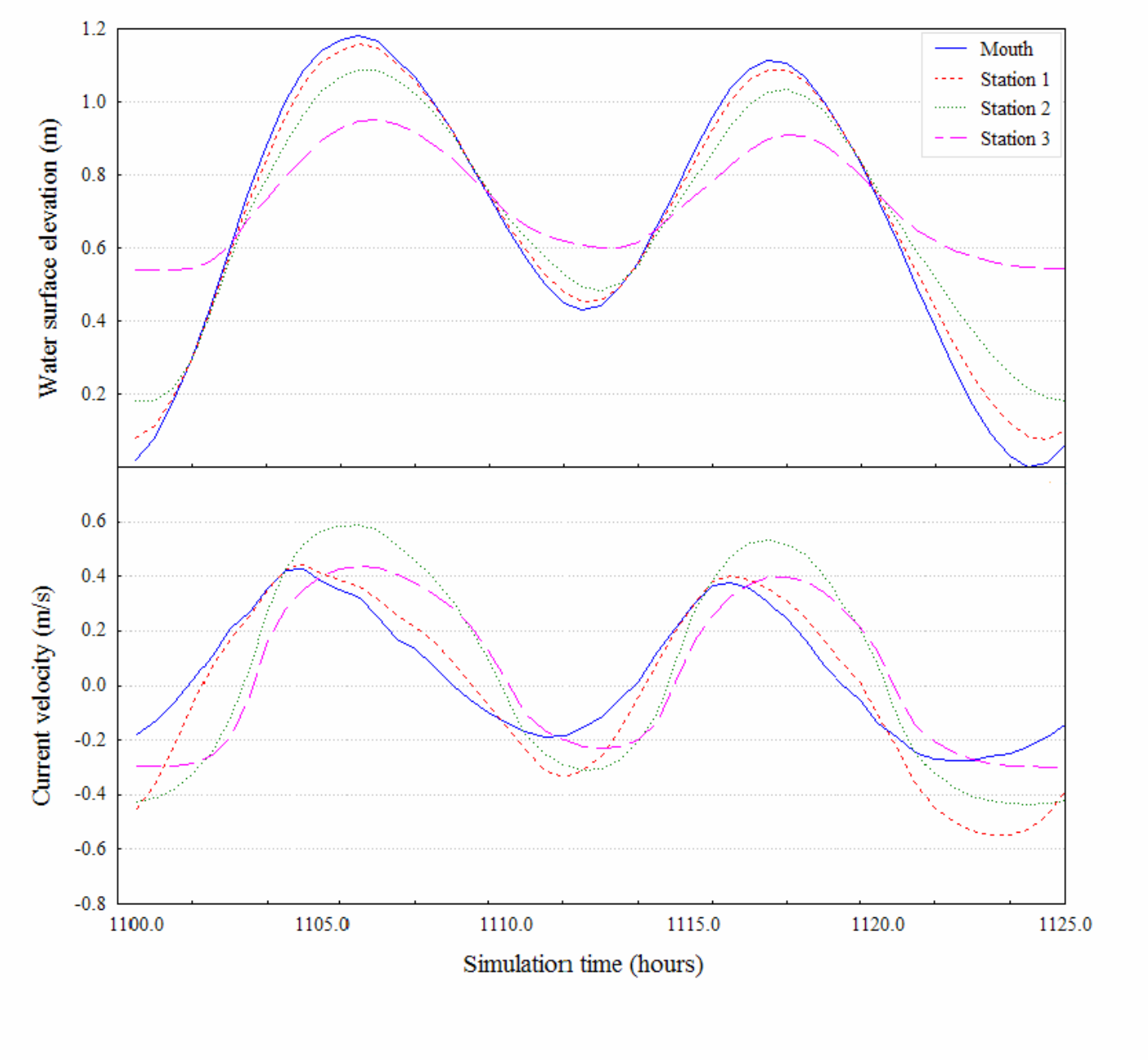

Figure 18 The water surface elevation and current velocity magnitudes are plotted together to illustrate the flow structure of the progressive tide in the Itajuru Channel during spring cycle.

There is significant variation in the tidal range from spring to neap tides. Figure 19 shows the tidal ranges measured at the Mouth and Station 3. The maximum range at the Mouth was 1.18 m, whereas minimum range was 0.1 m during spring and neap tides, respectively. Mean ranges for all stations are shown in Table 5. Mean values for the rising tide are greater than the falling tide at the Mouth, Station 1 and Station 2 during both spring and neap tides. Due to the short data set analyzed the range inequality in the mean values should not be considered as a general trend but a product of tidal harmonics. Over a longer period this inequality would disappear.

Tidal attenuation along the channel is greater during neap tides than during spring. An average of 57% of the off-shore tidal amplitude was lost between the ocean and Station #3 during spring tides. An average of 65% of the off-shore amplitude was lost during neap tides.

b) Current velocities

Tidal environments are characterized by regular flow reversals due to the changing hydraulic gradients. The mean current velocities shown in Table 6 indicate that flood velocities are greater than ebb velocities at the Mouth, Stations 2, and Station 3. At Station 1, the mean velocity is very small but ebb directed. Maximum current velocities occur during spring tides when the tidal range is at its maximum. Maximum flood currents at the Mouth and Station 2 are 35% and 27% greater than maximum ebb currents, respectively.

Peak current velocities are consistently greater during the rising limb of the spring and intermediate tidal cycles at the Mouth, Station 2, and Station 3. Conversely, strong peak currents in the ebb direction are consistently present at Station 1 (Figure 20). During

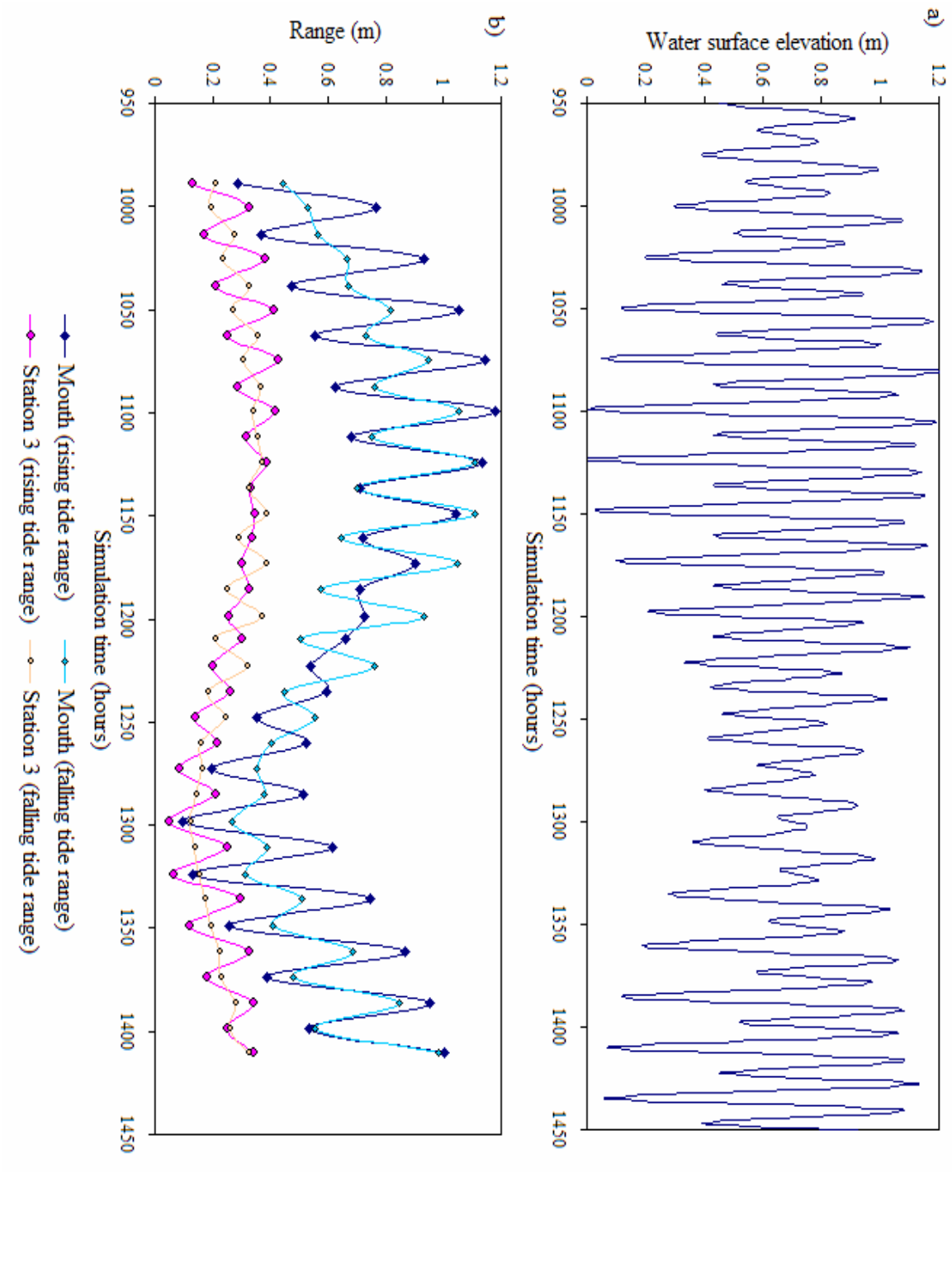

Figure 19 a) Mixed, semi diurnal tide curve used to force model for simulations. b) Range inequality at different phases of the tidal cycle is shown for the Mouth and Station 3. Wave amplitude is damped by an average of 57% and 65% between the mouth and Station 3 during spring and neap tides, respectively.

Table 5 Mean values for the rising and falling tidal ranges with variation computed to the first standard deviation.

	Mean rising range (m)	Standard deviation	**Mean falling range (m)**	Standard deviation
Mouth				
Spring	**0.95**	0.27	**0.92**	0.16
Intermediate	**0.67**	0.23	**0.66**	0.18
Neap	**0.39**	0.23	**0.35**	0.05
Station 1				
Spring	**0.88**	0.25	**0.85**	0.14
Intermediate	**0.63**	0.21	**0.62**	0.17
Neap	**0.36**	0.21	**0.33**	0.05
Station 2				
Spring	**0.74**	0.20	**0.72**	0.11
Intermediate	**0.54**	0.17	**0.53**	0.14
Neap	**0.31**	0.18	**0.28**	0.04
Station 3				
Spring	**0.34**	0.05	**0.35**	0.02
Intermediate	**0.27**	0.07	**0.27**	0.06
Neap	**0.13**	0.09	**0.14**	0.01

Table 6 Mean, maximum flood, and maximum ebb current velocities for the baseline conditions.

Velocity (m/s)	**Mouth**	**Station 1**	**Station 2**	**Station 3**
Mean	0.026	-0.003	0.032	0.029
Max flood	0.435	0.444	0.602	0.444
Max ebb	-0.277	-0.547	-0.437	-0.303

a)

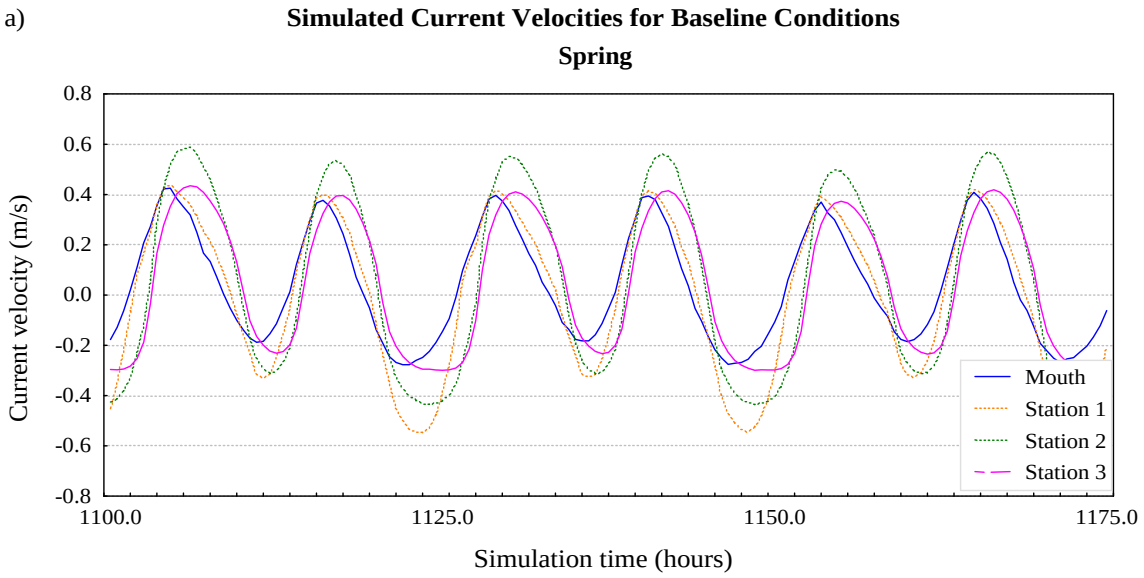

b)

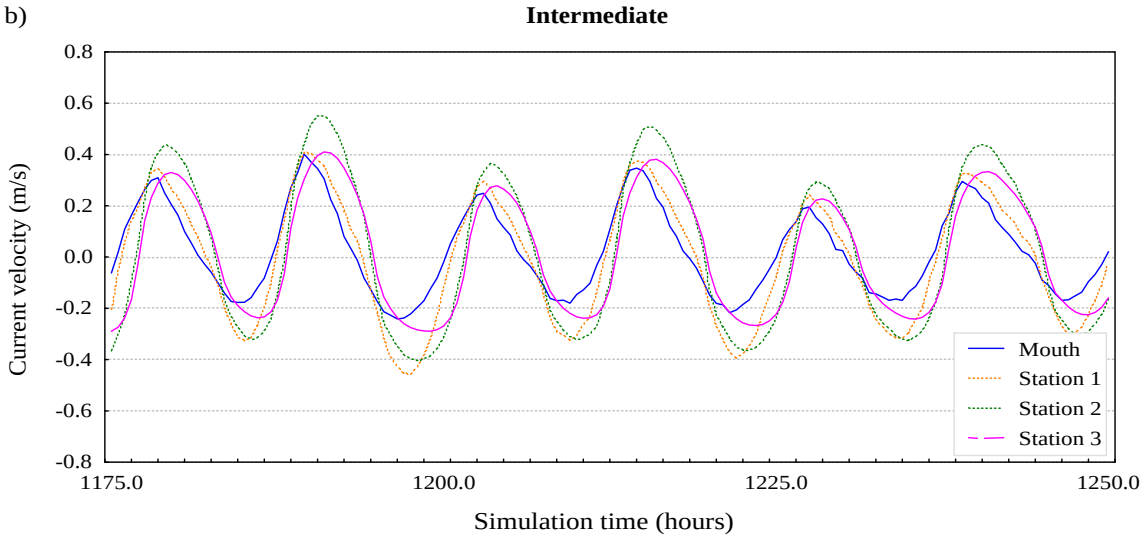

c)

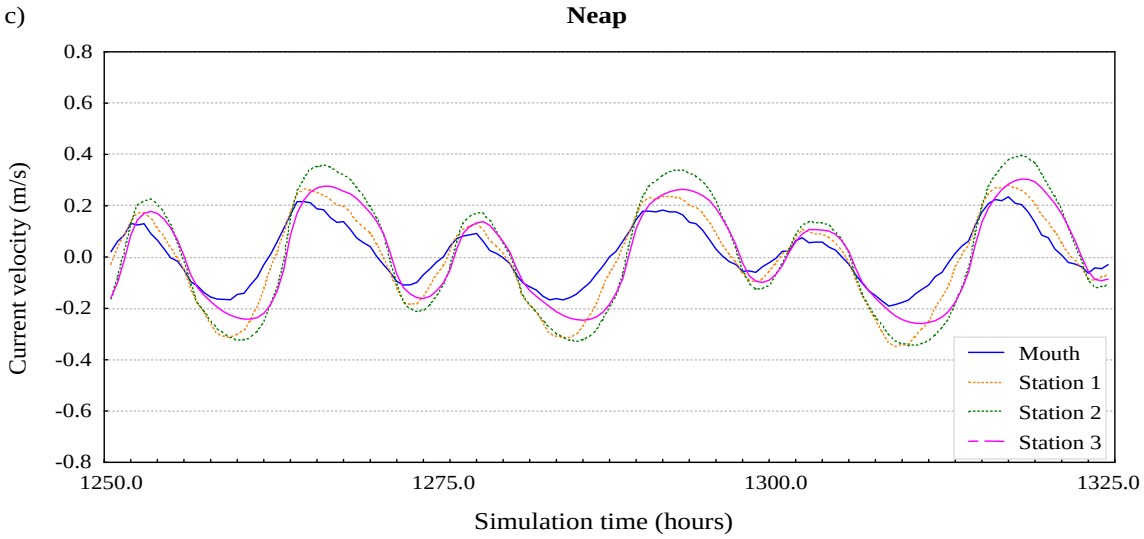

Figure 20 Three consecutive segments of current velocity magnitude output for a) spring, b) intermediate, and c) neap tides.

neap tides, current velocities reduce and the asymmetry between flood and ebb flows decreases due to the deeper channel, particularly at low water. Additionally, neap tidal cycles are characterized by smaller tidal ranges and, consequently, a larger proportion of the channel area remains actively conveying water. Spring and intermediate tidal cycles, due to much larger tidal ranges, are accompanied by dramatic variations in the estuarine morphology. Therefore, because of continuity larger volumes of water must be conveyed through a narrower channel resulting in greater ebb flow magnitude, particularly evident at Station 1.

The hydraulic gradient is the primary forcing mechanism of the current velocity and therefore a greater hydraulic gradient should result in larger magnitude current velocities. Figure 21 plots the hydraulic gradient and the current velocity for the baseline conditions. Positive values represent hydraulic gradients of rising water and flood directed currents. Negative values represent hydraulic gradients of falling water and ebb directed currents. In the flood direction, current velocities are seen to increase as the hydraulic gradients increase. However, in the ebb direction, current velocities appear to approach a threshold value that limits their magnitude. This is most evident between Station 2 and 3 where the hydraulic gradient is increasing but it is not inducing flow magnitudes greater than ~0.3 m/s. The same trend is apparent between the Mouth and Station 1 and between Station 1 and Station 2 but not as strongly. The decreased water depth at low water is producing greater frictional forces on the flow, restricting the flow velocity.

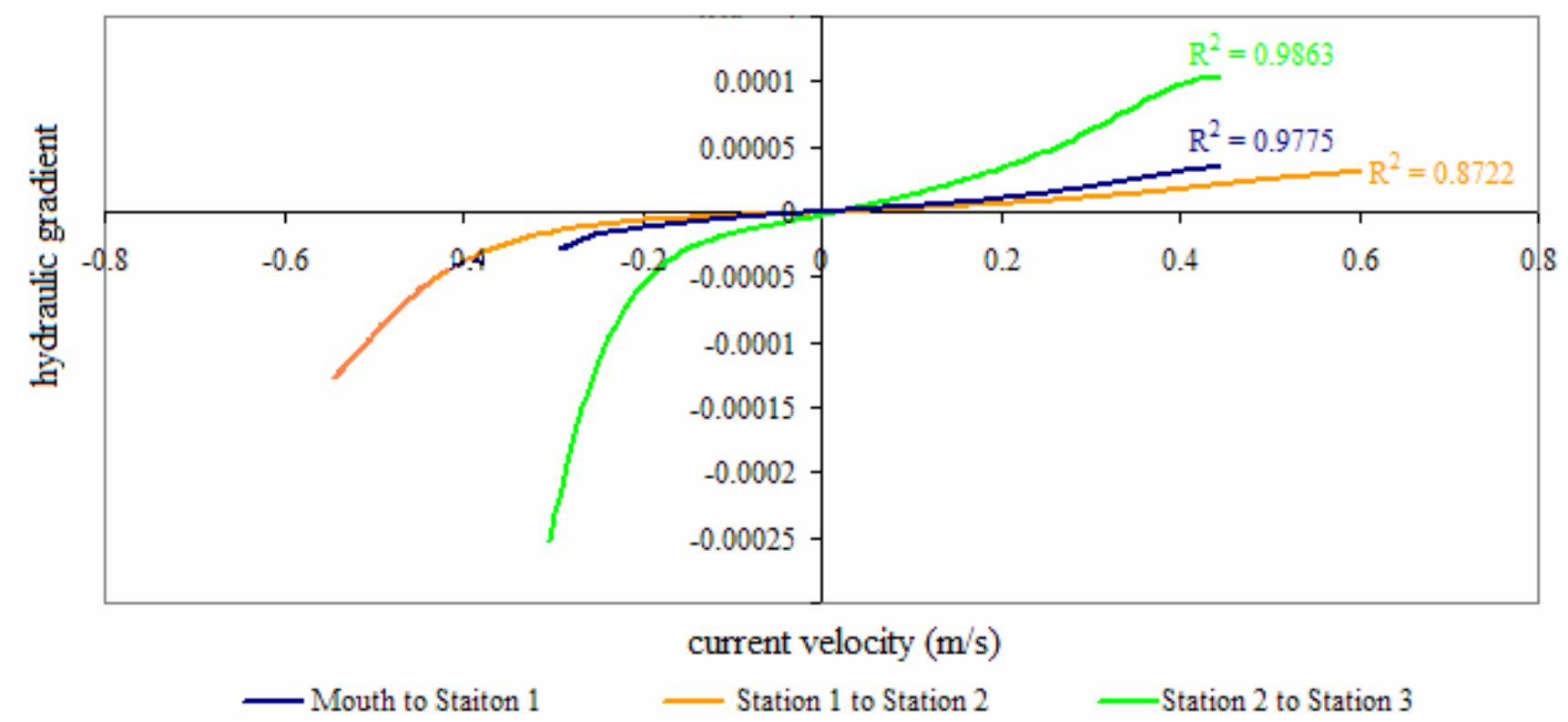

Figure 21 The hydraulic gradient is plotted with the current velocity for the baseline conditions. Positive values represent hydraulic gradients of rising water and flood directed currents. Negative values represent hydraulic gradients of falling water and ebb directed currents. A 6^{th} order polynomial represents the data with R^2 values are shown.

c) Water flux

The water flux is computed by the model as a scalar quantity at each time step and is representative of the tidal prism. The tidal prism is defined as the total volume of water entering the estuary on the rising limb of the tidal wave (Masselink and Hughes, 2003). The tidal prism is therefore represented in Figure 22 as the area under the curve of a single rising tide peak. Calculations of the tidal prism using the water flux output were conducted to check agreement with the tidal prism estimated by Lessa (1990). Using a sampling of tidal cycles from both spring and neap tides the tidal prism is estimated to be 2.5×10^7 m^3, 33% less than the tidal prism estimated by Lessa (1990). The predicted tidal prism from the RMA2 model is likely an underestimation of the actual tidal prism present in the Itajuru Channel. Lessa (1990) had tidal ranges within the lagoon of 0.25 meters, however, the model only predicted a range of 0.10 m. Lack of acceptable agreement between the wse field data and the wse model output is likely the primary cause of the large discrepancy since Lessa (1990) includes the additional volume in the lagoon which the model does not represent.

An analysis of the water budget within the lagoon was conducted to test the validity of the water flux output and check for the proper functioning of the model's evaporation function. Rising tide flux generally has greater peak magnitude than subsequent ebbing flux during both spring and neap cycles. Thus greater volumes of water are entering the lagoon than are leaving it. Evaporation parameters in the model remove an average of 8.1×10^6 m^3 of water from the lagoon over the tidal cycles examined, accounting for 78% of the difference between a rising tide flux and the subsequent falling tide flux. Clearly, the water budget must balance over a longer time

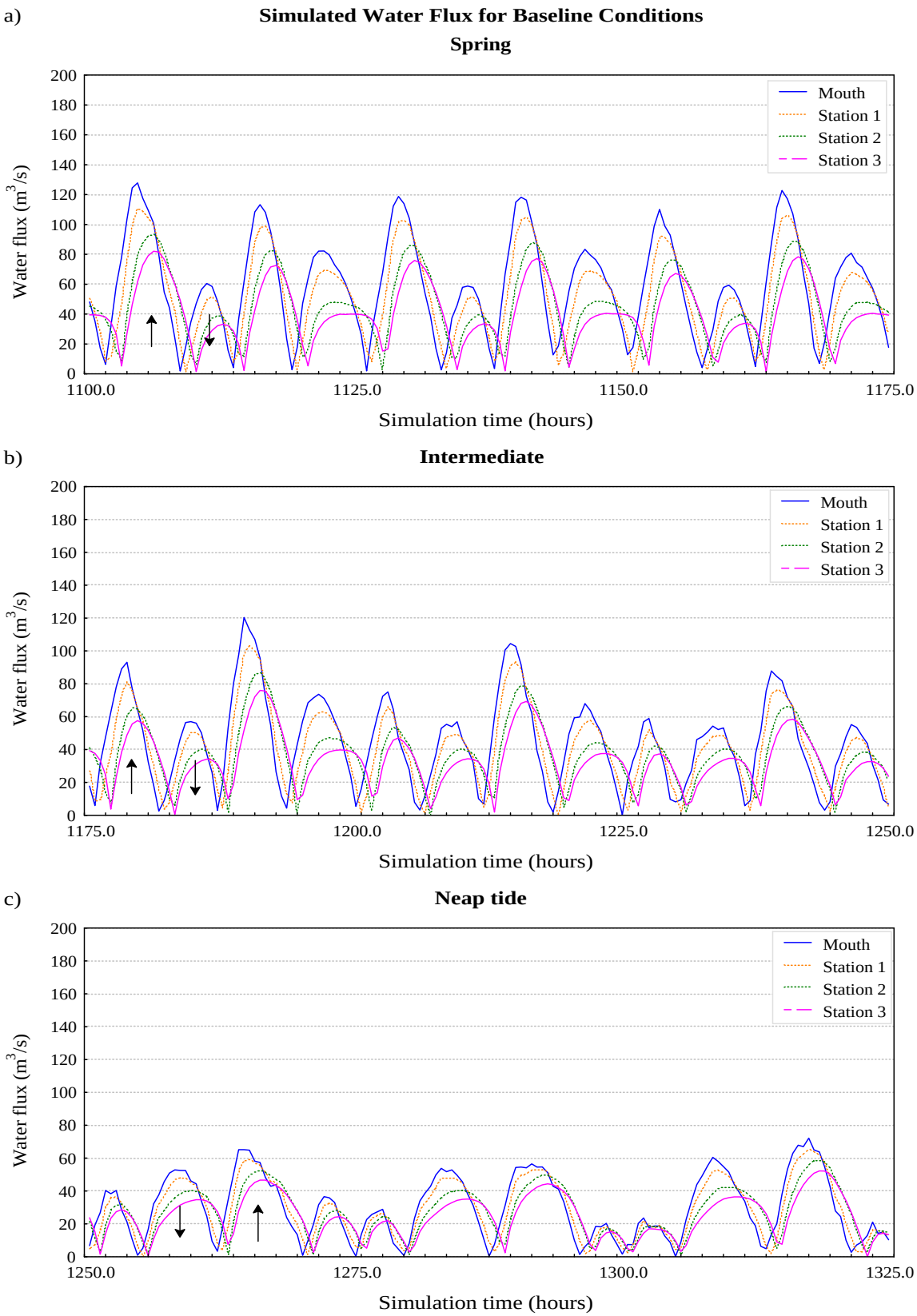

Figure 22 Three consecutive segments of water flux output for a) spring, b) intermediate, and c) neap tides. Arrows indicate rising (up arrow) or falling (down arrow) tide.

series and will need to be tested to confirm that input and removal of water in lagoon is modeled accurately. Due to the relatively short time series used in the simulation and the inherent range inequality of the input tidal curve, it appears that water budget is well represented.

As with the water surface elevation, the lag between peak water flux between stations is evident. Peak magnitudes occur 30 minutes before the crest or trough of the tidal wave passes the data station. Peak water flux magnitudes are in phase with the peak current magnitudes. Curves representing the flooding flux are narrow and pointed whereas curves representing ebbing fluxes are broader and flat. This difference in shape is representative of the duration asymmetry of the water surface elevation curve where ebb cycles are longer in duration than flood.

d) Tidal wave distortion and duration asymmetry

The tides in the Itajuru Channel are asymmetric and characterized by a short duration rising tide and a longer duration falling tide. This distortion increases as the tidal wave propagates along the channel. The duration ratios (rising tide duration/falling tide duration) at all stations are plotted against the low water level in Figure 23a. Of the 144 duration ratios, 91% of the values are less than 1, indicating that shorter flood durations dominate. Variation appears to be greatest during spring cycles. Of the 13 values greater than 1 (i.e. ratios favouring longer ebb durations), 70% of them occur during the spring tide and 15% during neap tides. The average flood/ebb duration ratio for each station is shown in Figure 23b, demonstrating the increasing tidal wave distortion as it progresses up the channel, reaching its maximum at Station 3. The variation in the average duration ratio is similar at most locations in the channel with greatest variation at the Mouth.

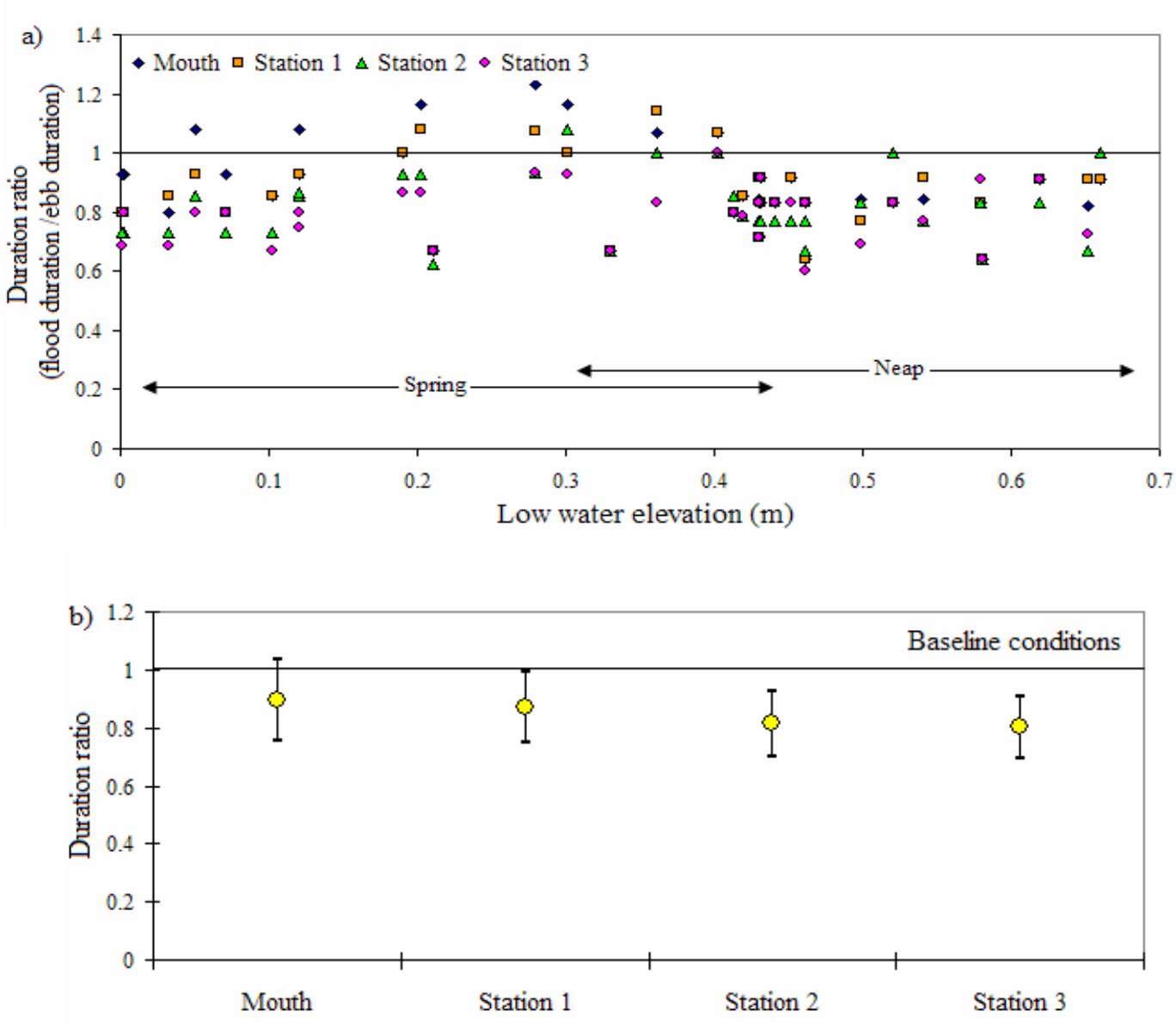

Figure 23 a) Duration ratios (rising tide duration/falling tide duration) is plotted against low tide level . Arrow indicate the range of values within spring and neap cycles. Of the 144 points, 131 (91%) are less than 1 indicating that a majority of the tidal cycles have shorter flood durations compared to subsequent ebb durations. b) Mean values with error bars representing the distribution (±σ) around the mean.

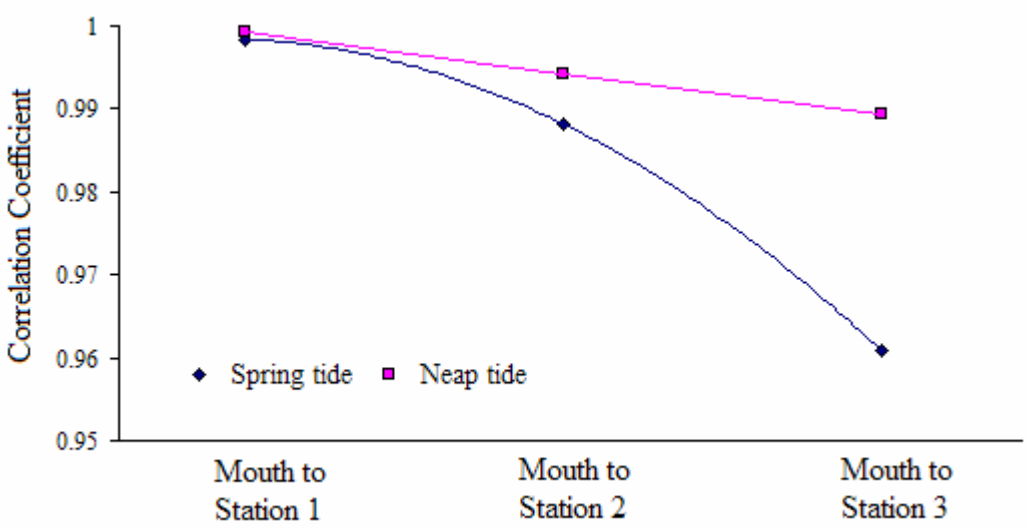

Figure 24 Cross-correlation coefficients comparing wse curves at different data stations become progressively smaller up the channel due to tidal wave distortion and time lag. Spring tides are shown to be more distorted than neap tides.

Table 7 The cross-correlation coefficients from a comparison of the water surface elevation curve at the mouth with the water surface elevation curves at the other data stations. Cross-correlation coefficients plotted in Figure 24 are bolded. A 0.5 hour lag is detected between the Mouth and Station 3.

Spring	-2	-1	0	1	2
Mouth to Station 1	0.8792	0.9661	**0.9984**	0.9416	0.8333
Mouth to Station 2	0.9093	0.9773	**0.9882**	0.9099	0.7828
Mouth to Station 3	0.9116	**0.9609**	0.9530	0.8654	0.7322

Neap	-2	-1	0	1	2
Mouth to Station 1	0.9281	0.9839	**0.9993**	0.9696	0.9006
Mouth to Station 2	0.9484	0.9920	**0.9942**	0.9512	0.8698
Mouth to Station 3	0.9565	**0.9894**	0.9805	0.9268	0.8370

A cross-correlation of the wse curves was performed to attempt to further quantify the distortion of the tidal wave as it propagates up the channel for both spring and neap tides. As the wave propagates up the channel the change in its shape and position can be quantified using the correlation and lag coefficients, respectively. Decreasing correlation would thus represent increasing distortion of the wave. Lag values would indicate the number of time steps out of phase the wave is with the ocean wse.

The wave is measured to be most distorted at Station 3. Spring tides were observed to become more distorted by the progression through the channel than neap tides. The correlation coefficients are shown in Table 7 and plotted in Figure 24. A lag of 0.5 hours (1 time step) was detected by the analysis between the wse curve at the Mouth and the wse curve at Station 3. Lags at the other stations are present but not detectable by this method using a 0.5 hour time resolution used in the model.

Mixed, semi-diurnal tides present some challenges with respect to analyzing the duration and current magnitude asymmetries. For example, during the neap tides, the range inequality over individual tidal cycles reaches a maximum. During these extremes, large variation from the typical conditions occurs and often influences tidal durations and current magnitudes.

The duration ratio is dependent on the tidal range. Figure 25 plots the duration ratio with the range ratio (rising range/falling range). A linear regression of the scatter points at each station show progressive weakening of the relationship up the channel. For the Mouth and Station 1, where little distortion of the wave has occurred, higher duration inequality favouring shorter rising tides are associated with range inequality that favours

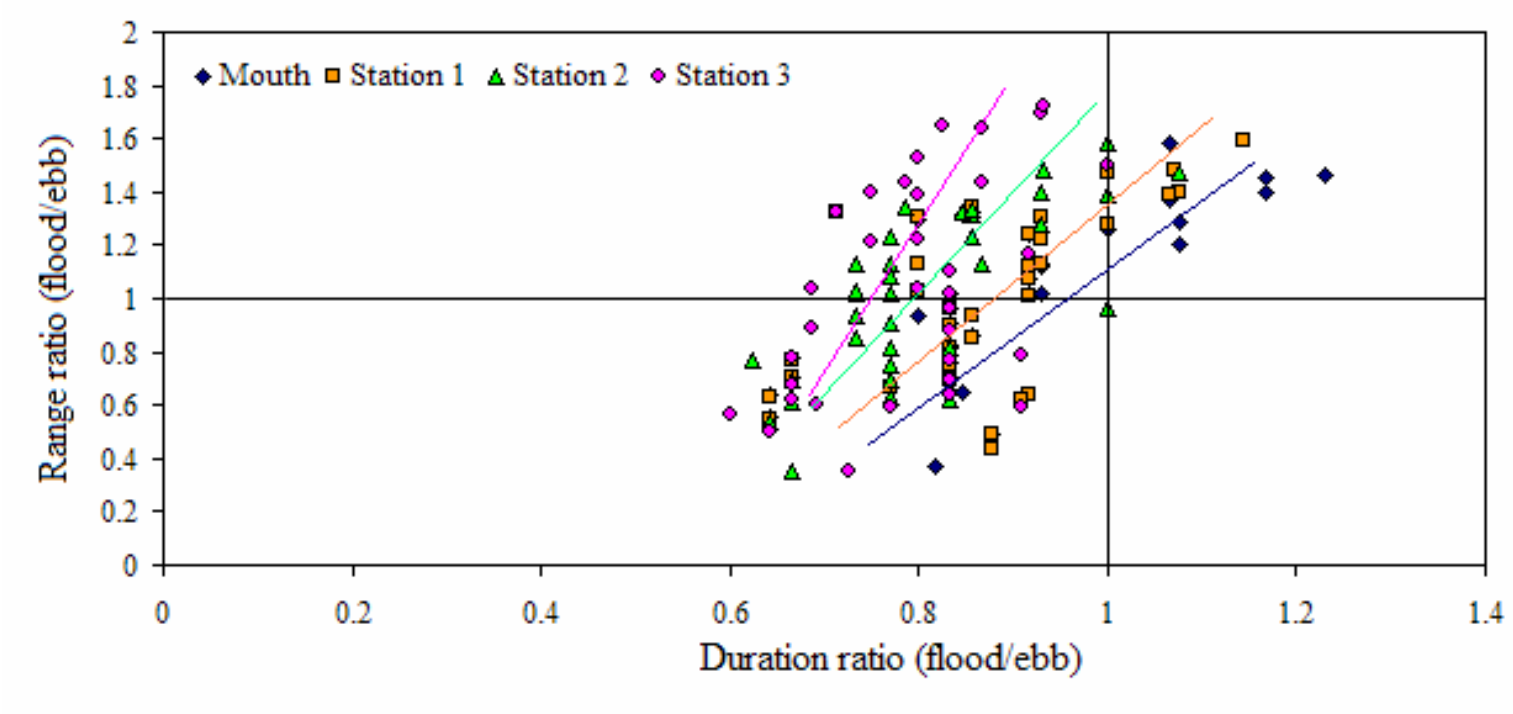

Figure 25 The range ratio (rising tidal range/falling tidal range) is shown to have a relationship with the duration ratio, where small flood ranges relative to ebb are associated with shorter flood durations. Linear regression of the data points from each station show relationship between the range ratio and the duration ratio diminishes up the channel.

e) Current velocity magnitude asymmetry

Although duration asymmetry is often a useful indicator of current magnitude asymmetry, it cannot account for the effect of the changing channel dimensions on the current magnitudes. Estuaries can have duration ratios that indicate shorter rising tide but have ebb currents that are of greater magnitude than flood because of the morphological effects on the flow at low water. Therefore analysis of the current velocities is necessary to determine current dominance.

The current velocity at all stations has a strong relationship with the tidal range. Figure 26 shows that higher peak current velocities are associated with large tidal range at all stations. Maximum current velocities on the flooding tide are seen to be of greater magnitude than the ebbing velocities at similar ranges. However at Station 1, ebb and flood currents appear to have similar magnitudes at various ranges. Maximum current values during spring tides were an average of 92% greater than those during neap tides.

The expected flood current dominance, anticipated from the asymmetry in the vertical tide discussed in the previous section, is confirmed by Figure 27. The current ratio (maximum flood velocity/maximum ebb velocity) is plotted against low water level and shows that flood currents are often greater than ebb currents at the Mouth, Station 2, and Station 3. Seventy-four percent of the points have values greater than 1 (flood dominance). Of the 30 points that have values of less than 1, 67% are from Station 1. Due to the constriction of the flow during spring tides, Station 1 has current ratios which show greater magnitude ebb directed flows. During neap tides where the low water level

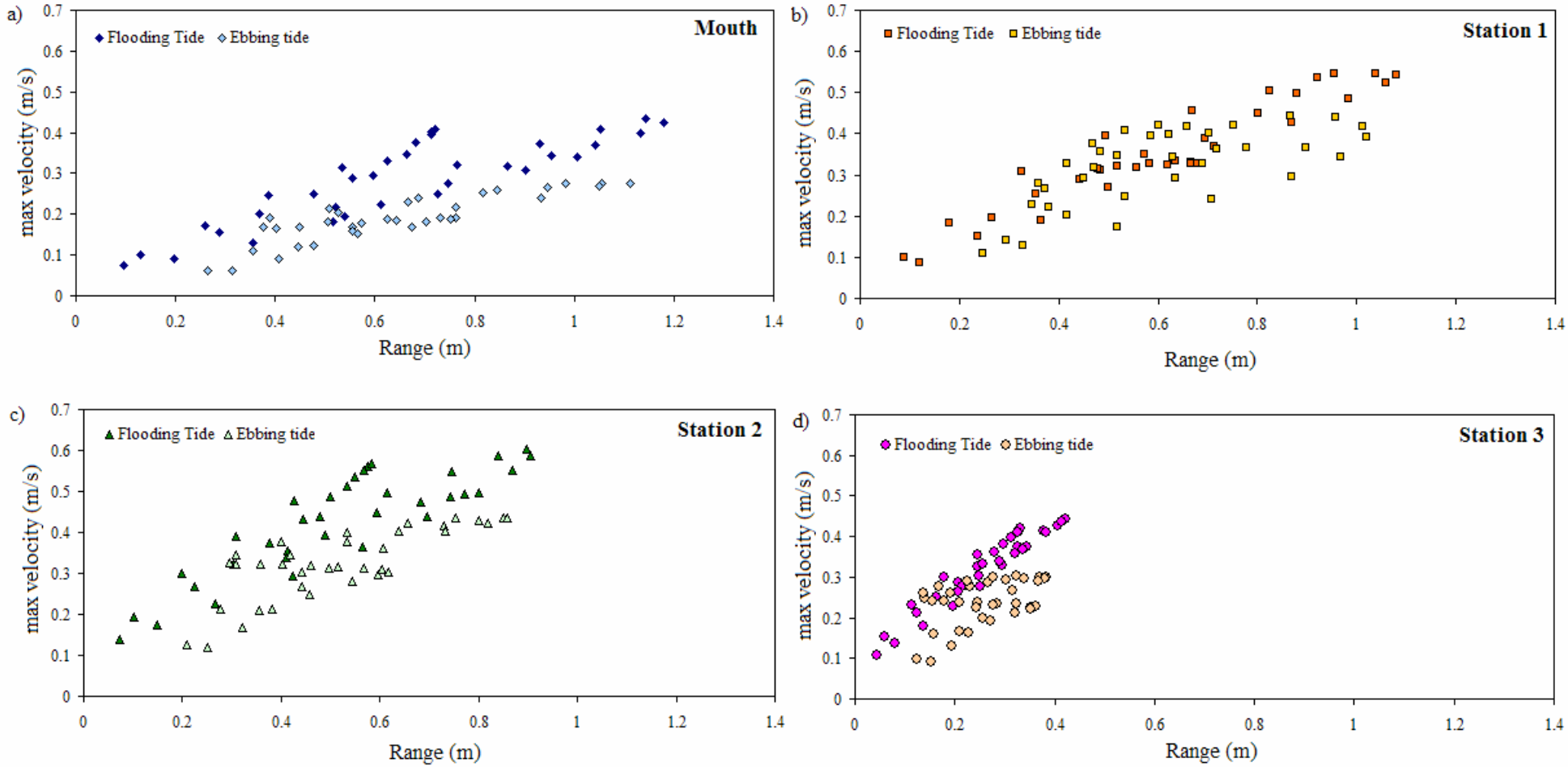

Figure 26 Peak current velocities are associated with tidal range at all stations. At the a) Mouth, c) Station 2, and d) Station 3 flooding currents are seen to be greater than ebbing currents at similar ranges. At Station 1, flood and ebb currents have similar magnitude at various ranges.

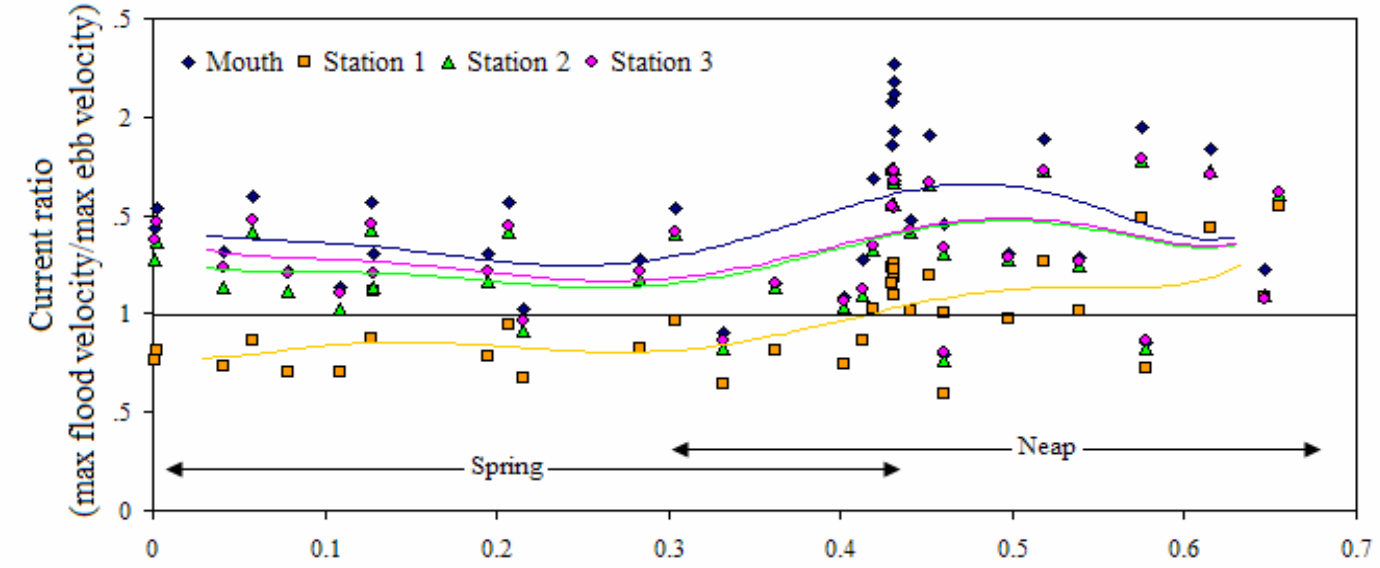

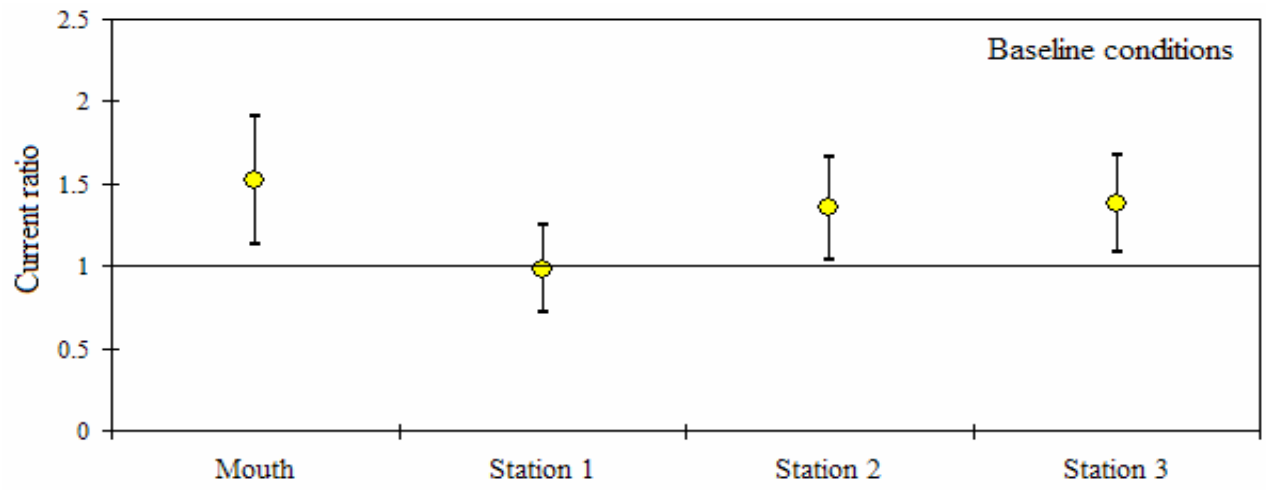

Figure 27 a) Current ratios (maximum flood current/maximum ebb current) are plotted against low tide level. Arrows indicate the range of values within spring and neap cycles. Of the 144 points, 106 (74%) are greater than 1 indicating that a majority of the tidal cycles have greater magnitude flood current magnitudes compared to subsequent ebb current magnitudes. Sixth order polynomial regression lines are included to show the trend at each station. b) Mean values with error bars representing the distribution (±σ) around the mean.

remains high enough to keep the whole channel conveying water, flood dominant flows are also present at Station 1. Three values of the current ratio from each station are seen to demonstrate ebb directed flow dominance at ranges of 0.33, 0.46, and 0.59 meters. Examination of the data reveals that these values occur when the range ratio and duration ratio strongly favours the ebb direction due to very small rising ranges.

A very strong relationship between the duration ratio and the current ratio is evident in Figure 28. Short flood durations relative to ebb durations (duration ratio < 1) have current velocities that are faster on the rising tide. Seventy-two percent of the points have flood dominant current magnitude and short flood duration. Seven points from the Mouth shown in Figure 26 have duration ratios favoring ebb dominance (duration ratio > 1) but current ratios are showing flood dominance. These points occur during an intermediate phase when tidal range is progressively getting larger from spring to neap and the rising range is consistently larger than the falling range.

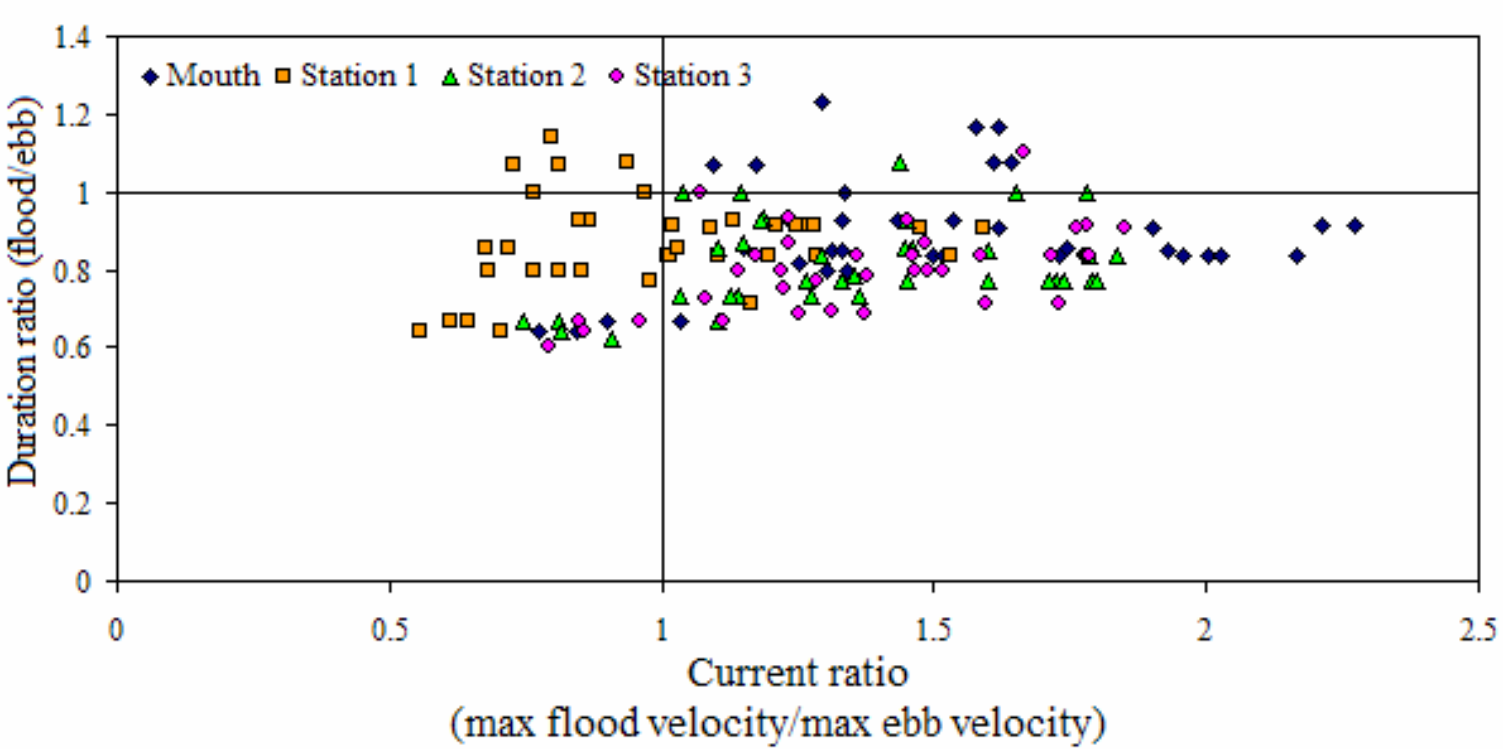

Figure 28 Duration ratio is plotted against the current ration showing that 72 % of the points have shorter duration, faster rising tide compared to the subsequent ebb.

f) *Sediment transport implications*

Fine sand particles are carried into suspension whenever an upward force caused by turbulence is greater than the gravitational settling force (Sumer and Deigaard, 1981). With asymmetrical currents, sediment transport can take place for varying time intervals and varying fluxes depending on the current magnitudes. The flood current dominance, shown in the previous section, has significant implications on the sediment flux in the Itajuru Channel.

A simple estimation of the sediment transport can be done if it is assumed that the Itajuru Channel sediments are cohesionless, nearly uniform in size and can be transported either as bed load or as suspended load. Non-cohesive sediment fluxes are proportional to the current velocity cubed provided that the current velocity is greater than a threshold of entrainment (Masselink and Hughes, 2003). A simple analysis of the sediment flux in Itajuru channel was conducted by cubing the current velocity, when it exceeded a threshold value of 0.2 m/s in the flood direction and -0.2 m/s in the ebb direction. A summation of the velocity cubed values over the 600 hour period equates to the values shown in Table 8. Both bed load and suspended load are assumed to adapt instantaneously to local flow conditions and thus scour and settling lags are neglected. The sediment flux at the Mouth and Station 2 are the greatest with values of 18.4 and 13.1 respectively. A small ebb directed sediment flux is predicted for Station 1.

Table 8 The summation of the cube of the velocity vector magnitudes produces sediment flux estimates listed for the four data stations.

	Mouth	**Station 1**	**Station 2**	**Station 3**
Estimated Sediment flux	+18.35	-1.68	+13.11	+6.10

Summary

The direction of sediment transport in the Itajuru Channel appears to be governed by the flood dominant conditions that have been established through the analysis of the duration asymmetry and current asymmetries. However, the morphological evolution of a system is dependent on the net sediment transport over much larger time frames than have been investigated here. For example, longer period tidal harmonics would affect the mixed, semi diurnal tidal regime and therefore variation in the magnitude of sediment transport would be expected.

The channel depth, particularly at low tide, appears to strongly govern the dynamics of the channel. Large magnitude ebb directed flows only occur when the channel has significantly narrowed due to the drying of the channel margins (Station 1) or when the range inequality is strongly favouring the ebb direction. During the flooding tide, when the channel is relatively deep, there is a positive relationship between the hydraulic gradient and the current velocities. However, during ebb flows, when the reduced depth in the channel limits the magnitude of the current velocity, despite relatively large hydraulic gradients. This result agrees with the model of Freidrichs and Aubrey (1988) where the flood or ebb dominance is determined by the ratio of tidal amplitude to the depth. The Itajuru Channel has a relatively large tidal amplitude when compared to its depth, and therefore would tend to become shallower due to flood dominant sediment transport.

ii) Dredged Conditions

The bathymetry of the finite element mesh was altered to represent a hypothetical scenario where the Itajuru Channel was dredged to a minimum depth of 3 m between the Mouth and Station 3 to allow for larger vessels to navigate the channel. Only nodal points with bathymetric values greater than -3 m were changed. The dredged channel was limited to an average width of 60 m but ranges from a minimum of 40 m to a maximum of 84 m. Due to the poor model performance within the lagoon, the bathymetry was not changed beyond the Itajuru Channel and thus the hydrodynamic conditions represented by the model in the lagoon are assumed to remain unchanged in the dredged scenario. The change from the baseline conditions to this experimental mesh is most noticeable in the cross sectional profiles at Station 1 and Station 3. The volume of the estuary, as measured by the model, increased 35% to 5.97×10^6 m^3. The Mouth and Station 2 were sufficiently deep that the cross sectional profiles remained unchanged from the baseline conditions. However, it should be noted that the channel depth on either side of Station 2 is significantly shallower due to the hypothetical dredging. Figure 29 shows the altered bathymetry for the channel and the cross-sectional profiles at each of the data stations.

The dataset for the dredged scenario was 500 simulated hours longer than the baseline simulation, totaling a period of 1100 simulated hours. It therefore includes two complete spring and neap cycles. Analysis of the wse, current velocities, and water flux data presented herein was conducted to include the additional data; however, analysis of the simulation data over the 600 hour period presented in the previous section for the baseline conditions was also done to check for consistency. The inclusion of the

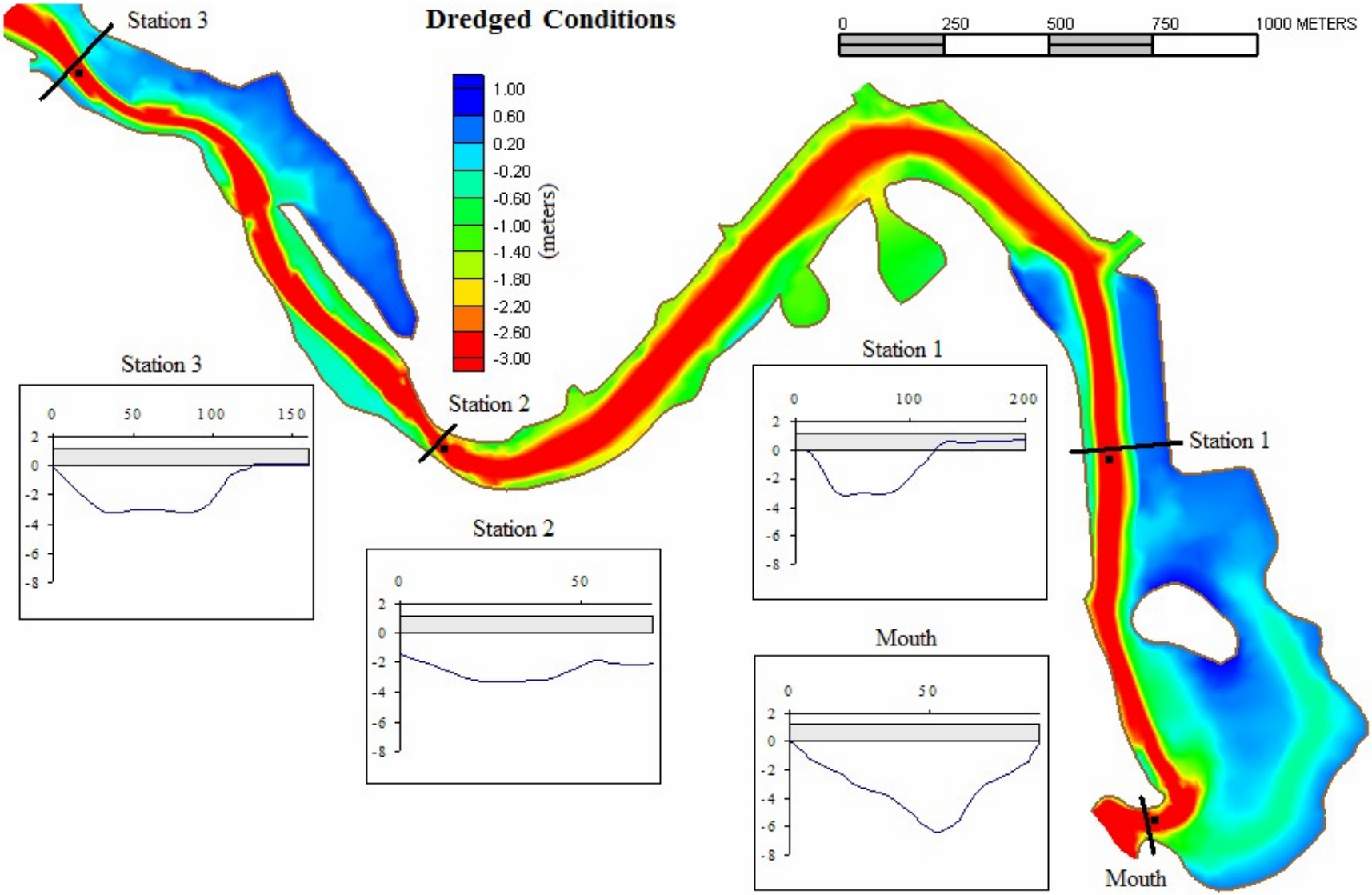

Figure 29 Bathymetry used for the hypothetical dredged conditions simulation. The locations of the four data stations are represented by the dark squares. The cross sectional profiles of the four stations are shown with vertical exaggeration (scale in meters). Dark bands in the cross-sectional profile diagrams show the maximum tidal range occurring at the highest spring tides.

additional data appears to reinforce, rather than alter, the observed trends in the shorter duration dataset for the dredged channel and therefore, have been included.

a) Water surface elevation

The asymmetry of the wse curves persists under the dredged conditions (Figure 30). However, cross correlations of the wse for the two scenarios indicates that only at the mouth are the curves identical (correlation coefficient of 1.0000). Close examination of the tidal range indicates that the amplitude of the wave is noticeably smaller under the dredged conditions. Furthermore, a plot of the ranges from the baseline conditions against those from the dredged conditions reveals that the change in the attenuation of the wave is greatest from the Mouth to Station 1 (Figure 31). Table 8 lists the values of the slope from a linear regression of the plotted points.

The decrease in the tidal range when compared to the baseline conditions consequently increases hydraulic gradients. Figure 32 shows a plot of the hydraulic gradient and the change in range (Δ range) between the Mouth and Station 1, where the greatest Δ range has occurred. Positive values represent hydraulic gradients of rising water and a change in range at high water. Negative values represent hydraulic gradients of falling water and a change in range at low water. Hydraulic gradients are seen to have increased in both the flood and ebb direction. However, in the ebb direction the change in range produces significantly larger hydraulic gradients, increasing the potential for greater magnitude ebb flows.

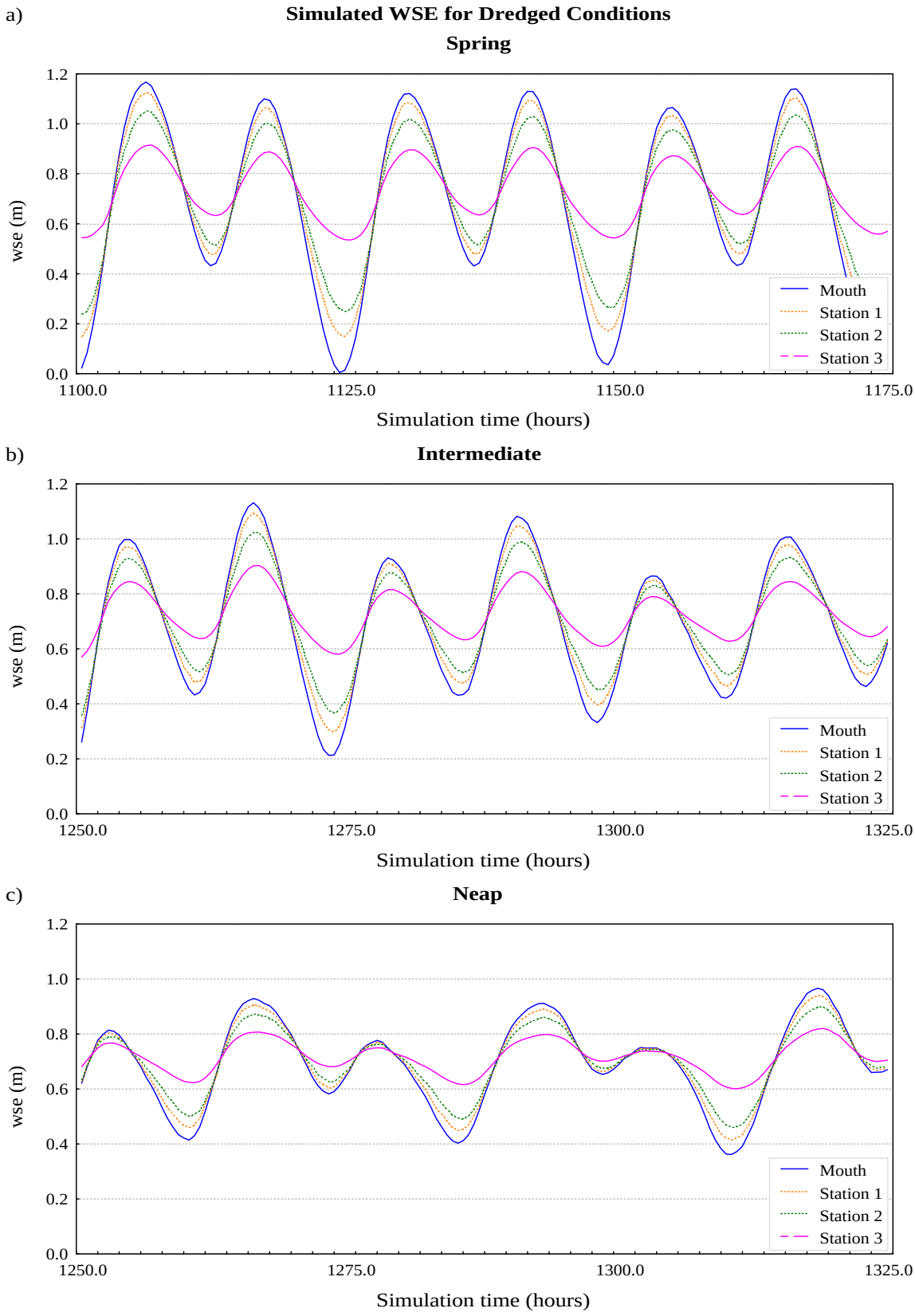

Figure 30 Three consecutive segments of the water surface elevation output for a) spring, b) intermediate, and c) neap tides using the hypothetical dredged bathymetry.

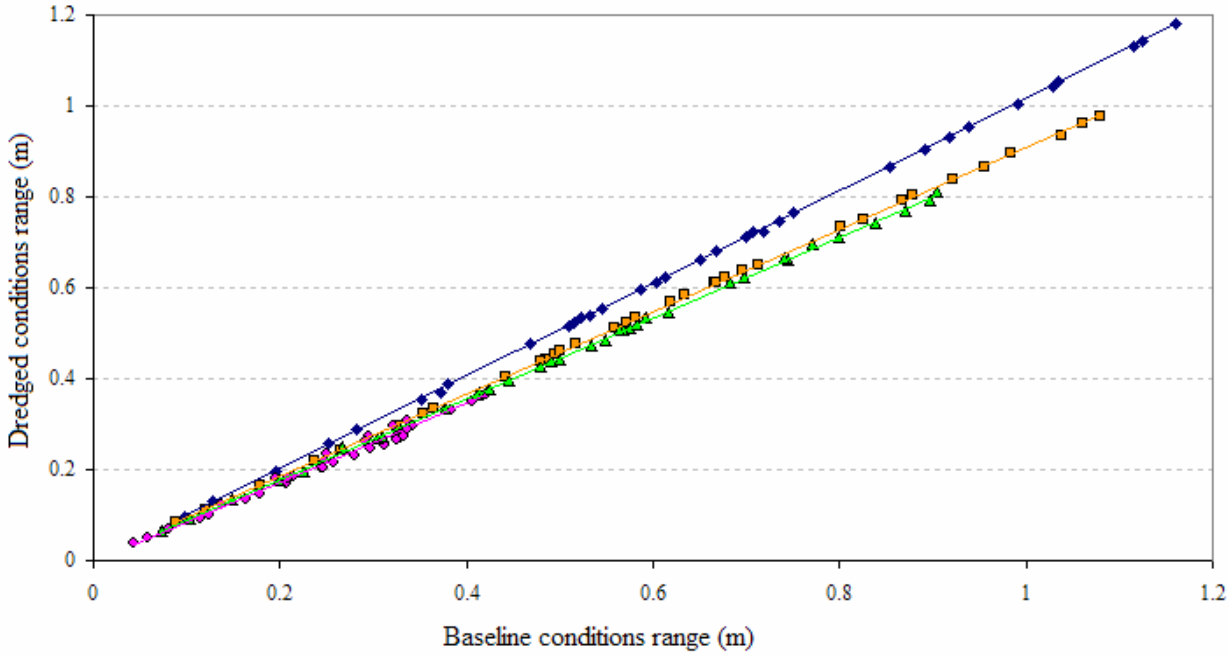

Figure 31 The dredged conditions tidal range (amplitude) plotted against the baseline conditions tidal range for all four stations. Wave amplitude, which creates the hydraulic gradient as it enters the channel, is less in the dredged channel.

Table 9 Slope values for the linear regression of the points shown in Figure 29.

	Mouth	**Station 1**	**Station 2**	**Station 3**
$\frac{R_{dredged}}{R_{baseline}}$	1.00	0.90	0.89	0.88

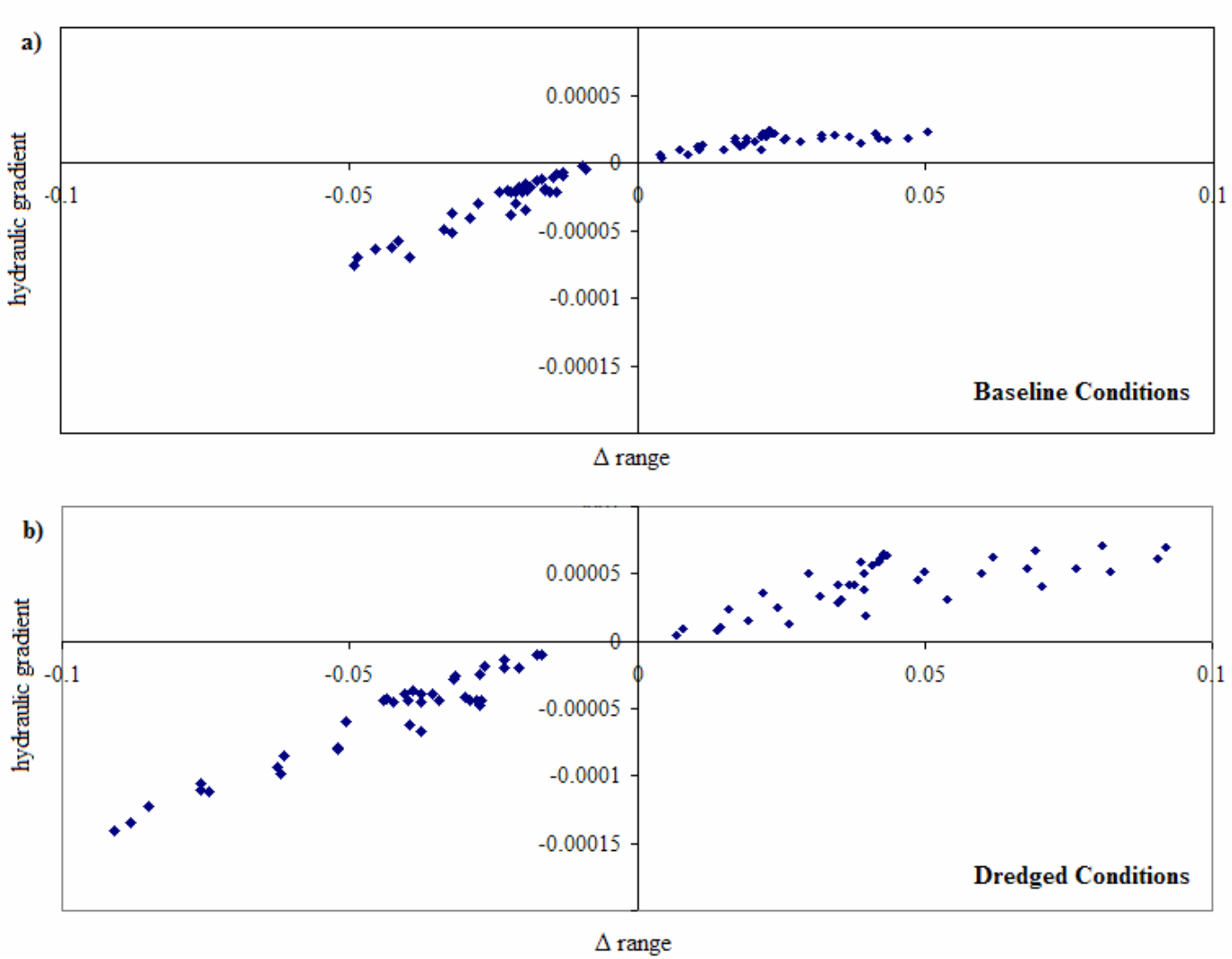

Figure 32 The hydraulic gradient and the change in range (Δ range) between the Mouth and Station 1 are plotted for the baseline and dredged conditions. Only points for the Mouth to Station 1 have been plotted because the change in range was the greatest between these stations. Positive values represent hydraulic gradients of rising water and a change in range at high water. Negative values represent hydraulic gradients of falling water and a change in range at low water. Greater change in ranges have created larger hydraulic gradients in the dredged conditions increasing the potential for greater magnitude flows.

b) Current velocities

The increased water depth has caused a shift in the peak tidal currents to be more in phase with high and low water. At the Mouth and Station 1 the peak current velocities occur just before the crest of the wave enters the Itajuru Channel as in the baseline conditions; however, the peak velocities are sustained for a much greater period only decreasing as the wse begins to drop (Figure 33). At Stations 2 and 3 peak currents occur in phase with high wse. As the wse begins to drop, flow deceleration occurs until slack water when all stations are at mean sea level simultaneously. Although the hydraulic gradient is eliminated at this point, slack water does not occur simultaneously because of inertia. Owing to the deeper channel at low water, flow retardation is reduced resulting in peak ebb current velocities in phase with the tidal wave trough and are of greater magnitude.

Current velocities are observed to increase during both spring and neap cycles (Figure 34). When comparing peak values to the baseline conditions, the flood current velocities are an average of 13% greater, whereas ebb current velocities are an average of 46% greater. This larger increase in the ebb directed flows has important implications on the flood dominant current asymmetry observed in the baseline conditions.

Cross correlation comparing the baseline and dredged conditions current velocities were done to quantify any changes that have occurred. The Mouth and Station 1 show highest correlation values at a lag of -1, demonstrating that the peak velocities occur approximately 0.5 hours later in the dredged conditions. Increases in the hydraulic

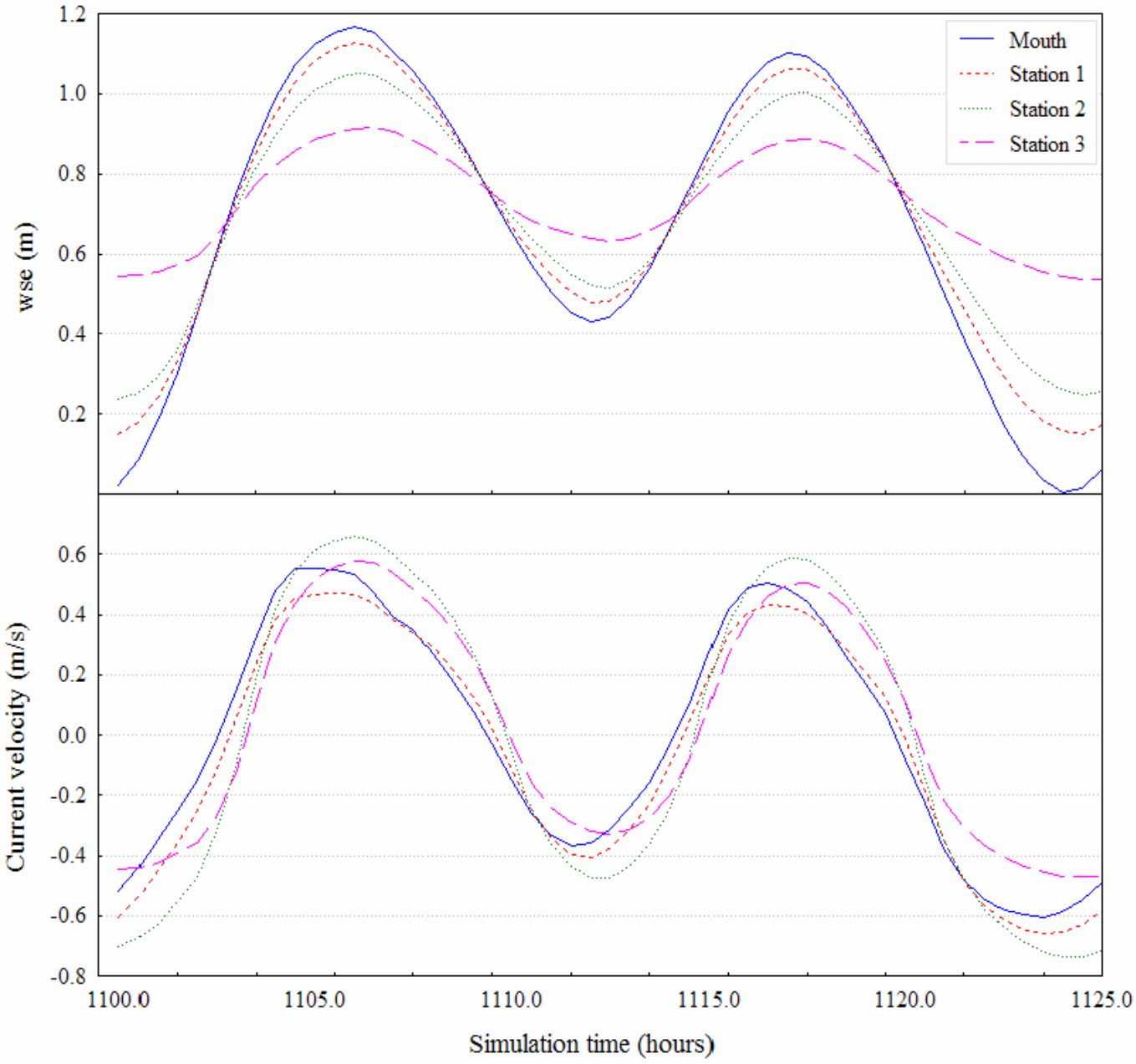

Figure 33 The water surface elevation and current velocity magnitudes are plotted together to illustrate the flow structure of the progressive tide in the Itajuru Channel during spring cycle under the dredged conditions.

a)

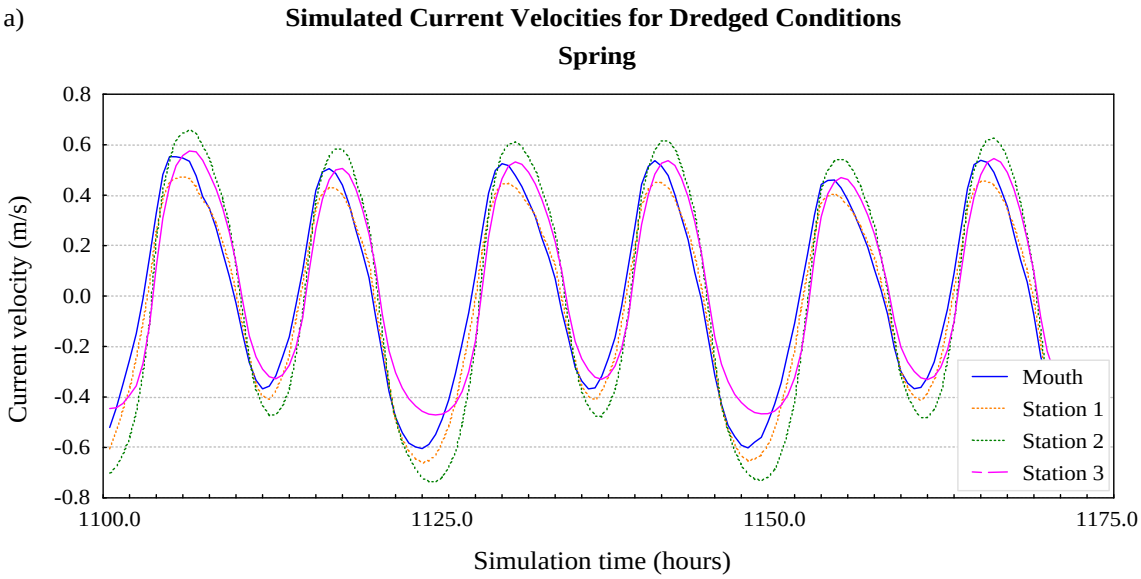

b)

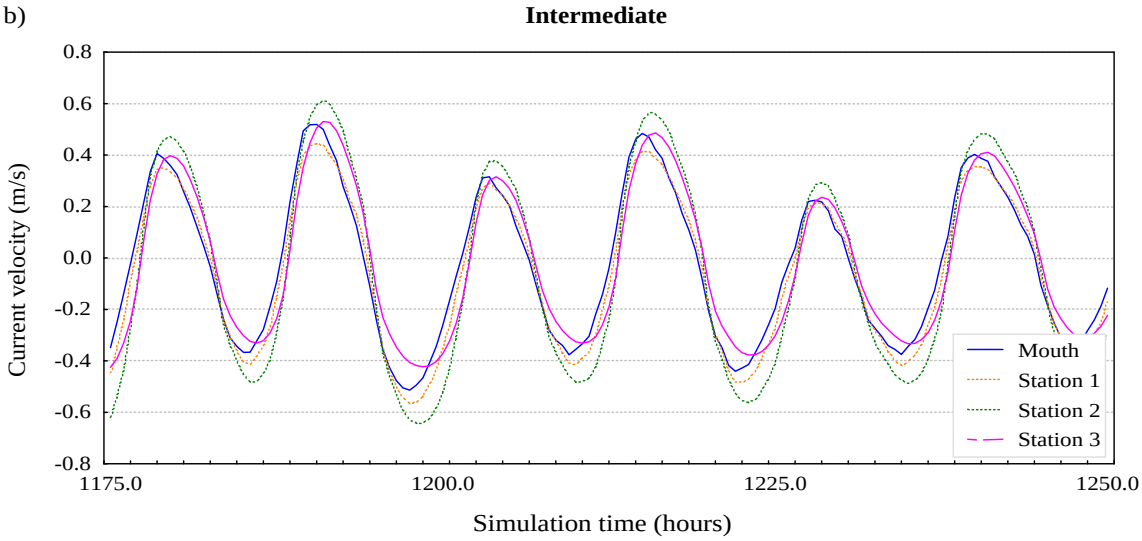

c)

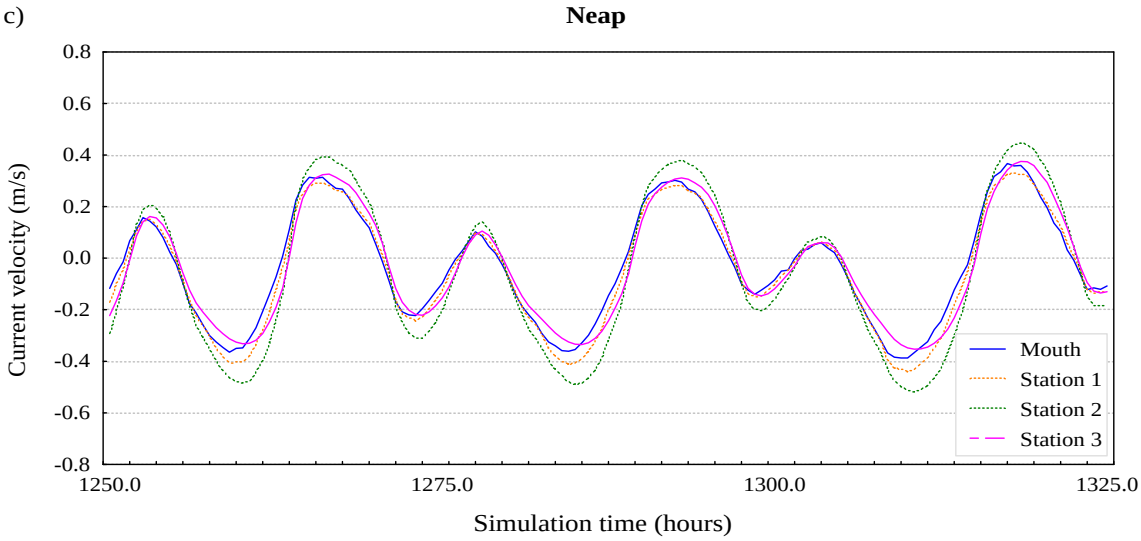

Figure 34 Three consecutive segments of current velocity magnitude output for a) spring, b) intermediate, and c) neap tides using the dredged conditions bathymetry.

gradient result in a longer period of flow acceleration. Thus the peak velocities are reached later and more in phase with the wse. The increase in tidal celerity and efficiency with which water can be conveyed appears to dominate the change in flow velocity magnitudes, particularly at low water.

Figure 35 plots the hydraulic gradient and the current velocity for the dredged conditions. In the flood direction, current velocities are seen to increase as the hydraulic gradients increase similarly to what was seen in the baseline conditions. In the ebb direction, the threshold value that apparently was limiting the magnitude of ebb flows has now increased. The reduction of channel friction due to increased channel depth has changed how the velocities are limited. This is most evident between Station 2 and 3 where the curve has shifted to the left indicating large flow velocities.. The same change in the trend is apparent between Station 1 and Station 2. The increased water depth at low water has reduced frictional forces on the flow, reducing the restriction on the flow velocity observed in the baseline conditions (Figure 21).

c) Water flux

Water fluxes are significantly greater in magnitude due to the increased conveyance capacity of the dredged channel (Figure 36). Like the baseline conditions, rising tide fluxes generally have greater peak magnitude compared to subsequent falling tide fluxes. Up channel lag of the peak magnitudes has decreased due to the increase in speed with which the tide propagates up the channel.

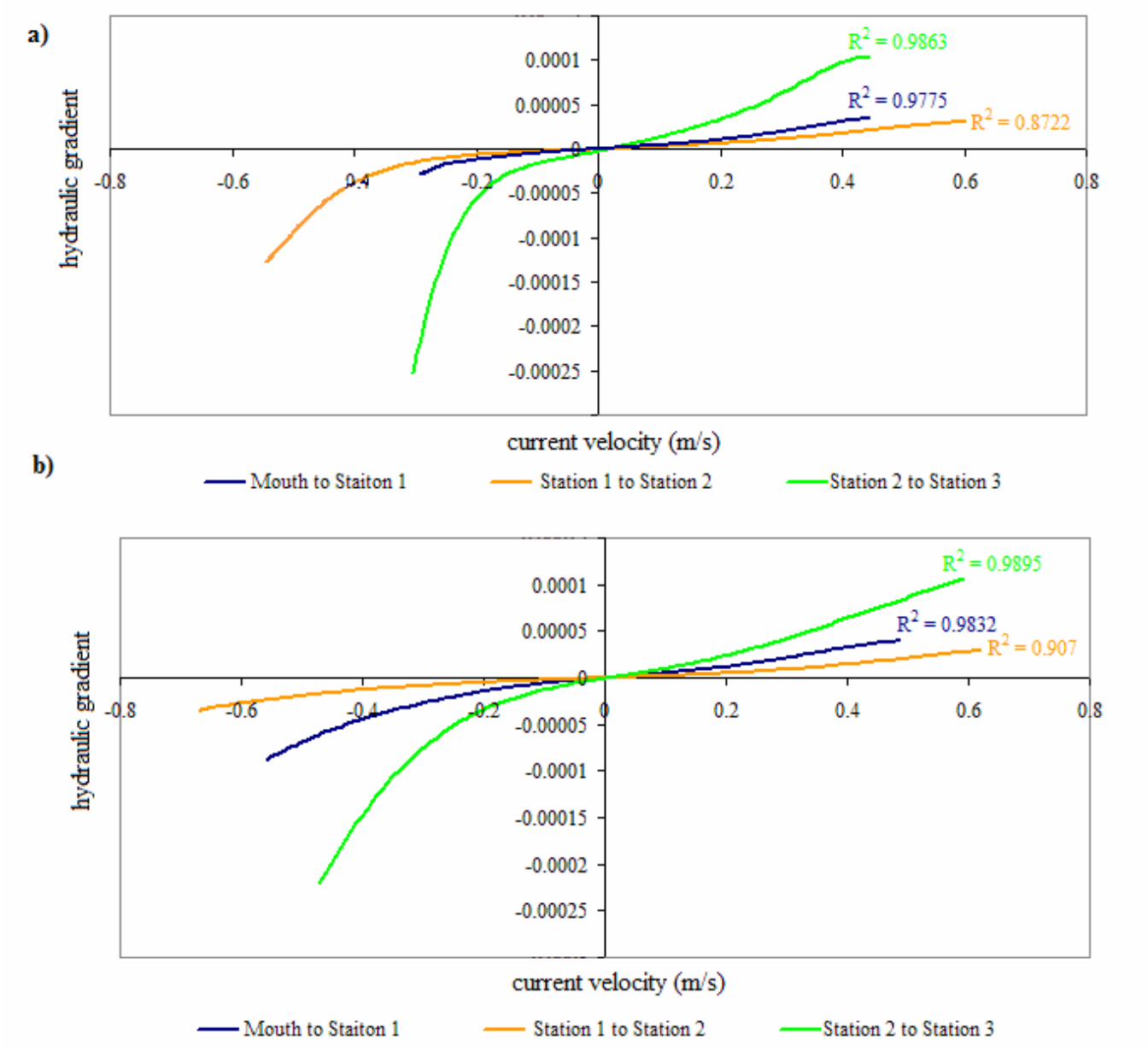

Figure 35 The hydraulic gradient is plotted with the current velocity for the a) baseline conditions (Figure 21 reprinted here for convenience) and b) dredged conditions. Positive values represent hydraulic gradients of rising water and flood directed currents. Negative values represent hydraulic gradients of falling water and ebb directed currents. A 6th order polynomial regression trendline represents the data with R^2 values shown. Ebb directed hydraulic gradients are shown to be able to produce greater magnitude ebb directed currents than those present in the baseline conditions.

a)

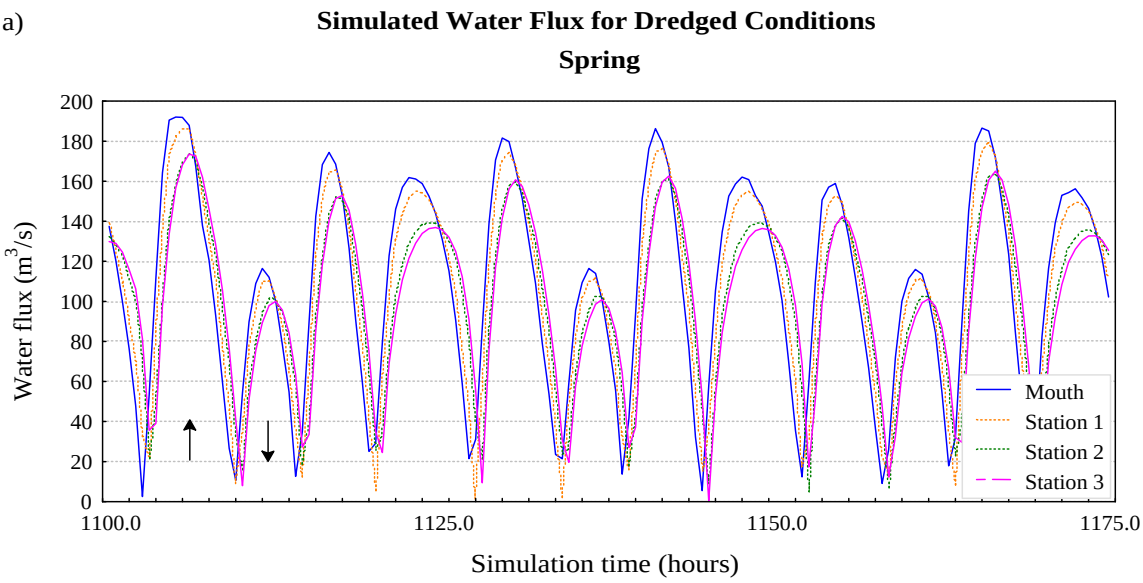

b)

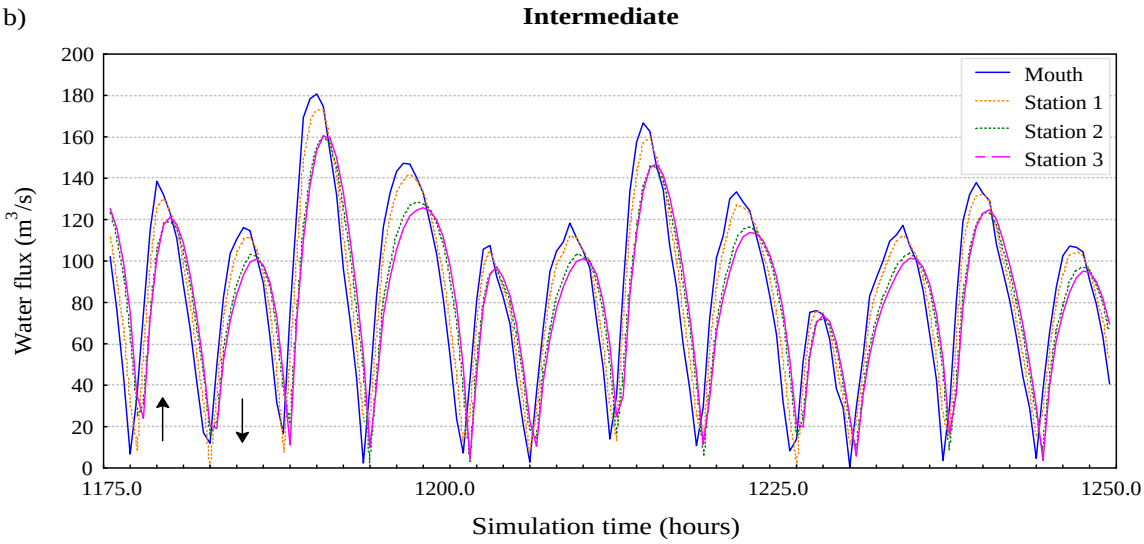

c)

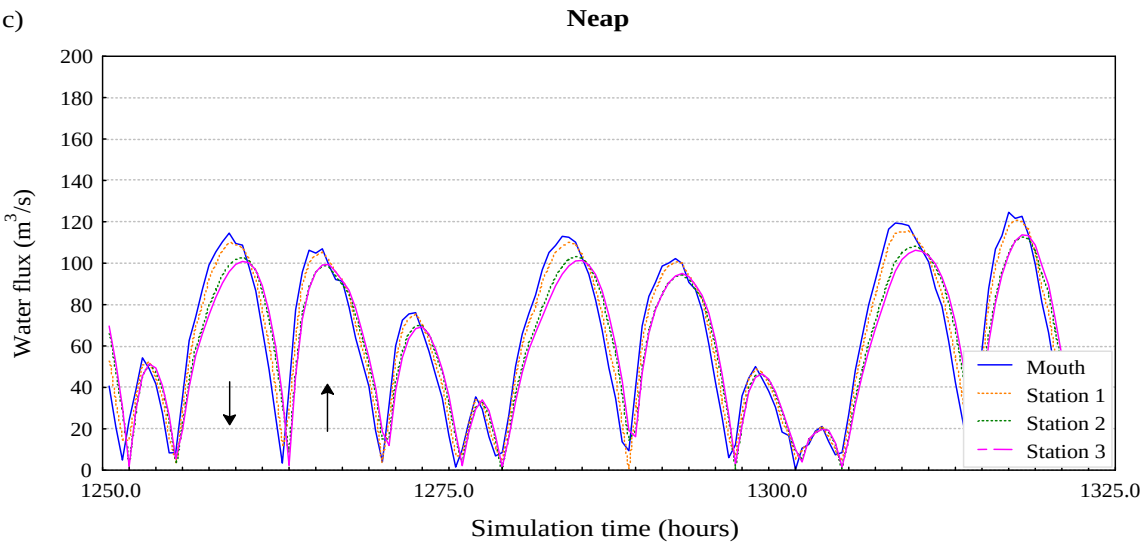

Figure 36 Three consecutive segments of water flux output for a) spring, b) intermediate, and c) neap tides using the dredged conditions bathymetry. Arrows indicate rising (up arrow) or falling (down arrow) tide.

d) Tidal wave distortion and duration asymmetry

The distortion of the tidal wave in the dredged channel is still present but of reduced magnitude. The duration ratio for the dredged channel is plotted against the low water elevation in Figure 37a. Of the 356 duration ratios, 90% of the values are less than 1, indicating that despite the increased depth in the channel, the rising tide durations are generally less than the falling tide durations. A small increase in the variation in the data is noticeable in the plot of mean values in Figure 37b, however, this is primarily due to the increased quantity of data and not the change in channel conditions. By examining the mean values of the duration ratio the increasing distortion of the tidal wave is shown to follow the same trend as that in the baseline conditions where maximum distortion occurs at Station 3.

The cross correlation of the wse curves shows that the wave distortion is measurably reduced with a deeper channel (Figure 38). Since the celerity of the tidal wave is related to the depth of the channel (Equation 1), the dredged configuration is more efficient at conveying water because the tidal wave can propagate through the channel at a faster rate. During rising tides the peak wse appears to occur simultaneously at all stations; however, in reality this indicates the crest of the wave is propagating faster than the model can detect at the present 0.5 hour time resolution. The tidal lag is only seen during falling tide where the shallower channel is reducing the speed of the wave trough sufficiently to be detected.

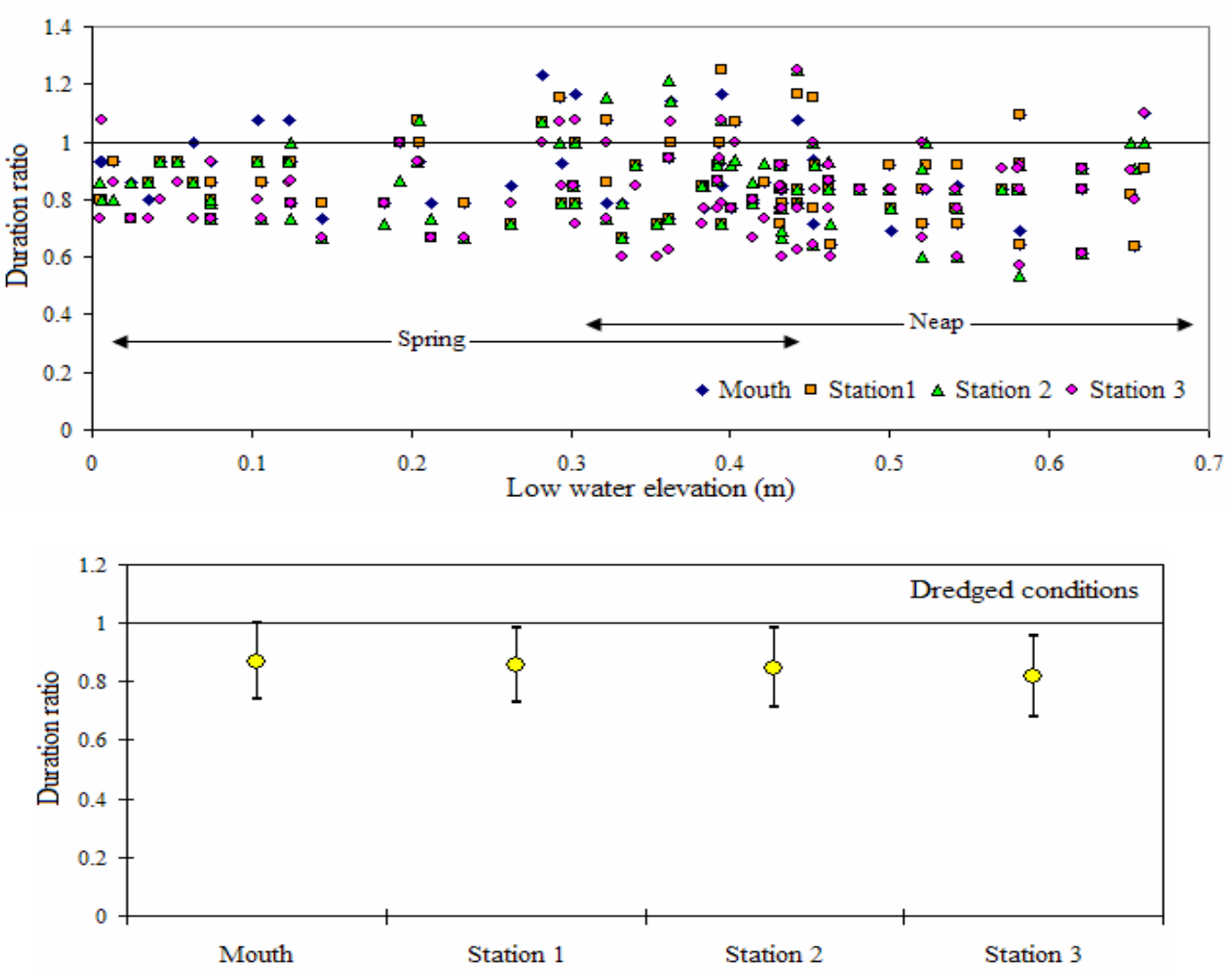

Figure 37 a) Duration ratios (rising tide duration/falling tide duration) is plotted against low tide level . Arrows indicate the range of values within spring and neap cycles. Of the 356 points, 321 (90%) are less than 1 indicating that a majority of the tidal cycles have shorter flood durations compared to subsequent ebb durations. b) Mean values with error bars representing the distribution (±σ) around the mean.

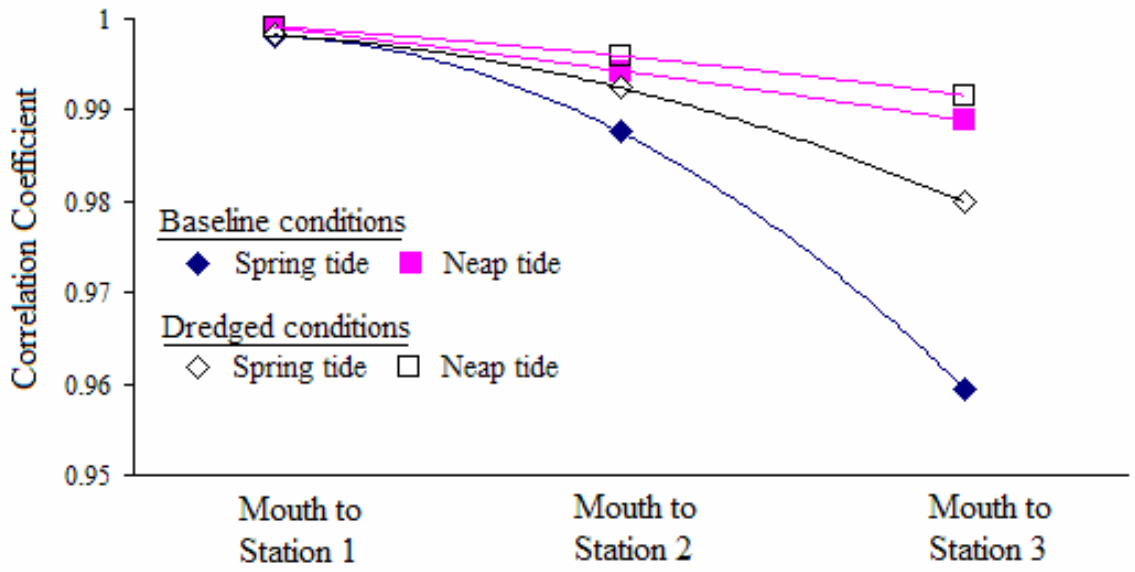

Figure 38 Cross-correlation coefficients comparing wse curves at different data stations become progressively smaller up the channel due to tidal wave distortion. The open points represent the correlation coefficients for the dredged channel. Wave distortion is shown to be reduced using the dredged conditions bathymetry.

e) Current velocity magnitude asymmetry

The strong relationship between peak current velocity and tidal range in the baseline conditions diminishes in the dredged scenario (Figure 39). No clear trend emerges when comparing the flood and ebb magnitudes at different stations. However, at Station 1 the ebb current velocities tend to be slightly stronger than flood velocities at similar ranges. The Mouth and Station 2 show significantly greater variation in the peak current velocity values at various ranges. Considering the channel bathymetry was unchanged at the Mouth, the reason for the significant change in trend and variation is unclear. However, at Station 2 the adjacent bathymetry was significantly changed and thus flow velocities approaching the data station would be increased.

Increased variation in the current ratio magnitudes for the dredged conditions is shown in Figure 40 where 59% of the current ratios have values of less than 1 (ebb dominance). No clear trends are apparent for the estuary as a whole. However, some trends are present upon examination of individual stations. The Mouth and Station 1 have primarily ebb dominant current ratios during spring tidal cycles. Greater variation and an increase in the current ratio values appears in intermediate and neap tide cycles. Conversely, Station 2 has flood dominant current ratios during spring tides but exclusively ebb dominant ratios during neap. Mean values of the current ratio show that the generally flood dominant conditions that were present in the baseline conditions are not present in the dredged scenario.

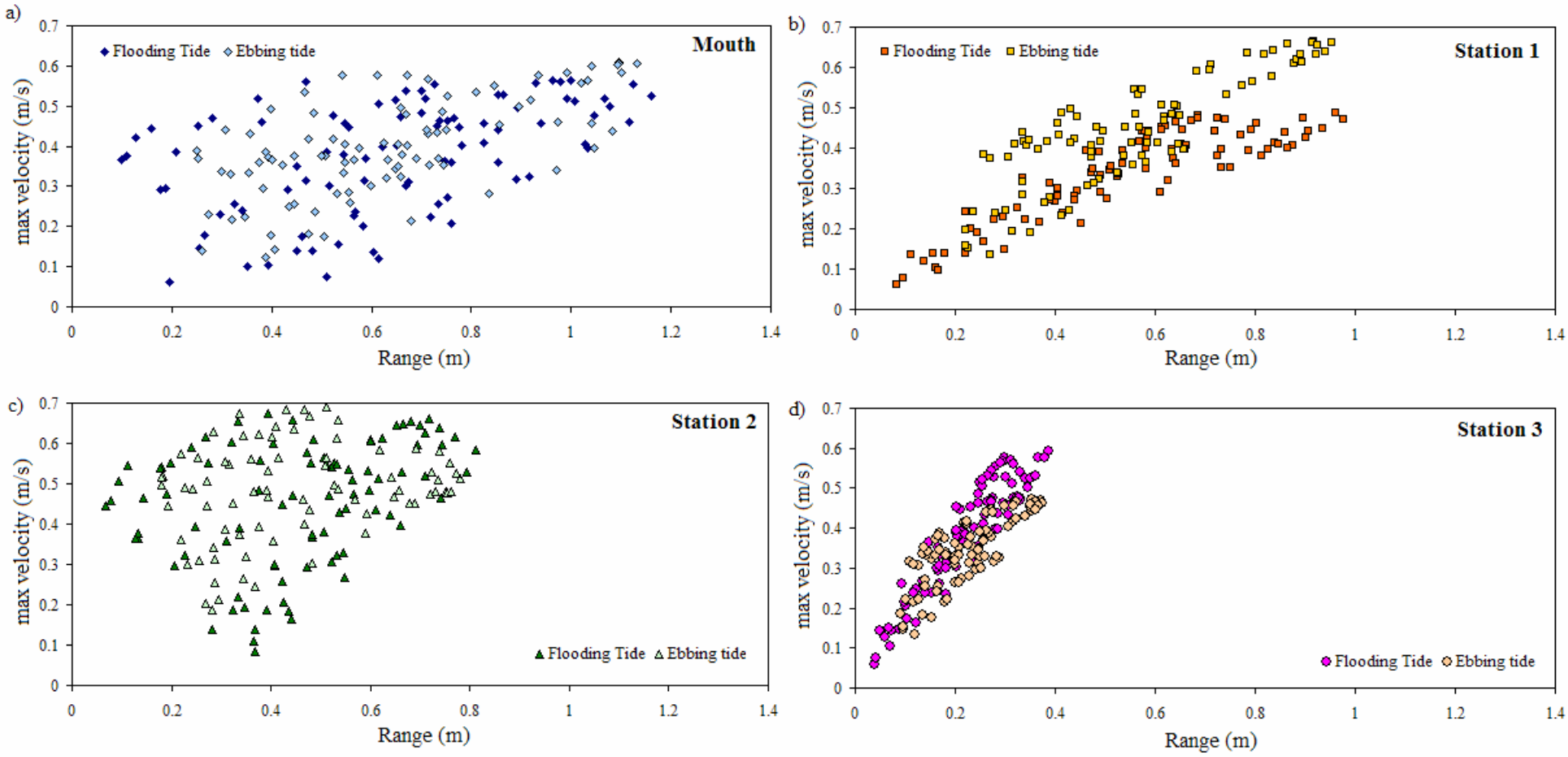

Figure 39 Peak current velocities are plotted with tidal range at all stations. At the a) Mouth, c) and Station 2 variation has significantly increased because of the dredged channel bathymetry. At Station 1 (b), peak ebb currents are now greater than the flood currents at various ranges.

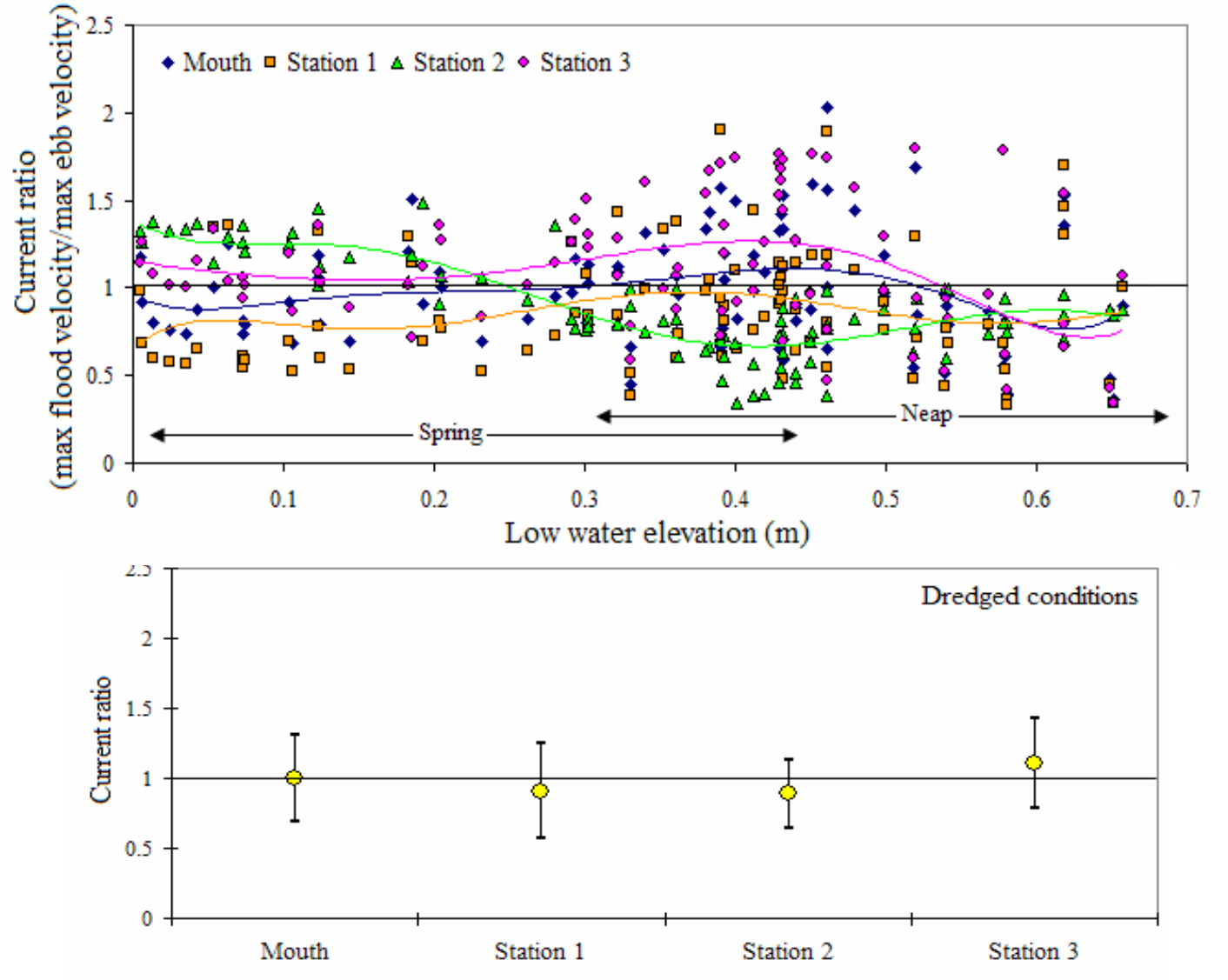

Figure 40 a) Current ratios (maximum flood current/maximum ebb current) are plotted against low tide level. Arrows indicate the range of values within spring and neap cycles. Of the 356 points, 210 (59%) are less than 1 indicating that a shift toward less asymmetrical current magnitudes has occurred using the dredged conditions bathymetry. Sixth order polynomial regression lines are included to show the trend at each station. b) Mean values with error bars representing the distribution (±σ) around the mean.

The positive relationship between the short duration rising tide and flood dominant current ratios is no longer present in the dredged scenario. Greater increases in the ebb current velocities when compared to flood current velocities have reduced the current magnitude asymmetry. Figure 41 plots the duration ratio against the current ratio and shows that 51% of the points can be described as having shorter relative flood durations and greater magnitude ebb current velocities.

f) Sediment transport implications

The increase in both ebb and flood velocities cause greater sediment flux over individual tidal cycles. Additionally, flow velocities are greater than the threshold of entrainment (0.2 m/s) for longer periods and as such potentially transport more sediment in a single tidal cycle. Net values of sediment transport indicate that over the period examined the estuary has a slight ebb directed sediment flux. The dredged channel sediment flux estimates are shown in Table 10. The largest magnitude flux appears at Station 1 where the channel still narrows during low low water. Only at Station 3 do positive sediment flux values persist. This result suggests that the hypothetical dredging of the Itajuru Channel has reduced the flood dominant transport of sediment to levels where the channel can potentially stabilize.

Table 10 The summation of the cube of the velocity vector magnitudes produces sediment flux estimates listed for the four data stations using the dredged conditions bathymetry.

	Mouth	**Station 1**	**Station 2**	**Station 3**
Estimated Sediment flux	-0.15	-2.26	-0.89	+0.69

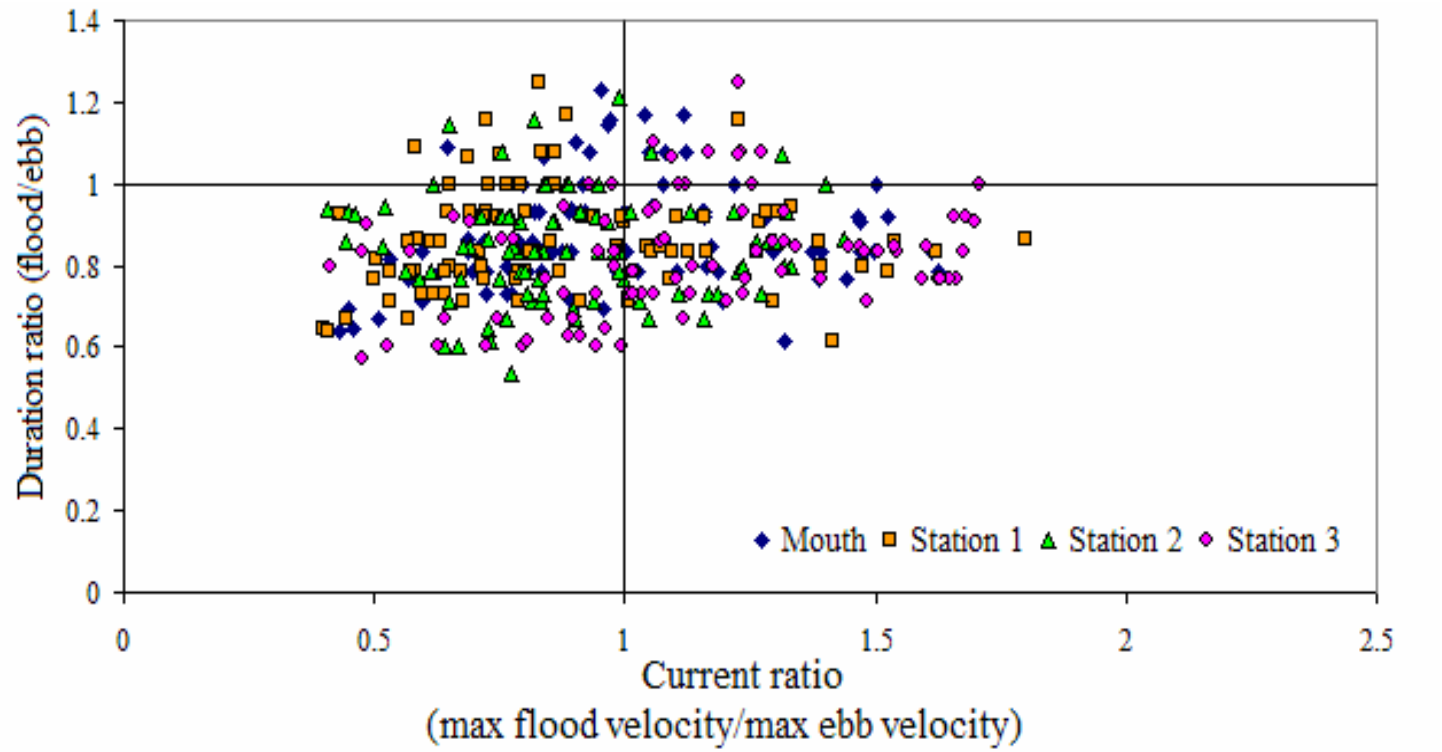

Figure 41 Duration ratio is plotted against the current ratio showing that 59 % of the points have longer duration, faster falling tide compared to the subsequent rising tide.

Summary

The hypothetical dredging of the channel appears to have significant implications for the Itajuru Channel dynamics. Increasing the depth of the channel has the effect of dramatically increasing the ebb flows at low water levels to a much greater extent than the effect on flooding flows at high water levels. Thus, the flood dominance that was observed in the baseline conditions is diminished when the channel is dredged.

The results of the sediment transport analysis suggest that the Itajuru Channel could be deepened to achieve long-term stability. However, it is more likely that the effect of a dredging operation such as this would only be temporary. The predicted net ebb directed transport is relatively small at all locations. However, the flux of sediment over individual tidal cycles due to the increased current velocities is significantly greater than in the baseline conditions. Thus, settling and scour lag effects would be magnified in the dredged conditions resulting in transport likely to still favour the flood direction.

CONCLUSIONS

i) Hydrodynamic Modelling

The RMA2 model has been successfully implemented for the Itajuru Channel, where water surface elevation and current velocity magnitude data were available for validation. The model calibration was performed by comparing the model output with the field data using statistical techniques to measure the correlation of the two datasets. The model was further verified through examination of the output results with estimates of the tidal prism. The model validation showed, on average, very good agreement between the measured field data and the simulation output.

Using the model results, the characteristics of the tide, current magnitudes, water flux, duration and current magnitude asymmetry, and implications for sediment transport were presented and discussed in detail. Additionally, the construction of the finite element mesh provides an adaptive and functional experimental tool to access baseline estimates of the estuarine volume, surface area, and mean and localized water depth distribution. Furthermore, the utility of the model to investigate hypothetical scenarios of anthropogenic (i.e. dredging) or natural (i.e. higher mean sea level predicted by climate change models) changes of the estuarine hydrodynamics remains largely unexplored.

The important parameters presented for the baseline tidal dynamics include a distinctive form of the tidal asymmetry in the tidal phase durations and current velocity magnitudes. Flood durations are consistently shorter than the subsequent ebb durations. When the rising tide is of shorter duration than the falling tide, flood velocities often are greater because of continuity. Asymmetry in the current magnitudes is characterized by flood velocities that are up to 92% greater than ebb velocities.

The origin of the tidal asymmetry can be attributed to the depth distribution along the channel causing varying frictional effects and attenuation of the tidal wave as it enters the mouth of the Itajuru Channel. Evaluation of the hydraulic gradient at low and high water reflect the potential cause of the flood dominant asymmetry, where ebb flow magnitudes are limited by frictional effects of a shallower channel. The ebb directed hydraulic gradient is seen to be significantly larger than the flood directed hydraulic gradient, yet does not result in faster flows.

The morphologic response to a flood dominated current regime is evident in the large sand shoals shown in the aerial photograph of the Itajuru Channel (Figure 2b) and historical anecdotal evidence of internal sedimentation. Marine sediments in proximity of the mouth are transported into the estuary due to the stronger flood currents caused primarily by the duration asymmetry. Additionally, net sediment transport is also related to the water surface elevation. The ability of the channel to transport sediment is, in part, related to the channel cross-sectional profile with respect to high and low water levels. Peak ebb flows occur in phase with low water when the channel is narrower. Thus, the available volume of sediment to be potentially transported is less during low water than during high water because the wet surface area of the estuary is significantly smaller. The ebb transport capacity is reduced for much of the peak flow duration.

Although the model is considered to be able to represent the hydrodynamic conditions of the channel well, some limitations should be highlighted. The model appears to be only representing the hydrodynamics of the Itajuru Channel well. Results obtained for the Lagoa de Araruama wse and flow velocities were not included because

of poor agreement with field data. Further investigation into why the model is functioning poorly inside the lagoon is certainly required.

The model runs were of relatively short duration and therefore limit the scope of the results presented. Trends that have been discussed need to be confirmed with longer simulation runs. For example, the effect of range inequality is unclear without additional data to examine. Lessa (2000) stresses that classification of a shallow estuary as flood or ebb dominant should take into account the hydrodynamic regime during extreme tidal events. This has not been done with the short simulation conducted. Furthermore, Fortunato and Oliveira (2005) warn that predictions of estuarine morphodynamics based on short-term simulations are potentially misleading. Despite the potential for misinterpretation due to the short datasets, the output appears to be a reasonable representation of the Itajuru Channel and the consistency between the results for the two experimental scenario data sets (600 simulated hours and 1100 simulated hours) is promising.

The relatively low resolution time step of 0.5 hours prevented a more robust quantitative measure of the wave distortion. A time step of 0.25 hours may achieve a better balance between computational time and the utility of the model output.

And finally, the major assumption that the instantaneous adjustment of the sediment flux to the transport capacity is unrealistic. Hoekstra and Maren, (2004) found that the suspended load transport rate is not only influenced by the degree and orientation of the maximum flow asymmetry, but also by the asymmetry of the flow acceleration. Asymmetries in maximum flow velocities are capable of generating residual transport of suspended load that is approximately five times larger than that caused by lag effects in

symmetrical flow. Thus, evaluation of settling and scour lag effects on the sediment flux and incorporation of a morphodynamic model that can estimate sediment flux more accurately would be an appropriate addition to the current model.

ii) Anthropogenic stress

Historical documents and bathymetric data spanning 400 years indicate that internal sedimentation has been occurring since the 16th century, possibly as a result of anthropogenic stress. The restriction of the channel mouth between 1615 and 1880 effectively reduced the cross-sectional area causing the hydrodynamics to strongly favour flood dominant sediment transport. Reclamation of the intertidal area, the construction of salt evaporation ponds, and the urban development along the estuary margins further enhanced the potential for internal sedimentation. Thus, the modelling of an anthropogenic stress on the Itajuru Channel to improve the circulation in the channel and diminish the flood dominant asymmetry seems appropriate.

The hypothetical dredging scenario is shown to have significant effects on the estuarine hydrodynamics. The modification of the bathymetric data was done to emulate dredging proposals that have been presented in local media sources (Freitas, 2004). The results demonstrate that the duration asymmetry that characterized the tidal wave in the baseline conditions is still present when there is a deeper channel. Comparisons of the tidal wave in the dredged scenario with the baseline conditions show that the wave distortion is reduced. The deeper channel allows the wave trough to propagate faster than in the baseline conditions, reducing the distortion.

The amplitude of the wave was shown to be reduced with a deeper channel, particularly between the Mouth and Station 1. The modelling results of Boon and Byrne

(1981) indicate that when impedance at the mouth of a tidal inlet is reduced the tidal range observed in the channel should increase (Figure 8). Assuming that the deeper channel near the mouth of the Itajuru Channel reduced the impedance when compared to the baseline conditions, the range observed at Station 1 should have increased. Thus, the observed decrease in range does not agree with the Boon and Byrne (1981) model. It appears that the range reduction observed in the Itajuru Channel model output is related to the increased flow capacity of the channel and the faster propagation of the tidal wave. The lag of the peak wse that was detected in the baseline conditions between the Mouth and Station 3 is reduced in the dredged scenario demonstrating faster propagation of the peak wse. Thus, the shape of the tidal wave is broader, spreading the water over a larger area and effectively reducing wave amplitude. This could be confirmed by examination of the wse in the lagoon when it is appropriately calibrated.

The change in range is shown to be representative of the change in hydraulic gradient. Thus, the smaller tidal wave amplitude in the dredged conditions equates to a larger hydraulic gradient between data stations in both the flood and ebb directions. Since hydraulic gradients ultimately drive the flow of water in the Itajuru Channel, there is greater *potential* for increased current velocities.

The flood dominant current asymmetry that normally accompanies shorter duration rising tides is no longer present in the dredged conditions. Olievera et al. (2006) also found that dredging operations to deepen the channels in the Patos Lagoon, Portugal increased tidal prisms and reduced the flood dominance causing internal sedimentation. Current velocities in the Itajuru Channel were shown to have increased 13% in the flood

direction and 46% in the ebb direction. Consequently, the flood dominant asymmetry is eliminated due to a greater increase in the ebb directed current velocities.

The change in the hydraulic gradient, which created the potential for faster flows, caused increased current magnitudes in both directions, but more so in the ebb direction. The dramatic increase in the ebb directed flow is attributed to the increased channel depth. Friction is reduced and faster flows are observed. Therefore, in agreement with the modeling results of Freidrichs and Aubrey (1988), the tidal amplitude to depth ratio appears to be the critical factor in determining the magnitude of tidal asymmetry in Itajuru Channel.

The elimination of the current magnitude asymmetry in the dredged scenario reduces the predicted net sediment transport. However, sediment fluxes over individual tidal cycles would increase due to the greater current velocities. Further investigation into the dynamics of sediment transport and the importance of settling and scour lag need to be addressed before concluding that the predicted low ebb directed net sediment flux would imply long-term channel stability.

DIRECTIONS FOR FUTURE STUDY

Based on the limited field data for model calibration and the largely untapped potential of the Itajuru Channel hydrodynamic model, the following directions for future study are proposed:

1. Further model validation is required to supplement the calibration procedure presented herein. Field data sets were relatively short in duration and should include more than one tidal cycle. Thus, a supplementary field campaign is proposed to collect wse and current velocity data for a consecutive period ranging from spring to neap.
2. Investigation into the poor performance of the model with respect to the field data collected in the Lagoa de Araruama is required before the model can be considered complete.
3. The construction of a second finite element mesh representing the bathymetric conditions described in the historical record prior to colonization would provide the context with which to test the speculative hypothesis that a hydrodynamic switch from ebb to flood dominance occurred as a direct consequence of the anthropogenic stresses that have occurred over the past 400 years.
4. Implementation of the morphodynamic model (SED2D module) available for SMS 8.1 and RMA2 would provide greater insight into the sedimentation patterns that exist in the Itajuru Channel since static bathymetries are unrealistic in dynamic environments.
5. Further investigation into dredging scenarios that maximize the natural effects of the feedback mechanisms between the hydrodynamics and morphodynamics

would be of particular value to find sustainable management strategies for estuarine harbours in the context of the increasing socio-economic demands on these environments.

REFERENCES

Aldridge, J. N. (1997). Hydrodynamic Model Predictions of Tidal Asymmetry and Observed Sediment Transport Paths in Morecambe Bay. *Estuarine, Coastal and Shelf Science, 44*, 39–56.

Arcement, G., & Schneider, V. (1989). *Guide for Selecting Manning's Roughness Coefficients for Natural Channels and Flood Plains* (Water Supply Paper 2339): United States Geological Survey.

Aubrey, D. G., & Speer, P. E. (1985). A Study of Non-Linear Tidal Propagation in Shallow Inlet/Estuarine Systems Part I: Observations. *Estuarine, Coastal and Shelf Science, 21*, 185-205.

Bertin, X., Chaumillon, E., Sottolichio, A., & Pedreros, R. (2005). Tidal inlet response to sediment infilling of the associated bay and possible implications of human activities: the Marennes-Oleron Bay and the Maumusson Inlet, France. *Continental Shelf Research, 25*, 1115 - 1131.

Boon, J. D., & Byrne, R. J. (1981). On basin hyposmetry and the morphodynamic response of coastal inlet systems. *Marine Geology, 40*, 27-48.

Burau, J. R., & Cheng, R. T. (1989). *A general method for generation bathymetric data for hydrodynamic computer models* (Open file report 89-28): United States Geological Survey.

Byrne, R. J., & Boon, J. D. (1976). *Speculative hypothesis on the evolution of barrier island-inlet-lagoon systems, 2. A Case Study* (Abstract): Geological Society of America Annual Meeting, 8:159.

Castaing, P., & AlIen, G. P. (1981). Mechanisms controlling seaward escape of suspended sediment from the Gironde: A macrotidal estuary in France. *Marine Geology, 40*, 101-118.

Cheng, R. T., Casulli, V., & Gartner, J. W. (1993). Tidal, Residual, Intertidal Mudflat (TRIM) Model and its Applications to San Francisco Bay, California. *Estuarine, Coastal, and Shelf Science, 36*, 235-280.

Cunha, M. (2004). *Uma Historia de Cabo Frio*. Rio de Janeiro: Editora Schwarcz Ltda.

de Claye, J. V. (Cartographer). (1574). *Le vrai pourtraict du geneure et du Cap de Frie* [Historical map].

Compania Brasileira de Dragagem. (Cartographer). (1985). *Sobdagam Batimetrica do Canal de Itajuru - Folhas 1,2, and 3* [Bathymetric chart].

Dronkers, J. (1986). Tidal Asymmetry and Esturine Morphology. *Netherlands Journal of Sea Research, 20*(2/3), 117-131.

Elias, E., Stive, M., Bonekamp, H., & Cleveringa, J. (2003). Tidal Inlet Dynamics in Response to Human Intervention. *Coastal Engineering Journal, 45*(4), 629-658.

Fernandes, E. H. L., Dyer, K. R., & Moller, O. O. (2005). Spatial Gradients in the Flow of Southern Patos Lagoon. *Journal of Coastal Research, 21*(4), 759-769.

Fitzgerald, D. M., Buynevich, I. V., Fenster, M. S., & McKinlay, P. A. (2000). Sand circulation at the mouth of a rock-bound, tide-dominated estuary. *Sedimentary Geology, 131*, 25-49.

Fitzgerald, D. M., Nummedal, D., & Kana, T. W. (1976). Sand Circulation patterns at Prince Inlet, South Carolina. *Proc. 15th Conference on Coastal Engineering, A.S.C. E.*, 1868-1880.

Fortunato, A. B., & Oliveira, A. (2005). Influence of Intertidal Flats on Tidal Asymmetry. *Journal of Coastal Research, 21*(5), 1062-1067.

Franco (1988) – *full reference pending*

Freitas, W. (2004, 21/06/2004). Serla anuncia obras na Lagoa de Araruama. *O Globo*.

French, J. R., & Clifford, N. J. (2000). Hydrodynamic modelling as a basis for explaining estuarine environmental dynamics: some computational and methodological issues. *Hydrological Processes, 14*, 2089-2108.

Friedrichs, C. T., & Aubrey, D. G. (1988). Non-linear tidal distortion in shallow well-mixed estuaries: a synthesis. *Estuarine, Coastal and Shelf Science, 27*, 521-545.

Friedrichs, C. T., Lynch, D. R., & Aubrey, D. G. (1992). Velocity asymetries in frictionally-dominated tidal embayments longitudinal and lateral variablity. In D. Prandle (Ed.), *Dynamics and Exchanges in Estuaries and the Coastal Zone* (pp. 37). Washington: American Geophysics Union.

Hoekstra, P. & Maren, B. (2004) Flow asymmetry associated with astronomical tides: implications for the residual transport of sediment. Conditionally accepted by the *Journal of Geophysical Research.* (Course notes: Dr. Bob Dalrymple, Surficial Processes, Queen's University, 2004)

King, I., Donnell, B. P., Letter, J. V., McAnally, W. H., & Thomas, W. A. (2005). *Users Guide to RMA2 WES Version 4.5*. Valhalla: Environmental Modeling Research Laboratory.

King, I. P. (1990). *Program Documentation - RMA2 - A Two Dimensional Finite Element Model for Flow in Estuaries and Streams*. Lafayette: Resource Management Associates.

Kjerfve, B., & Magill, K. E. (1989). Geographic and Hydrodynamic Characteristics of Shallow Coastal Lagoons. *Marine Geology, 88*, 187-199.

Kjerfve, B., Schettini, C. A., Knoppers, B., Lessa, G., & Ferreira, H. O. (1996). Hydrology and Salt Balance in a Large Hypersaline Coastal Lagoon: Lagoa de Araruama, Brazil. *Estuarine, Coastal, and Shelf Science, 42*, 701-725.

Lanzoni, S., & Seminara, G. (2002). Long-term evolution and morphodynamic equilibrium of tidal channels. *Journal of Geophysical Research, 107*(C1), 1-13.

Lessa, G., & Masselink, G. (1995). Morphodynamic evolution of a macrotidal barrier estuary. *Marine Geology, 129*, 25-46.

Lessa, G. C. (1990). *Dinamica de mare e transporte de sedimentos no Canal de Itajuru - Laguna de Araraumа.* Unpublished Dissertacao de Mastrado, UFRJ, Rio de Janeiro.

Lessa, G. C. (2000). Morphodynamic Controls on Tides and Tidal Currents in Two Macrotidal Shallow Estuaries, NE Austrailia. *Journal of Coastal Research, 16*(4), 976-989.

Lincoln, J. M., & Fitzgerald, D. (1988). Tidal Distortions and Flood Dominance at Five Small Tidal Inlets in Southern Maine. *Marine Geology, 82*, 133-148.

Masselink, G., & Hughes, M. (2003). *Coastal Processes and Geomorphology*. New York: Oxford University Press.

Medeiros, C., & Kjerfve, B. (2005). Longitudinal Salt and Sediment Fluxes in a Tropical Estuary: Itamaraca, Brazil. *Journal of Coastal Research, 21*(4), 751-758.

Mota-Oliveira, I. B. (1970). *Natural Flushing Ability of Tidal Inlets.* Paper presented at the 12th Coastal Engineering Conference, Washington D.C.

Muehe, D., & Correa, C. H. T. (1989). The coastline between Rio de Janeiro and Cabo Frio. In C. Neves (Ed.), *Coastlines of Brazil* (pp. 110-123). New York: American Society of Civil Engineers.

Norton, W. R., King, I. P., & Orlob, G. T. (1973). *A Finite Element Model for Lower Granite Reservoir*. Walla: Walla Walla District, U.S. Army Corps of Engineers.

Oliveira, A., Fortunato, A. B., & Rego, J. R. L. (2006). Effect of morphological changes on the hydrodynamics and flushing properties of the Obidos lagoon (Portugal). *Continental Shelf Research, 26*, 917-942.

Oliveira, M. (Cartographer). (1862). *Barra a Porto de Cabo Frio* [Historical Chart].

Perillo, G. M. E., & Kjerfve, B. (2005). Regional Estuarine and Coastal Systems of the Americas: An Introduction. *Journal of Coastal Research, 21*(4), 729-730.

Primo, P., & Bizerril, C. (2002). *Lagoa de Araruama* (Report). Cabo Frio, Estado do Rio de Janeiro: Secretaria de Estado de Meio Ambiente e Desenvolvimento Sustentavel.

Pugh, D. T. (1987). *Tides, Surges, and Mean Sea Level*. Avon (U.K.): John Wiley and Sons Ltd.

Ranashinghe, R., & Pattiaratchi, C. (2000). Tidal inlet velocity asymmetry in diurnal regimes. *Continental Shelf Research, 20*, 2347-2366.

Ribeiro, F., daSilva, R., Valentini, E., Rosman, P., Oliveira, V., & Cunha, A. (2002). *Modelagem da Lagoa de Araruama, RJ* (Report). Rio de Janeiro: Fundacao Coppetec - COPPE/UFRJ.

Roy, P. S., Thom, B. G., & Wright, L. D. (1980). Holocene asequences on an embayed high energy coast: an evolutionary model. *Sedimentary Geology, 26*, 1-9.

Speer, P. E., & Aubrey, D. G. (1985). A Study of Non-linear Tidal Propagation in Shallow Inlet/Estuarine Systems Part II: Theory. *Estuarine, Coastal and Shelf Science, 21*, 207-224.

Stanev, E. V., Brink-Spalink, G., & Wolff, J. O. (2004). *Transport-Controlled Sediment Patterns in the East Wadden Sea.* Paper presented at the International Workshop HWK - From Particle Size to Sediment Dynamics, Delmenhorst.

Strahler, A. N. (1952). Hypsometric(area-altitude) analysis of erosioal topography. *Bulletin of the Geological Society of America, 63*, 1117-1142.

Sumer, B. M., & Deigaard, R. (1981). Particle Motions Near the Bottom in Turbulent Flow in an Open Channel. Part 2. *Journal of Fluid Mechanics, 109*, 311-338.

Thomas, C. G., Spearman, J. R., & Turnbull, M. J. (2002). Historical morphological change in the Mersey Estuary. *Continental Shelf Research, 22*, 1775-1794.

Uncles, R. J. (2002). Estuarine Physical Processes Research: Some Recent Studies and Progress. *Estuarine, Coastal and Shelf Science, 55*, 829-856.

Van der Spek, A. J. (1997). Tidal Asymmetry and long term evolution of Holocene tidal basins in the Netherlands: simulation of paleotides in the Schelde estuary. *Marine Geology, 141*, 71-90.

Vasconcellos, L. (Cartographer). (1788). *Planta da Cidade de N. S. da Assumpcao de Cabo Frio* [Historical Chart].

Walters, R. A., & Werner, F. E. (1991). Non-linear generation of overtides, compound tides, and residuals. In B. B. Parker (Ed.), *Tidal Hydrodynamics* (pp. 298-320). New York: John Wiley and Sons Ltd.

Wang, Z. B., Jeuken, M., Gerritsen, H., de Vriend, H. J., & Kornman, B. A. (2002). Morphology and asymmetry of the vertical tide in the Westerschelde estuary. *Continental Shelf Research, 22*, 2599-2609.

Wang, Z. B., Louters, T., & Vriend, H. J. d. (1995). Morphodynamic modelling for a tidal inlet in the Wadden Sea. *Marine Geology, 126*, 289-300.